EPIGENETIC REGULATION OF THE HIF PATHWAY AND NOVEL THERAPEUTIC OPPORTUNITIES

A DISSERTATION IN
Pharmaceutical Sciences
and
Molecular Biology and Biochemistry

Presented to the Faculty of the University
of Missouri-Kansas City in partial fulfillment of
the requirements for the degree

DOCTOR OF PHILOSOPHY

by

VENKATA KRISHNA CHAITHANYA PONNALURI

M.E. (Hons.), Birla Institute of Technology and Science, 2007

Kansas City, Missouri

2014

EPIGENETIC REGULATION OF THE HIF PATHWAY AND NOVEL THERAPEUTIC OPPORTUNITIES

Venkata Krishna Chaithanya Ponnaluri, Candidate for the Doctor of Philosophy Degree

University of Missouri-Kansas City, 2014

ABSTRACT

The research presented in this dissertation is aimed at understanding the epigenetic regulation of the HIF pathway and the efficacy of treatment for retinal diseases and hemangioblastomas using HIF pathway inhibitors. Jumonji domain containing proteins demethylate tri- and dimethylated histone lysines and regulate chromatin structure. Substrate specificity of Jumonji domain-2 family histone demethylases (JMJD2A-C) was evaluated. A candidate substrate-based approach demonstrated that JMJD2A-C demethylate trimethylated lysine containing peptides from WIZ, CDYL1, CSB and G9a proteins, all constituents of transcription repression complexes. Also preference of Arg at –1 position and a smaller amino acid at –2 position was identified. The results obtained are consistent with lax substrate specificities observed for the iron (II), 2-oxoglutarate-dependent dioxygenases, and shed new light on the role of JMJD2 family of KDMs during epigenetic transcriptional regulation.

Hypoxia inducible factor (HIF) plays a critical role in cellular adaptation to hypoxia. Little is known about the epigenetic regulations during HIF-mediated transcription of pro-angiogenic genes in oxygen-dependent retinal diseases and hemangioblastomas. Hypoxic induction of a number of histone lysine demethylases (KDMs) and stem cell markers in retinal pigment epithelial cells and VHL–/– renal cell

carcinoma cells was evaluated. Also, expression of pro-angiogenic genes (*ADM*, *GDF15*, *HMOX1*, *SERPE1* and *SERPB8*) was determined to be dependent on KDMs under hypoxia. Further, treating cells with a general KDM inhibitor blocked the induction of these pro-angiogenic genes. Expression of stem cell markers in hemangioblastomas was determined to be due to activation of the HIF pathway. Further, honokiol, digoxin, and doxorubicin, three recently identified HIF inhibitors from natural sources effectively blocked the expression of stem cell markers. These results present the possible cytological origin of neoplastic stromal cells in hemangioblastomas. Based on our results we believe that inhibition of the HIF pathway is an attractive strategy for the treatment of hemangioblastomas and retinal diseases. Also, blocking of KDMs using specific inhibitors can inhibit the amplification of the HIF pathway.

TET2 is a Fe(II), 2OG dependent dioxygenase which can demethylate 5mC in a CpG context, a key epigenetic modification. In this study we developed a HPLC based analytical method for evaluating the catalysis by recombinant TET2 protein.

The undersigned, appointed by the Dean of the School of Graduate Studies have examined a dissertation titled " Epigenetic Regulation Of The HIF Pathway And Novel Therapeutic Opportunities," presented by Venkata Krishna Chaithanya Ponnaluri, candidate for the Doctor of Philosophy degree, and hereby certify that in their opinion it is worthy of acceptance.

Supervisory Committee

Mridul Mukherji, D Phil., Committee Chair

Division of Pharmaceutical Sciences

Simon Friedman, Ph.D.

Division of Pharmaceutical Sciences

Kun Cheng, Ph.D.

Division of Pharmaceutical Sciences

Santosh Kumar, Ph.D.

Division of Pharmacology and Toxicology

Jeffrey Price, Ph.D.

Department of Biological Sciences

Contents

LIST OF ILLUSTRATIONS

Figure Page

LIST OF TABLES

ACKNOWLEDGEMENTS

First, I would like to thank my advisor Dr. Mridul Mukherji for accepting me into the program and providing constant support and advice through the course of my doctoral studies. He has been very patient and helpful through some of the most difficult periods of my studies. He always pushed me to work harder and helped me succeed in my endeavors by constantly motivating me.

I would like to thank my supervisory committee; Dr. Jeffrey Price, Dr. Simon Friedman, Dr. Kun Cheng, and Dr. Santosh Kumar for their help and guidance throughout my thesis work. I also thank Dr. Sandeep Putty and Dr. William Gutheil for teaching and helping me with LC-MS analysis and providing their valuable suggestions. I thank Dr. Ashim K Mitra and Dr. Dhanjay Pal for allowing me to use their cell culture facility and Dr. Ramya Vadlapatla for helping with the initial qPCR experiments. I also thank Dr. Kun Cheng for his qPCR instrument, which enabled me publish multiple papers.

I would like to thank Dr. Divya Teja Vavilala for always being there and believing in me. She was the strongest critic and a staunch advocate of my work and thought process. She is one person in my life who stood by me when there was no one for me. She helped me develop into the person I am today in both professional and personal aspects. I am very grateful for the unconditional support, motivation and guidance that she gave me at every step of my PhD. I will forever be indebted to her for

this. I would also like to thank Swami Prakash and Shayak Samaddar for helping in my research and for maintaining a positive work culture in the lab.

Altaf Hirani played an important role in my initial years of my PhD. I thank him for countless hours of discussions late in the night about varied topics, which helped me get distracted from the frustrations of failed experiments in lab. I also thank Dr. Sudheer Bobba, Hari Krishna Ananthula, Ravi Vaishya, Viplendra Pratap Shakya, Surbhi Verma, Namita Giri, Jouliana Sadek and Gulshan Mehta for their support and encouragement in my professional and personal life. I thank you all for reaching out to help me even without asking. I also would like to extend my thanks to Sharon Self and Joyce Johnson for their constant help and support with all the administrative work and for their kind words.

Finally, I would like to express my utmost sincere gratitude to my father and mother who helped me realize the dream of pursuing a doctoral degree by constantly encouraging and supporting me. I thank them for always believing in my abilities. No words can express how grateful I am for having them as my parents. I am grateful to Sushma for being patient with me while I was working long hours in the lab to finish my dissertation and supporting me through tough times. She was there to support me when things didn't work and encourage me to work harder to get things done. She managed everything at home making sure I didn't have to worry about anything other than my work. I would also like to thank my in-laws for their constant support and encouragement. Lastly I would like to extend my appreciation to Lakshmi, Sagar, and Satish for supporting me through my studies.

DEDICATED TO MY PARENTS AND MY WIFE

CHAPTER I

INTRODUCTION

General introduction to epigenetics

DNA of a eukaryotic cell, which is several meters long, is present in the nucleus and is extremely compacted. To achieve this high degree of compaction, DNA associates with a set of highly basic proteins called histones. This compacted structure is called chromatin and is made up of nucleosomes. The nucleosome consists of a histone octamer of the four core histones, H2A, H2B, H3, and H4 and 147 base pairs of DNA wrapped around it. Furthermore these nucleosomes fold into progressively higher-order structures like a chromatin fiber and finally a chromosome [1]. Chromatin folding is observed to be a dynamic process, and the extent of folding determines the level of accessibility of DNA for processes like transcription, replication, and recombination. Occurrence of varying degree of folded chromatin regions plays an important role in regulating gene expression. The histone subunits have tail regions that protrude out of the nucleosome and are sites for extensive posttranslational modifications. These modifications modulate chromatin structure, thereby regulating accessibility of genes for effective transcription. Some of the observed post-translational modifications on histone tails are phosphorylation, acetylation, methylation, and sumolyation [2]. Interplay between these modifications determines the accessibility of DNA (Figure 1).

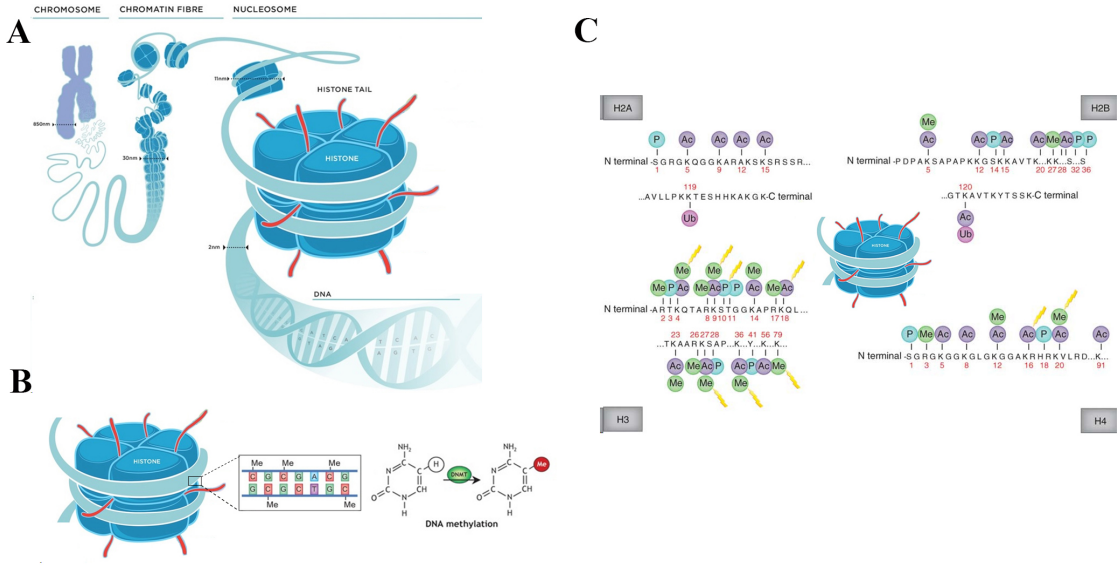

Figure 1: Chromatin architecture and epigenetic modifications observed on a nucleosome

The molecular mechanisms associated with packaging of DNA and how the RNA polymerase II (RNAPII) machinery and its regulatory factors access this packaged DNA sequences remain unclear. Regulation of transcription is found to be effected by factors like DNA methylation, histone modifications, and small nuclear RNAs [3]. This mode of regulation is termed “epigenetic regulation”, denoting an inherited state of gene regulation independent of any encoded genetic information from within DNA.

DNA methylation and demethylation

Methylation of DNA and post-translational modifications of histone proteins play an important role in regulating the chromatin architecture and gene expression. One of the most widely studied epigenetic marks in normal and cancer cells DNA is cytosine methylation at the C5 position within the dinucleotide CpG. It has been

shown that 3–6% of all cytosines are methylated in normal human DNA [4]. Owing to the low level of occurrence of modified cytosine in the genome, it is believed that 'methylable' CpG dinucleotides are distributed in the human genome in a non-random fashion. CpG-rich regions known as the CpG islands are found in the 5′ end region of many genes (promoter, untranslated region and exon 1) and for expressed genes are usually in an unmethylated state in normal cells. This unmethylated status is associated with the transcriptional ability of CpG-island containing genes. However in cancer cells, CpG-island-promoter hypermethylation is observed, which leads to transcriptional silencing of tumour-suppressor genes-key for the tumorigenic process [5].

In mammals, a family of DNA methyltransferases (DNMTs) which are the only known enzymes to facilitate the transfer of a methyl group to cytosine from S -adenosylmethionine (SAM) [6] carries out DNA methylation. In mammals there are three enzymatically active DNMTs: DNMT1, DNMT3A and DNMT3B; and one related regulatory protein, DNMT3L (devoid of catalytic activity). DNMTs use a conserved mechanism [7] that has been studied best using the bacterial 5mC methyltransferase (MTase) M.HhaI [8]; [9]; [10]; [11]; [12]. Briefly, the catalysis involves binding of MTase to the DNA, eversion of target nucleotide to project it out of the double helix (''base flipping''), a conserved Cys nucleophile covalently attacks the cytosine C6, followed by the transfer of the methyl group from AdoMet to the activated cytosine C5, and the various release steps. The epigenetic effects associated with methylation of cytosine results in maintaining the patterns of gene

expression in different cell types [13]. CpG methylation is found to play an important role in epigenetic processes like X-chromosome inactivation [14], genomic imprinting (Hore et al., 2007), reprogramming in transferred nuclei [15], gene silencing [16]; [17], and some elements of carcinogenesis [18].

Cytosine methylation on the DNA also occurs in the context of other known epigenetic modifications like histone acetylation, methylation and methyl-CpG-binding proteins. Methylated CpG islands are associated with the formation of nuclease-resistant chromatin and the DNA methyltransferases (DNMTs) are associated with histone deacetylases and histone methyltransferases, two key regulators of histone modification [19-21]. The levels of methylation and acetylation of specific lysine residues found in the tails of core histones of nucleosomes play a crucial role in regulating chromatin structure and gene expression [21]. Overall, histone hypermethylation and hypoacetylation are hallmarks of DNA regions that are methylated and repressed in normal cells like in the case of the inactive X chromosome in females, and silenced imprinted and tissue-specific genes.

DNA methylation is a relatively stable epigenetic modification compared to most histone modifications. However, loss of DNA methylation, or DNA demethylation, has been observed in different biological contexts. This loss of methylation can occur in an active or passive fashion. Active DNA demethylation is an enzymatic process which facilitates the removal or modification of the methyl group from 5mC. In contrast, passive DNA demethylation refers to the loss of 5mC

during replication when functional DNA methylation maintenance machinery is absent [22]. Recently a series of discoveries have identified a family of DNA demethylases called Ten Eleven Translocation (TET), which can actively remove the 5mC mark from the CpG islands [23-26].

TET proteins were first discovered in a search of analogous DNA-modifying enzymes based on the analysis of *Trypanosoma brucei* base J-binding protein 1 (JBP1) [24], a dioxygenase that hydroxylates thymine in DNA [27]. The mammalian TET family consists of three members: TET1, TET2, and TET3 [28] which can convert 5mC to 5hmC. Recent studies have shown that TET enzymes can further oxidize 5hmC to 5-formylcytosine (5fC) and 5-carboxylcytosine (5caC) in DNA [29]; [30]. All TET enzymes belong to 2-oxoglutarate (2-OG) and Fe(II)-dependent dioxygenase superfamily which is characterized by a C-terminal catalytic domain (CD). 5caC, which is an oxidation product of 5mC, can be further excised by thymine-DNA glycosylase (TDG) and replaced by unmodified cytosine through the base excision repair (BER) pathway [29].

Every 2OG-dependent oxygenase characterized to date requires Fe(II) for catalysis and oxidize the primary substrate (*e.g.* 5mC into 5hmC) with coupled oxidation of 2OG cosubstrate into succinate and CO_2. During this process one atom of oxygen gets incorporated into the carboxylic acid group of succinate, while the fate of the other oxygen atom of dioxygen molecule depends on the type of oxidation reaction catalyzed. In the case of dehydration and desaturation reactions, the other oxygen is assimilated into water. However, in epoxidation and hydroxylation reactions,

incorporation of oxygen occurs into the epoxide or alcohol products, respectively. Since these oxygenases incorporate both the atoms of molecular oxygen into the products (*e.g.* succinate and 5hmC), they are also known as dioxygenases (Figure 2).

To date two Fe(II), 2OG-dependent dioxygenase superfamilies catalyzing the oxidative modifications of nucleic acid bases have been identified; the AlkB- and the TET/JBP-family. The AlkB-family dioxygenases protect *E. coli* against the cytotoxic effects of methylating substances by directly dealkylating bases (1mA, 3mC, 1mG and 3mT) in DNA [31, 32]. In humans, at least nine potential homologues of *E. coli* AlkB have been identified. Interestingly, similar to *E. coli* AlkB, some human homologs (*e.g.* ABH3 and FTO) can efficiently demethylate bases in single-stranded DNAs (ssDNA) and RNAs along with double-stranded DNA (dsDNA) [33, 34]. It is not known whether the TET-family of dioxygenases prefer 5mC demethylation in dsDNAs, ssDNAs or even in RNAs. Interestingly, 5mC is also a major RNA modification without much known functional significance [35].

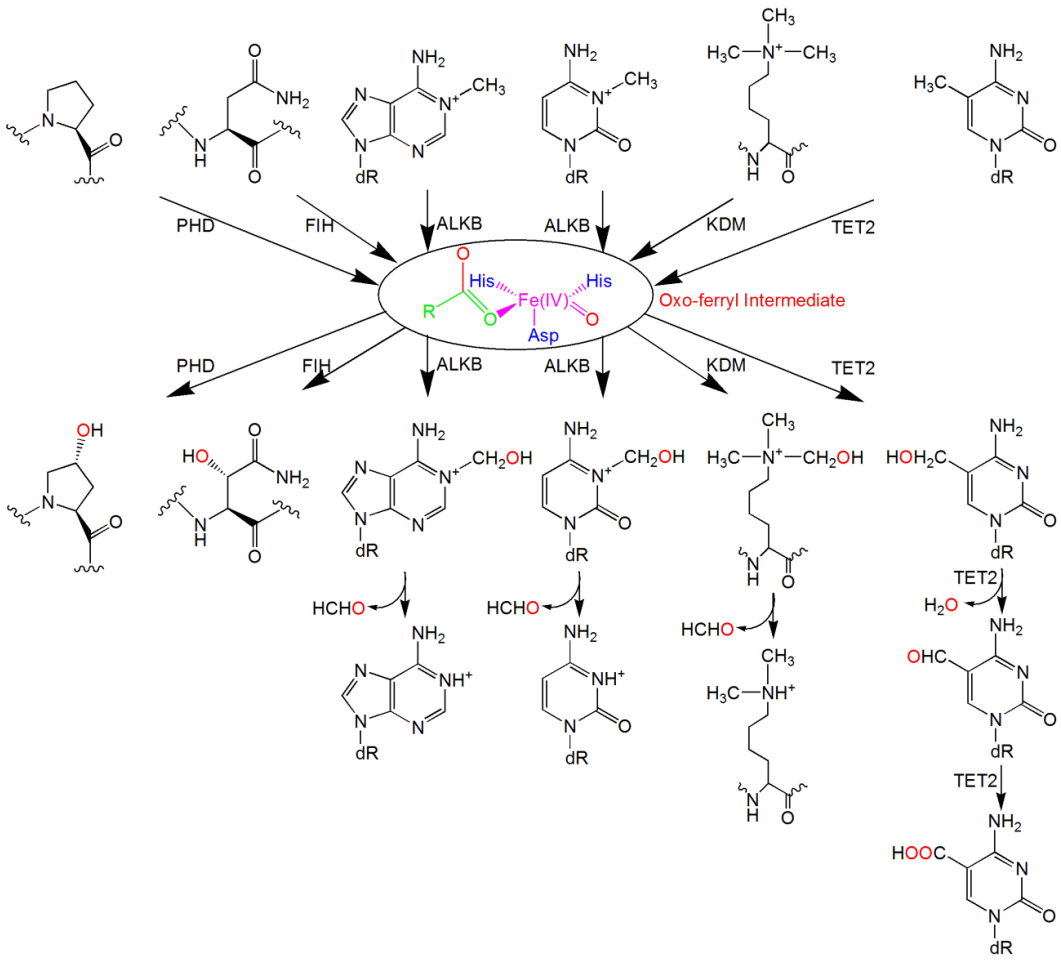

Figure 2 An overview of Fe(II), 2OG-dependent dioxygenases mediated oxidation of substrates involved in epigenetic regulation via a reactive oxo-ferryl [Fe(IV)=O] intermediate.

Bisulfide sequencing revealed that: (i) TET1-mediated 5mC demethylation is coupled with transcription because analysis of promoter truncated, transcriptionally inactive construct showed significantly less demethylation; (ii) demethylation is highly selective with few DNA strands being extensively demethylated while others are barely demethylated; (iii) of the two DNA strands in the transcribed region, 5mC demethylation is much more efficient on the non-transcribed (sense) strand than on the transcribed (antisense) strand [30]. All these observations suggest that the lax substrate specificity of TET1 is regulated by its interacting proteins which target it to specific sites of transcription initiation/elongation complexes.

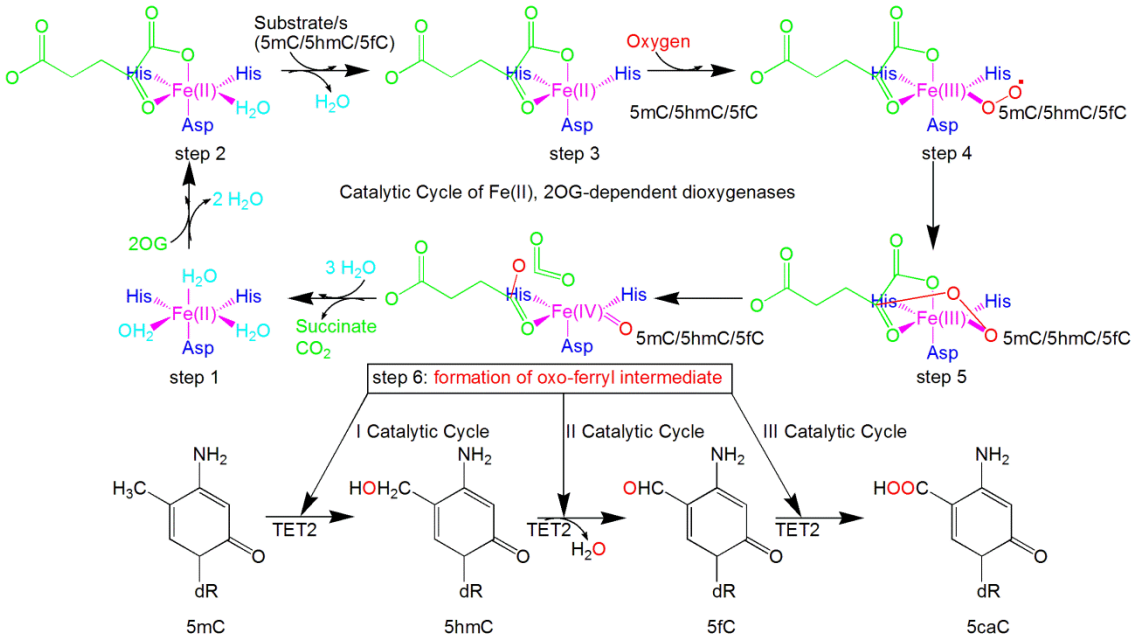

Figure 3: A catalytic cycle of Fe(II), 2OG-dependent dioxygenases showing sequential binding of the cofactors and substrates leading to the formation of reactive oxo-ferryl [Fe(IV)=O] intermediate. The two histidines and one aspartate residues, which form the active site core, are called the 2-His-1-carboxylate facial triad. The conversion of 5mC to 5caC is mediated by three iterative catalytic/oxidation cycles by the TET family of dioxygenases generating 5hmC and 5fC as intermediates.

Using a number of techniques, a detailed catalytic mechanism of Fe(II), 2OG-dependent dioxygenases has been proposed (Figure **3**) [36]. The TET-family dioxygenases convert 5mC into 5hmC, 5-formylcytosine (5fC) and 5-carboxylcytosine (5caC) by iterative oxidation steps [29]. Demethylation of 5mC takes place by the excision of 5caC, the final product in the TET-mediated oxidation reaction, by thymine-DNA glycosylase, a base excision repair enzyme [29]. It seems that TET dioxygenases prefer 5mC as substrate over 5hmC and 5fC [37], which could possibly explain the low genomic level of 5fC and 5caC compared to 5hmC [29, 37]. It is interesting to note that during the first and third TET-mediated oxidation reactions (from 5mC to 5hmC and then from 5fC to 5caC), the oxo-ferryl intermediate possibly abstracts a hydrogen atom from the substrates (*e.g.* 5mC and 5fC) and then hydroxylates it in a rebound mechanism. While during the conversion of 5hmC into 5fC, the second TET-mediated oxidation reaction, hydroxylation is proceeded by a dehydration reaction producing water and 5fC. Thus TET enzymes are the first example of a bifunctional Fe(II), 2OG-dependent dioxygenase in the mammalian system.

Histone acetylation and deacetylation

Chromatin immunoprecipitation assays performed with antibodies that are selective for hyperacetylated histones, demonstrated presence of high density of acetylated histones in regions correlating with general DNase I sensitivity. This fits well with transcriptional competence, as sensitivity to nuclease digestion and histone acetylation are often considered as salient features of chromatin accessible for transcription.

Acetylation on histone is observed on lysine residues. DNA, owing to its high negative charge, associates with positively charged side chains of amino acids like lysine and arginine to form a compact structure. Acetylation of these residues results in loss of this charge – charge interaction between histone tail amino acids and DNA, resulting in weakened histone:DNA contacts. This altered state of histone tails can modulate the interactions between the adjacent nucleosomes. Also, changes in the nucleosome structure could affect the binding ability of other regulatory proteins, thus modulating chromatin structure. Taken together, alteration of the charge on the histone tail by the addition or removal of acetyl group could influence the structure of the individual nucleosome and also its higher order folding. These changes regulate the presence of an open or closed chromatin structure for transcription. In the last decade, several classes of enzymes have been identified which can add an acetyl group and ones that can remove this acetyl group. These discoveries have facilitated better understanding of chromatin dependent regulation of gene expression.

Histone methylation and demethylation

Modulation of chromatin structure through covalent histone modification is one of the fundamental ways of regulating DNA accessibility during processes such as gene transcription, DNA replication and DNA damage repair. Methylation of histones can be done on either arginine or lysine residues [38-41]. On the lysine residue, ε-nitrogen undergoes methylation by either the SET domain- or non-SET domain containing lysine histone methyltransferases (PKMTs). As shown in the Figure 4, lysine residue could be modified by the addition of up to three methyl groups at each lysine producing a total of four methyl states: unmethylated, monomethylated, dimethylated or trimethylated. However, an arginine residue in histone proteins can only be mono- or dimethylated and this could be in either symmetric or asymmetric configuration.

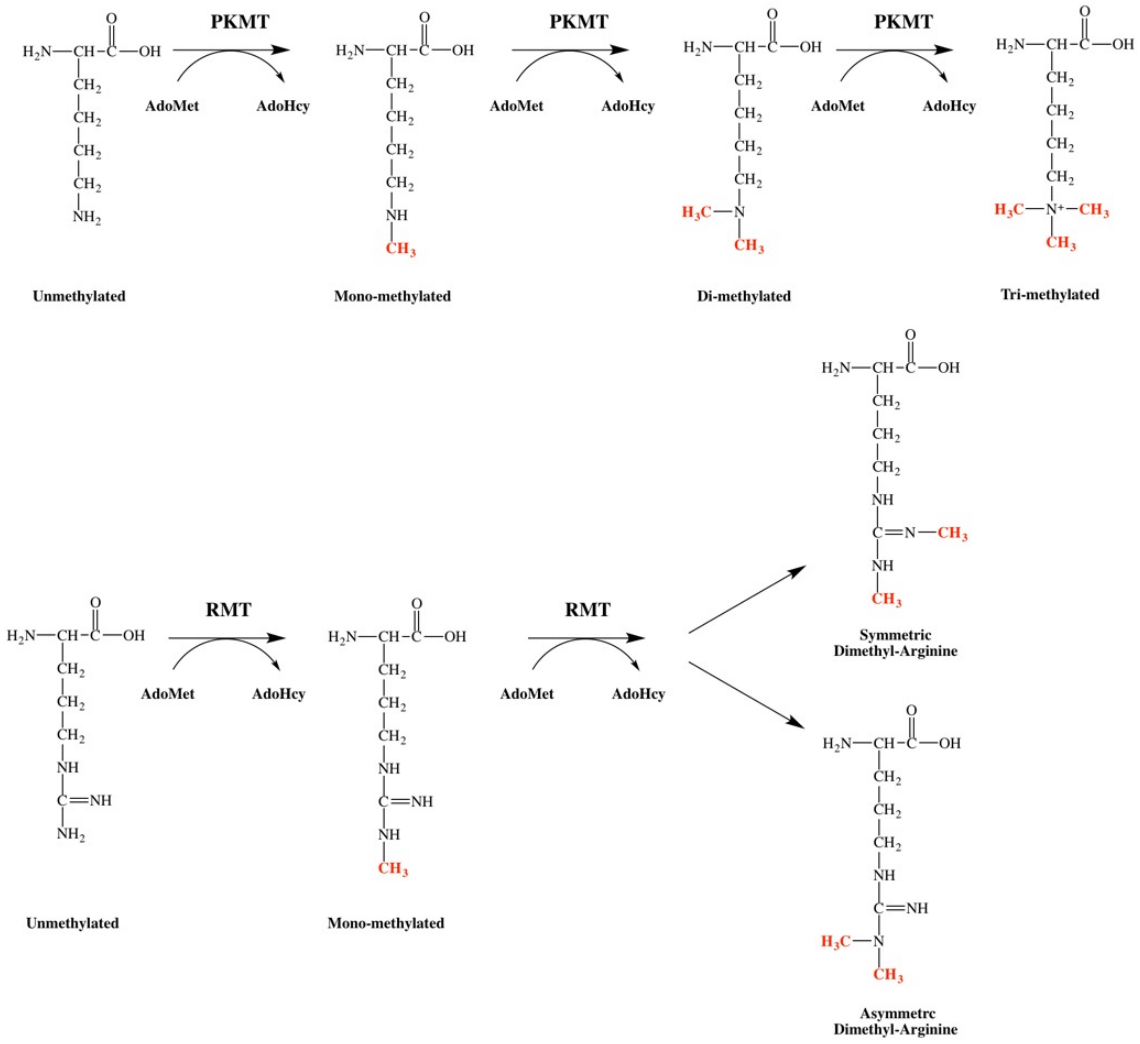

Figure 4: Methylation of lysine and arginine residues by PKMTs

For a long time it was believed that methylation of histone proteins on their lysine and arginine residues was a static modification. However, three distinct classes of enzymes with an ability to remove the methylation mark were eventually identified. PADI4 (Petidylarginine deiminase 4), the first enzyme identified converts methyl arginine into citrulline through a deimination reaction. In 2001, LSD1 (lysine specific demethylase 1), a histone lysine demethylase, was identified

and can remove methyl marks form H3-K4 and H3-K9 residues (mono or dimethylation) [42-44]. LSD1 catalysed through an oxidative demethylation reaction involving flavin as a cofactor. Other proteins like CoREST complex are necessary for full enzymatic activity, indicating involvement of regulatory subunits for modulation of their demethylase activity. A third class of enzymes containing a putative Jmj domain was identified, with various histone variants being the only known substrates. These Jmj domain-containing histone demethylases catalyzed demethylation of histone lysine residues through an oxidation reaction involving iron (II) and 2-oxoglutarate as cofactors. In humans ~25-30 putative Jmj domain containing histone demethylases (KDMs) have been identified and classified into seven families based on sequence similarities [45, 46].

With the identification of KDMs and the dynamic nature of methylation, the effects of histone methylation on gene expression were shown to be site specific. Both activation and inhibition of gene expression by methylation of specific lysine residue has been observed. For example, methylation of the H3-K4 residue signifies presence of an open/active chromatin structure and H3-K27 signifies presence of closed/inactive form. The observed distribution patterns for H3K4me3, H3K27me3 underlie the existence of diverse cellular states with varying gene expression profiles. This variation among cell types facilitates pluripotency and lineage differentiation. As epigenetic regulation of gene expression *via* histone modification plays a key role in determining cell fate, it is believed that it may help establish the tumour-initiating cell population early in tumorigenesis. Several studies have shown

existence of altered global histone modification patterns in several types of cancer, providing evidence for the role of epigenetic landscape and cellular context in tumorigenesis.

The enzymatic machinery involved in histone methylation

Methylation of histone proteins was known to exist for many decades, but the significance of this modification and its role in modulation of chromatin structure and thus gene expression were not understood. A methyl group is added to either specific lysine or arginine residues on histone proteins, where SAM acts as a methyl donor. The enzymes associated with methylation of histone proteins are known as Histone methyltransferases and are classified into three classes, lysine-specific SET domain-containing histone methyltransferases (PKMTs) involved in methylation of lysines 4, 9, 27, and 36 of histone H3 and lysine 20 of histone H4; non-SET domain-containing lysine methyltransferases involved in methylating lysine 79 of histone H3; and arginine methyltransferases involved in methylating arginine 2, 17, and 26 of histone H3 as well as arginine 3 of histone H4 [47]. The SET domain in PKMTs is ≈130 amino acids and is highly conserved [48]. It also contains a Pre and Post SET domain, and forms a characteristic β fold, which constitutes the pseudoknot structure. This pseudoknot structure incorporates the two most conserved sequence motifs of SET domain (RFINHXCXPN and ELXFDY) to form a catalytically active site next to the methyl donor and peptide-binding cleft. Molecular dynamics studies of the enzyme substrate interactions gave clues about the mechanism of these enzymes. Each methylation step includes the formation of a water channel to allow proton dissociation from protonated

charged lysine into solvent (step 1), methylation of a neutral lysine by $^{+}$AdoMet (step 2), and product formation (step 3) [49]. These SET domain containing PKMTs can be classified into seven families; SUV39 family, SET 1 family, SET 2 family, RIZ family, SMYD family, EZ family, and SUV4-20 family based on the sequence surrounding their SET domain.

Reaction mechanism and substrate specificity of histone demethylases

The JmjC domain containing KDMs are members of non-heme iron (II)-dependent dioxygenases that require molecular oxygen and 2-oxoglutarate (2OG) for catalysis. The reported crystal structures of 2OG-dependent dioxygenases [50, 51] have demonstrated the emergence of a common structural motif called the "2-His-1-carboxylate facial triad" [52]. These structures reveal a β-strand core containing eight sheets folded into a distorted "jelly-roll" motif with an active site containing two histidine and a carboxylate ligands [53], occupying one face of the iron(II) coordination sphere. Of the remaining three sites of the iron(II) coordinate, the carboxyl and keto oxygens of the 2OG bind to the metal centre in bidentate manner. Whereas, the last site is occupied by O_2, *trans* to any one of the three ligands of the 2-His-1-carboxylate facial triad. The 5-carboxylate group of 2OG binds to either arginine (present on the eighth β-sheet of the "Jelly-roll") or lysine (present on the fourth β-sheet of the "Jelly-roll") residue from the enzyme (Figure 5).

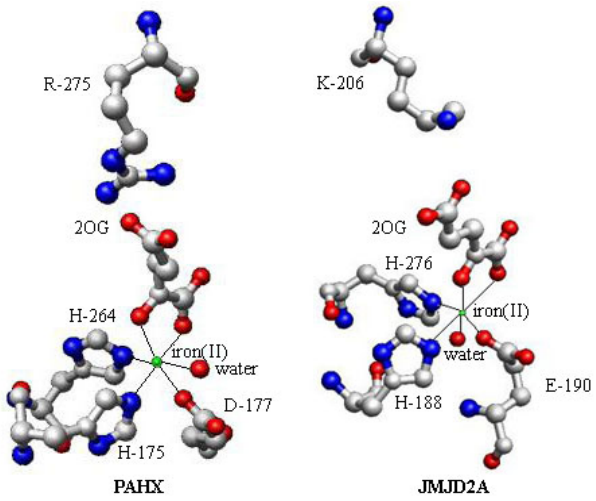

Figure 5: A conserved active site structures of PAHX and JMJD2A derived from their crystal structures. The 5 carboxylate group of 2OG binds either arginine, as in PAHX, or lysine, as in JMJD2A.

The demethylation proceeds in two steps. In the first step, these enzymes directly hydroxylate the affected methyl group of the substrate (e.g. H3-K9me3). In the second step, which does not require dioxygenase activity, formaldehyde is spontaneously released from hydroxylated methyl group to generate dimethylated product (e.g. H3-K9me2). In all 2OG-dependent dioxygenase reactions, the oxidation of the prime substrate is coupled to the conversion of 2OG into succinate and CO_2. One of the oxygen atoms of the dioxygen is incorporated into the carboxyl group of succinate while, in the case of hydroxylation reactions, the other oxygen atom is incorporated into an alcohol product [10] (Figure 6)

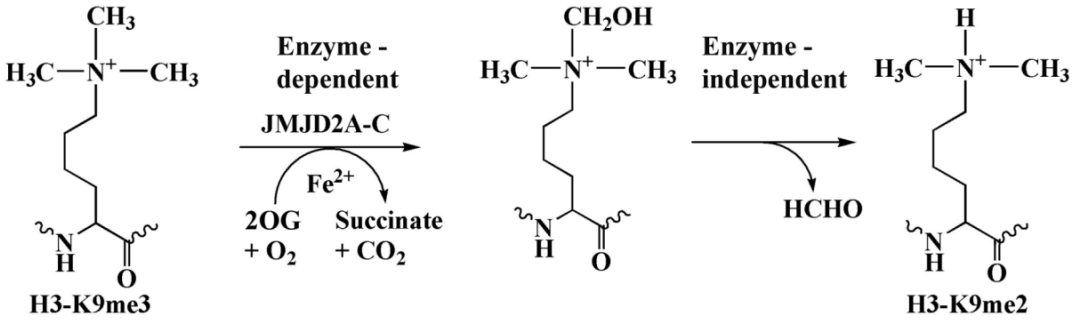

Figure 6: Reaction scheme showing formation of dimethylated product from H3-K9me3 by JMJD2A-C KDMs.

General introduction to hypoxia

Oxygen is an essential element for the survival of an aerobic organism. Oxygen acts as the final acceptor of electrons in the mitochondrial respiratory chain which is essential in the generation of cellular energy, in the form of adenosine triphosphate (ATP). ATP is essential for maintaining cellular viability. In a normoxic cell, there is abundance of oxygen which facilitates maintenance of a high and constant ratio of cellular ATP/ADP essential for the survival of the cell. This need for a high and constant ATP/ADP ratio highlights the dependence of the cell on oxygen. Any drop in then normal oxygen supply triggers hypoxia and alters cellular processes [54, 55].

Hypoxia is experienced in many physiological processes (such as wound healing, embryonic development, etc.,) and also in patho-physiological conditions, such as obstructive sleep apnea, atherosclerosis, ischemic diseases (stroke), mountain sickness, retinal diseases, and cancer [56, 57]. Tissues and cells experiencing lower than normal oxygen tension could be due to reduced oxygenation of the blood (hypoxemia), a decrease in the oxygen supply sufficient to impair cellular function (hypoxia) and a

combination of hypoxia and lowered blood flow to the tissue/cells (Hypoxia-ischemia) [58, 59].

Further response to hypoxia can be differentiated based on the duration of exposure into an acute, intermediate, and a chronic response; based on levels of oxygen concentration into a moderate (5-8% O2) and an anoxic level (<1 O2) (normoxia is 21% O2) [56, 60].

Hypoxia inducible factor (HIF) is a central molecule that plays a vital role in eliciting the effect of oxygen tension at the cellular level by modulating gene expression [61]. HIF-1α was originally identified while studying the human *EPO* gene, which encodes the glycoprotein hormone erythropoietin that regulates erythrocyte production [61]. DNA affinity purification assays revealed that HIF is a heterodimer consisting of HIF-1α and HIF-1β subunits [62, 63]. Also, HIF-1α protein levels increase as the O_2 concentration lowers [64]. Homology based search using HIF-1α sequence identified HIF-2α, which can also dimerize with HIF-β and initiate transcription by binding to the same recognition motif as HIF-1α [65]. HIF-1α (and HIF-2α) protein stability is negatively regulated by hydroxylation mediated by iron(II), 2-OG dependent prolyl hydroxylase domain protein (PHD). This hydroxylation of the HIFα isoforms leads to recognition and ubiquitination by E3 ubiquitin ligase von Hippel–Lindau protein (VHL) and targeting to proteasome-dependent degradation under normoxic conditions (9–11). Also, the transactivation ability of HIF-1α (and HIF-2α) is negatively regulated by factor inhibiting HIF-1 (FIH-1) in the nucleus [66]. FIH-1-dependent asparaginyl hydroxylation hinders the association of the coactivators CBP (CREB-binding protein)

and p300 with the HIF heterodimer [67, 68]. Thus, the stability and activity of the HIFs are regulated *via* their hydroxylation in an O_2 dependent manner, thereby transducing the changes in O_2 availability to changes in transcriptional activity of the cell.

Epigenetic modulators induced by hypoxia

As discussed histone lysine demethylase are classified into two classes, LSD1 and JmjC domain-containing KDMs. LSD1 is a flavin dependent enzyme, while most JmjC domain-containing histone demethylases are dioxygenases and are similar to FIH1, whose activities require Fe(II), α-ketoglutarate, and oxygen. As a result of this there is a possibility that their enzyme activities are affected by oxygen tension. In addition, recent studies have demonstrated that JMJD1A and JMJD2B are HIF targets, and other JmjC domain-containing proteins may also be upregulated by hypoxia or HIF [69-72]. Seven additional JmjC domain-containing proteins, including JMJD1B, JMJD2C, JMJD6, PLU-1, SMCX, RBP2, and KIAA1718 could be regulated by hypoxia. A chromatin immunoprecipitation (ChIP) sequencing approach also found 17 out of 22 JmjC family KDM genes upregulated under hypoxic conditions, with four (including PLU-1, JMJD1A, JMJD2B, JMJD2C) being direct HIF-1 targets [69]. It is still not clear what is the role of these KDMs in the hypoxic response and warranted more work in this area. Expression of the recently identified TET2 family of DNA demethylases has also been found to be modulated under hypoxia in cells originating from various tissues. These findings suggest a possible mechanism associated with regulating the expression of HIF target genes under hypoxic conditions *via* these epigenetic modulators.

CHAPTER II

ENZYMATIC CHARACTERIZATION OF JMJD2 (JUMONJI DOMAIN CONTAINING) FAMILY OF HISTONE DEMETHYLASES

Introduction

Epigenetic mechanisms which govern cell fate and identity are regulated by histone modifying enzymes. Eukaryotic histone proteins undergo extensive modifications which constitutes the 'histone code' [2]. This controls the accessibility and usage of genetic information. Covalent histone modifications, specifically acetylation and methylation, play a major role in scripting the 'histone code'. Histones are methylated on lysine or arginine residues. The predominant sites of lysine methylation are H3-K4, -9, -27, -36, -79 and H4K20 [2]. The SET domain containing protein lysine methyltransferases (PKMTs) methylate histone and non-histone proteins. Most histone methylating enzymes perform mono-, di- or trimethylation of the lysine side chain [73]. The SET domain in these enzymes is ≈130 amino acids. They also contain a Pre and Post SET domain, and form a characteristic β fold, which constitutes the pseudoknot structure [48]. This pseudoknot structure incorporates the two most-conserved sequence motifs of the SET domain (RFINHXCXPN and ELXFDY) to form a catalytically active site next to the methyl donor and peptide-binding cleft.

In the active site of PKMTs, the substrate and the cofactor (*S*-adenosylmethionine / $^{+}$AdoMet) bind at two adjacent sites of the conserved SET domain. The $^{+}$AdoMet methyl group approaches the target lysine of the substrate to form Enz-LysNH_3^+·$^{+}$AdoMet complex. The Enz-LysNH_3^+ [or Enz-Lys$N(Me)H_2^+$ or

Enz-LysN(Me)$_2$H$^+$] must be deprotonated before methylation because only a neutral LysNH$_2$ [or LysN(Me)H or LysN(Me)$_2$] can be methylated by the $^+$AdoMet cofactor.

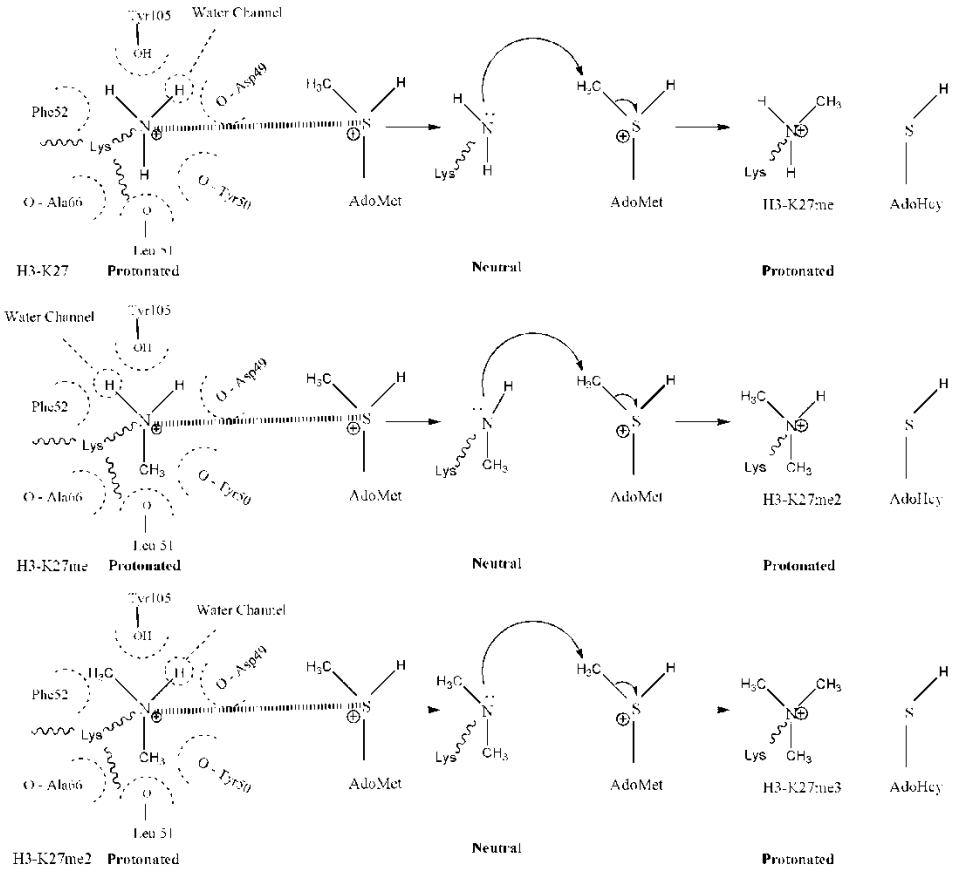

Figure 7: Catalytic scheme of SET domain containing lysine methyltransferases showing the formation of water channels.

Molecular dynamics simulations of a number of Enz-LysNH$_3^{+}$.$^+$AdoMet complexes suggest the formation of a water channel after the establishment of the complex (*e.g.* G9a-Lys9NH$_3^{+}$.$^+$AdoMet). This water channel allows proton transfer from the protonated substrate to the solvent. Methyl transfer does not occur if a water channel is not formed. The number of accessible water channels determines whether a

PKMT transfers one, two, or three methyl groups to target lysine residue. Thus each methylation step includes the formation of a water channel to allow proton dissociation from protonated charged lysine into solvent (step 1), methylation of a neutral lysine by $^{+}$AdoMet (step 2), and product formation (step 3) (Figure 7) [49].

LSD1, the first histone lysine demethylase (KDM) identified, can demethylate mono- and dimethylated H3-K4 and H3-K9 residues [43]. More recently, a number of Jumonji (Jmj) domain containing KDMs have been identified which can also demethylate trimethylated lysine residues of histone tails [44, 46, 74, 75]. The Jmj domain containing KDMs are members of non-heme iron (II)-dependent dioxygenases that require molecular oxygen and 2OG for catalysis. The demethylation proceeds in two steps; in the first step (enzyme-dependent), JmjD2 members directly hydroxylate the affected methyl group of H3-K9me3. In the second step (enzyme-independent), which does not require dioxygenase activity, formaldehyde is spontaneously released from the hydroxylated methyl group to generate H3-K9me2 (Figure 6).

In light of the spectroscopic data [76, 77] and crystallographic studies [50, 78-85], a detailed catalytic mechanism of the 2OG-dependent enzymes has been proposed (Figure 8). Stoichiometric binding of iron (II) to apoenzyme forms a distorted six coordinate octahedral ferrous active site (step 1). The affinity of 2OG binding is higher when iron (II) is present in the active site and results in a strong direct bidentate interaction between 2OG and iron(II). The keto carboxylate moiety of 2OG becomes much more planar when 2OG binds to iron(II) producing a new six coordinate octahedral geometry (step 2).

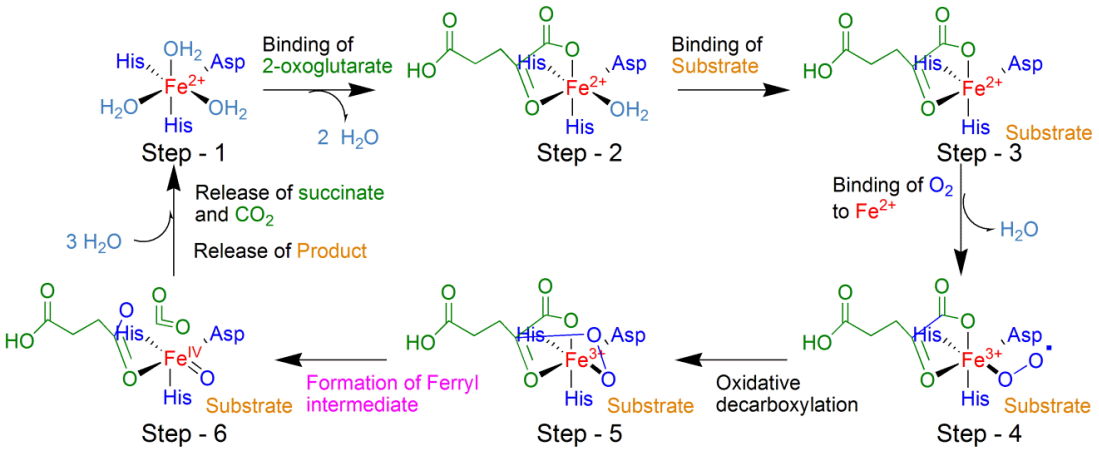

Figure 8: Catalytic scheme of iron(II), 2OG-dependent dioxygenases showing the 'ferryl' intermediate [Fe(III)-O., equivalent to FeIV=O] and the effect on substrate oxidation. The two histidines and one aspartate form the active site core called the "2-His-1-carb

The six coordinate iron(II) site is relatively unreactive toward O_2, thus limiting the rate of the uncoupled conversion of 2OG to succinate and CO_2 in the absence of a substrate. Substrate binding, with 2OG present in the active site, dramatically changes the spectra of the iron site, indicating the formation of a square-pyramidal five coordinate species creating an open iron(II) coordinate site for O_2 to bind (step 3). The fact that the open coordination position at the iron (II) site becomes available only when both substrate and cosubstrate are present supplies a critical coupling mechanism for the decarboxylation of 2OG and hydroxylation of the substrate. Dioxygen then reacts at the open coordination position of the five coordinate iron (II). The partial electron transfer from iron (II) to O_2, gives oxygen a superoxo radical anion character (O_2^-) (step 4). This

activates O_2 for the nucleophilic attack on the keto-carbon of 2OG (step 5). The resulting bridged intermediate then undergoes a concerted decarboxylation of 2OG and a heterolytic cleavage of the O-O bond, forming an oxo-ferryl [Fe^{IV}=O] intermediate (step 6). The oxo-ferryl intermediate abstracts a hydrogen atom from the substrate and then hydroxylates it in a rebound mechanism with significant exchange of oxygen from water [86], thus generating the product.

In humans ~25-30 putative Jmj domain containing KDMs have been identified with various histone variants being the only known substrates [46, 75]. The JmjC domain containing KDMs have been classified into 7 families based on their sequence. The Jumonji domain-2 (JMJD2) family consist of four members, JMJD2A-D, and demethylates the trimethylated histone H3-lysine-9 (H3-K9me3), and also H3-K9me2 and H3-K36me3 residues, albeit at lower rates [87]. JMJD2A-C are closely related isoforms with JMJD2D being the distinct one based on sequence homology. JMJD2A-C comprise an N-terminal catalytic core composed of JmjC and JmjN domains, a linker region, and a C-terminal region containing two PHD and Tudor domains.

We believed that JMJD2 family of enzymes may have additional non-histone substrates because of the following three reasons. First, in the proposed reaction mechanism of iron (II), 2OG-dependent dioxygenases, substrate is not directly involved in generating the reactive oxo–ferryl intermediate (Figure 8).

Consequently, the iron(II), 2OG-dependent dioxygenases generally have lax substrate specificity [88-90]. Second, a substrate profile of histone lysine methyltransferase G9a (which catalyzes the formation of H3-K9me1 and H3-K9me2, as

well as H3-K9me3 at a lower rate) identified a number of non-histone substrates [91]. This suggests the possibility for the existence of demethylases which can reverse methylation marks from non-histone proteins. Finally, the crystal structure of JMJD2A revealed that the binding of the methylated peptide substrates to the active site is achieved by few polar side chain interactions [50]. This provides a degree of plasticity in substrate recognition by JMJD2 family KDMs, an unusual feature for sequence specific enzymes.

Therefore, in the first part of the current study we investigated if JMJD2A-C can accept peptides from non-histone proteins as substrates and demonstrated that these can indeed demethylate alternate peptide substrates (WIZ-K305me3, CDYL1-K135me3, CSB-K170me3, CSB-K297me3, CSB-K448me3, CSB-K1054me3 and G9a-K185me3, automethylation site of G9a) from four different proteins (WIZ, CDYL1, CSB and G9a). Surprisingly, all the non-histone substrates are components of transcription complexes. In the second part of the study, in order to determine the essential amino acids required for the identification of substrates by the Jmjd2a-c KDMs we searched for the existence of a consensus motif in these eight peptides (one histone and seven non-histones). These studies suggested preference for a smaller amino acid at –2 position and conservation of Arg at the –1 position (the methylated lysine is used as reference position 0 for amino acid numbering throughout the text). However, the conservation of Arg at the –1 position may be due to G9a (H3-K9 methyltransferase) substrate specificity rather than Jmjd2 KDMs because all the non-histone substrates examined were G9a substrates [92]. In this study we identified the role of –1 and –2

residues in the substrate recognition by Jmjd2a-c KDMs. Surprisingly we also found similarities in the substrate specificities of G9a PKMT and Jmjd2a-c KDMs, although both the enzymes have different reaction mechanisms and structure.

Materials and Methods

Cloning and expression of JMJD2A, JMJD2B, and JMJD2C (GASC1)

Human cDNA clones of all three genes were used as the template for PCR. The N-terminal catalytic cores (1-349 amino acids) were amplified using the following primers: 5'-JMJD2A-SphI, SalI, SmaI, BamHI: 5'-ACTAGTGTCGACACCCGGGAGGATCCCTGGAAGTTCTGTTCCAGGGGCCC ATGGCTTCTGAGTCTGAAAC-3', 3'-JMJD2A-NotI, NdeI, HindIII, PstI: 5'-CTGCAGAAGCTTCATATGGCGGCCGCCTATTCTGGCGTGGGCAG-3', 5'-JMJD2B-SalI, KpnI: 5'-GTCGACGGGGTACCCTGGAAGTTCTGTTCCAGGG GCCCATGGGGTCTGAGGACCAC-3', 3'-JMJD2B-NotI, XhoI: 5'-CTCGAGGCGGCCGCTTACGCCGTGGGCCGCGT-3', 5'-JMJD2C-XhoI, SalI, SmaI, BamHI: 5'-CTCGAGGTCGACACCCGGGGGGATCCCTGGAAGTTCTGTTC CAGGGGCCCATGGAGGTGGCCGAGGTG-3' and 3'-JMJD2C-NotI, HindIII, PstI: 5'-CTGCAGAAGCTTGCGGCCGCCTAAGTAGGCTTCGTGTGATC-3'. The amplified DNA sequences were gel purified and cloned into pGEM®-T vector (Promega, Madison, WI). The sequences of JMJD2A-C genes were verified by DNA sequencing using SP6 and T7 promoter primers. The verified genes were subcloned into pGEX-4T1 vector (GE Healthcare, Piscataway, New Jersey). The JMJD2A and JMJD2C were cloned using BamHI / NotI restriction sites, while SalI / NotI sites were used for JMJD2B. The recombinant vectors were transformed into *E. coli* BL21(DE3) cells for protein expression. Cells were grown in Luria-Bertani broth containing 100 μg/ml ampicillin at 37°C, until the $O.D._{600}$ of the culture reached 0.8. The optimized

condition for recombinant protein expression was found to be 0.25 mM IPTG induction of bacterial culture ($O.D._{600}$ = 0.8) for 4 hrs at 37ºC. All three JMJD2 isoforms were produced at ~10% of the total soluble protein observed using 12% SDS-PAGE analyses.

Protein purification

All three recombinant JMJD2 protein isoforms were purified from 12 liter of culture. Bacterial cells were pelleted and either stored at –80°C or lysed immediately for protein purification. This step onwards all the steps of protein purification were performed on ice. The cells were resuspended in 30 ml of lysis buffer (PBS-10 mM Na_2HPO_4, 1.8 mM KH_2PO_4, 2.7 mM KCl, 140 mM NaCl, pH 7.3 containing 10% glycerol) and sonicated at an intensity of 5 for 6 mins with 6 pulses every 30 seconds (Sonic Dismembrator 550, Fisher Scientific). The lysate was spun down at 15,000 rpm for 20 min (Beckman J2-HS centrifuge) and the supernatant was collected and filtered through 0.45µ filter. Glutathione Agarose 4B resin (USB, Cleveland, Ohio) was used for purification of GST tagged proteins. The resin (100 ml) was packed into a XK50 FPLC column (Pharmacia now GE Healthcare, Piscataway, New Jersey) and equilibrated in 10 bed volumes of wash buffer (PBS-10 mM Na_2HPO_4, 1.8 mM KH_2PO_4, 2.7 mM KCl, 140 mM NaCl, pH 7.3) using an Akta FPLC system (Pharmacia/GE Healthcare). A constant flow rate of 1 ml/min was used for all steps. Clarified cell lysate was loaded onto the column and washed with the wash buffer (~ 300 ml) till the flow through was clear. Elution of the bound protein was carried out using a gradient from the wash buffer to the elution buffer (50 mM Tris-HCl, 20 mM Glutathione, pH 7.5). 0 to 50% of elution buffer was reached in 60 min, followed by

holding at 50% elution buffer for 90 min and then at 0% elution buffer for 30 min. Samples of cell lysate before and after column loading, along with all the elution fractions (30 ml each) were collected and analyzed by SDS-PAGE. Selected fractions containing the desired protein (fractions 3-5) were concentrated to 3 ml using an Amicon Ultrafiltration stir cell (Millipore, USA). Concentrated protein was dialyzed using 12-14 kDa cut off dialysis membrane in 100 mM NaCl, 50 mM Tris-HCl, pH 7.5 for 6-8 hrs, to remove glutathione used during elution. After dialysis, 15% glycerol was added to the protein, and aliquotes were stored at –80°C.

Synthesis and purification of trimethylated peptide substrates

Peptides containing the trimethylated lysine residues at the specific sites (Table **1**) were custom synthesized (Abgent, San Diego, California). These peptides were purified using an Agilent Zorbax Eclipse XDB-C18 column (4.6 x 250 mm, 5 μm particles). Liquid chromatography (LC) used the following conditions: flow rate of 300 μL/min, with a gradient of 100% solvent A (0.1% TFA in water) for 3 min, 0% to 100% of solvent B (0.1% TFA in 30:70 water:acetonitrile) in next 5 min, then 0% to 100% of solvent C (0.095% TFA in acetonitrile) in next 7 min, then 0% to 100% of solvent A in next 1 min followed by a linear gradient of 100% A for 5 min. Trimethylated peptide peaks were collected and concentrated using a freeze dryer.

Table 1: Sequences of the custom synthesized trimethylated peptide substrates used in the study.

Protein name	Peptide name	Peptide sequence	Position
Histone	H3-K9me3	KQTARK(me3)STGGKAPRK	4-18
WIZ	WIZ-K305me3	SPPPTARK(me3)MFPGLAA	298-312
CDYL1	CDYL1-K135me3	TSPNNARK(me3)QISRSTN	128-142
CSB	CSB-K170me3	TSRDINRK(me3)LDSVKRQ	163-177
CSB	CSB-K297me3	CNKRAARK(me3)APAPVTP	290-304
CSB	CSB-K448me3	EGGGGGRK(me3)VGRYRDD	441-455
CSB	CSB-K1054me3	ADHDVPKRK(me3)KFPASN	1046-1060
G9a	G9a-K185me3	KVHRARK(me3)TMSKPGNG	179-193

A second set of peptides (Table 2) were synthesized in house using an Apex 396 peptide synthesizer (AAPPTec, Louisville, KY). Synthesis was performed with Wang resin at 75 mg scale using the standard Fmoc chemistry. Amino acid loaded resin was swelled in dimethylformamide (DMF) for 10 mins with shaking. The transient protecting groups were removed with 20% piperidine in DMF. The resin was washed with DMF to remove any residual piperidine, followed by activation with HCTU and DIEA for coupling of the next amino acid. This cycle was repeated 14 times, and finally, the peptides were cleaved off the resin using 88% TFA v/v, 5% water v/v, 2% triisopropylsilane v/v and 5% phenol w/v. Cleaved peptides were precipitated in cold ether and centrifuged. The pellet was air dried overnight and resuspended in either

water or water/acetonitrile mixture. Diluted samples were infused into mass spectrometer to confirm the synthesis of the desired peptides.

Purification of these peptides was carried out on Shimazdu preparative HPLC system using Beckman ODS semi preparative column (10 mm X 150 mm, 5 μm particles). Liquid chromatography (LC) used the following conditions: flow rate of 2000 μL/min, with a gradient of 100% solvent A (0.1% TFA in water) for 5 min, 0% to 70% of solvent B (0.095% TFA in acetonitrile) in next 15 min, then 70% to 100% of solvent B in next 3 min, then 0% to 100% of solvent A and 0% of solvent B in next 2 min, followed by a linear gradient of 100% A for 5 min. Multiple fractions were collected during the purification chromatography. All the fractions were analyzed on mass spectrometer by infusion. Fractions containing the desired peptide were pooled and concentrated by freeze drying, and was resuspended in 200 μl of millipore water.

Table 2: Sequences of trimethylated peptide substrates synthesized in the lab.

Protein name	Peptide name	Peptide sequence	Position
Histone	H3-K9me3	KQTARKSTGGKAPRK	4-18
WIZ	WIZ-K305me3	SPPPTARKMFPGLAA	298-312
WIZ	WIZ-R304A-K305me3	SPPPTAAKMFPGLAA	298-312
WIZ	WIZ-A303W-K305me3	SPPPTWRKMFPGLAA	298-312
G9a	G9a-K185me3	KVHRARKTMSKPGNG	179-193
G9a	G9a-R184A-K185me3	KVHRAAKTMSKPGNG	179-193
G9a	G9a-A183W-K185me3	KVHRWRKTMSKPGNG	179-193
G9a	G9a- R184A -A183W-K185me3	KVHRWAKTMSKPGNG	179-193
DNMT1	Dnmt1-K70me3	DLETKLRKEELSEEG	63-77
KLF 12	KLF12-K313me3	SESPDSRKRRIHRCDF	305-321
ACINUS	ACINUS-K654me3	RSASSNSRKSLSPGV	646-660
HDAC	HDAC1-K432me3	EEGEGGRKNSSNFKKA	425-440

Purity of the peptides was confirmed using LCMS analysis. LCMS analysis was carried out on an ABI 2000 Q-Trap mass spectrometer fitted with electro-spray ionization (ESI) source and interfaced to an Agilent 1100 series HPLC system equipped with a diode array detector. LCMS was performed using an Agilent Zorbax Eclipse XDB-C18 column (2.1 x 150 mm, 3.5 μm particles) with the conditions described

above (TFA was replaced with formic acid for LCMS). Detection of ions by the mass spectrometer was performed in Q1 positive multiple ion mode. Source temperature was set at 300 ºC and ion spray voltage at 5500 V. The declustering potential (DP) and entrance potential (EP) were set at 70 and 9, respectively.

Demethylation assay:

All assays were performed in duplicate in 50 µl reaction volume with final concentrations of 500 µM $FeSO_4$, 4 mM 2-oxoglutarate, 10 mM ascorbate, 50 mM Tris-HCl, pH 7.5, and 22.5 µg of purified enzyme. 50 nmoles of trimethylated peptide substrates were used in the assay. The reactions were carried out at 22 °C for 4 hrs and stopped by adding 50 µl of 0.25 M EDTA. Half of the assay reaction (50 µl) was loaded on an Agilent Zorbax Eclipse XDB-C18 column (2.1 x 150 mm, 3.5 µm particles) and analyzed by a Shimadzu 2010C HPLC system, while of the remaining sample 40 µl was analyzed by the LCMS method described earlier. The specific activities (nmole/min/mg) of the enzymes were determined by the disappearance of substrates. This was done by converting % reduction in the substrate peak area into nmole using 22.5 µg of enzyme for 240 min.

Results

Cloning, expression and purification of JMJD2A-C

Truncated human JMJD2A-C (tJMJD2A-C) consisting of the N-terminal catalytic cores (1-349 amino acids) were PCR amplified using the primers described in the methods section (Figure 9).

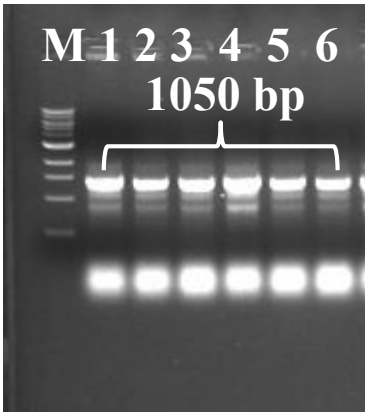

Figure 9: PCR amplification of truncated JMJD2A-C (1-349 amino acids). M – 1 Kb ladder, Lanes 1-2 JMJD2A, 3-4 JMJD2B and 5-6 JMJD2C.

The amplified product was subsequently cloned into pGEMT vector and verified by restriction digest and sequencing (Figure 10A). Verified gene fragments were transferred into pGEX4T-1 vector as described in methods section and confirmed by restriction digest (Figure 10B, 10C, and 10D). The target genes were expressed as GST-fusion proteins in *E. coli*. All three isoforms were produced at ~10% of the total soluble protein by SDS-PAGE analysis (Figure 11). The fusion proteins were purified (>90% purity) using GST affinity chromatography. The total size of the GST-tagged JMJD2A-C was found to be 67.3 kDa.

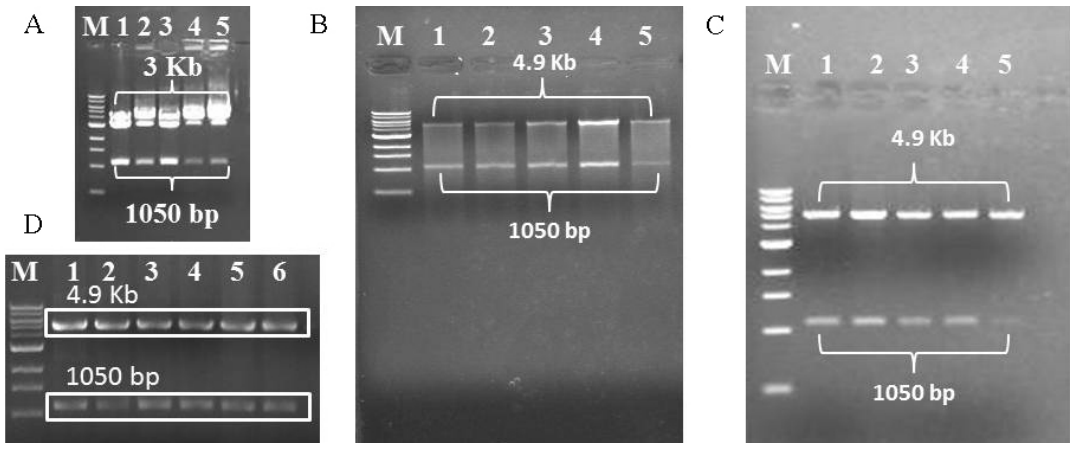

Figure 10: (A) Double digest of pGEMT-JMJD2A (Lanes 1-2) and pGEMT-JMJD2C (Lanes 4-5) clones with BamHI and NotI and pGEMt-JMJD2B (Lane 3) with SalI and NotI releasing 1050 bp insert. (B) Double digest of pGEX-4T1-JMJD2A with BamHI and NotI releasing 1050 bp JMJD2A insert. (C) Double digest of pGEX-4T1-JMJD2C with BamHI and NotI releasing 1050 bp JMJD2C insert. (D) Double digest of pGEX-4T1-JMJD2B with SalI and NotI releasing 1050 bp JMJD2B insert. M stands for 1 Kb ladder in all the panels.

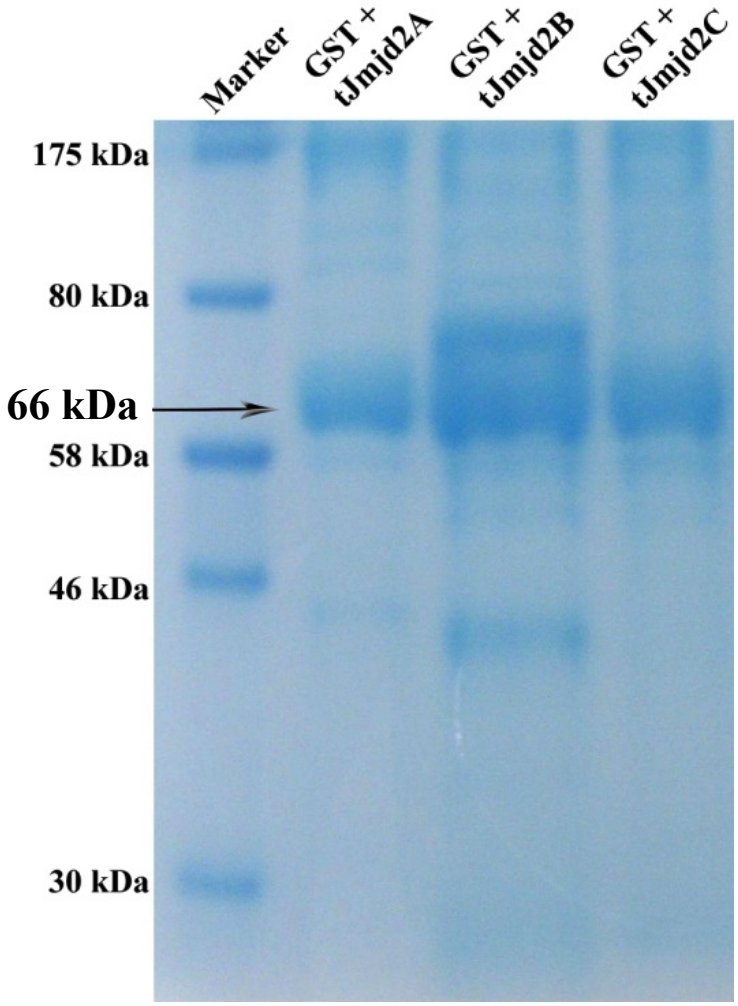

Figure 11: SDS-PAGE analysis of purified GST-tJMJD2A-C proteins. The total size of the GST-tagged proteins is 67.3 kDa as indicated by the arrow.

Peptide Synthesis and Purification

Nine 15-mer peptides were synthesized at 75 mg scale using an Apex 396 peptide synthesizer and purified as described in materials and method section. All the peptides synthesized were solubilized in either water or water/acetonitrile mixture. The peptide samples were loaded onto a preparative HPLC column as described in methods section and all fractions observed in the chromatogram were collected and analyzed by infusing into a mass spectrometer. Peaks corresponding to the desired peptides are identified in the individual chromatograms (Figure 12A-I). Purity of all the peptides was assessed to be ≥98% by LCMS analysis using an Agilent Zorbax Eclipse XDB-C18 column (2.1 x 150 mm, 3.5 μm particles). In the purified peptides no peaks corresponding to di or monomethylated impurities were detected by LCMS analysis (Figure 13).

Figure 12: Liquid chromatography profiles of synthesized non-histone peptides: A) Dnmt1-K70me3, B) KLF12-K313me3, C) ACINUS-K654me3, D) HDAC1-K432me3, E) G9a-R184A-K185me3, F) WIZ-R304A-K305me3, G) G9a-R184A-A183W-K185me3, H) WIZ-A303W-K305me3 and I) G9a-A183W-K185me3.

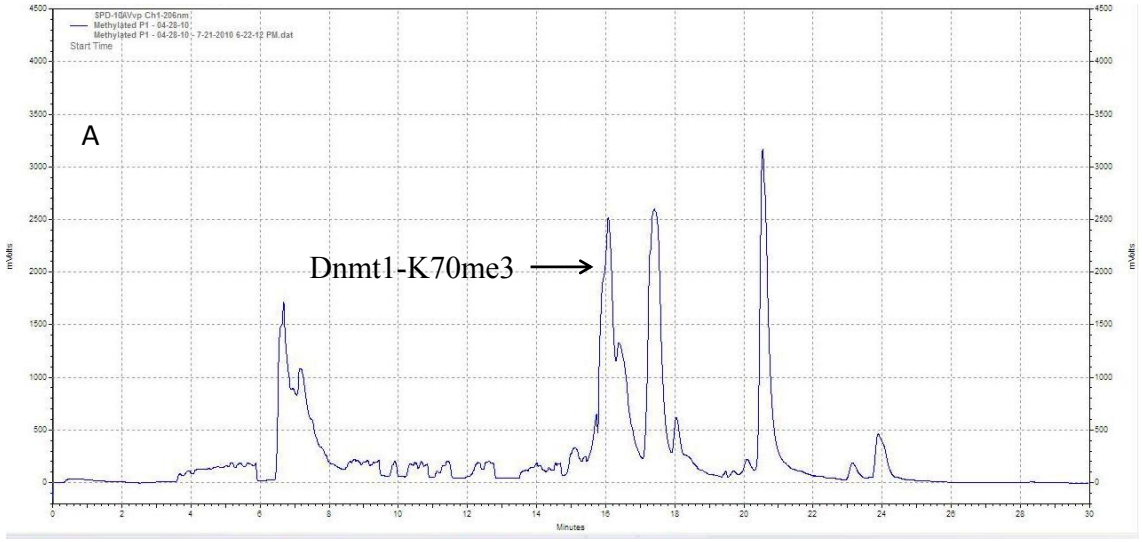
A
Dnmt1-K70me3
mVolts
Minutes

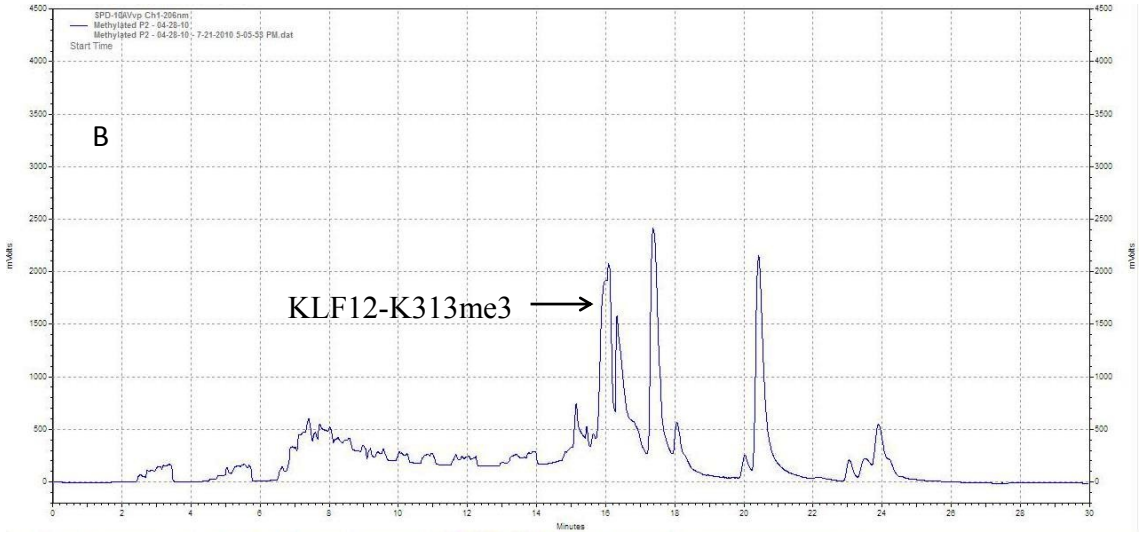
B
KLF12-K313me3
mVolts
Minutes

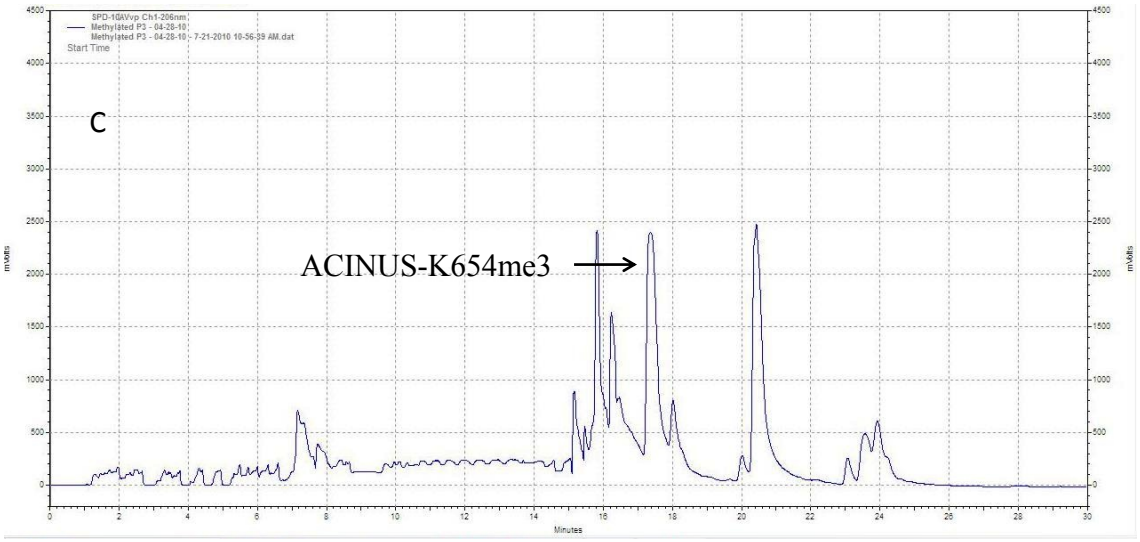
C
ACINUS-K654me3
mVolts
Minutes

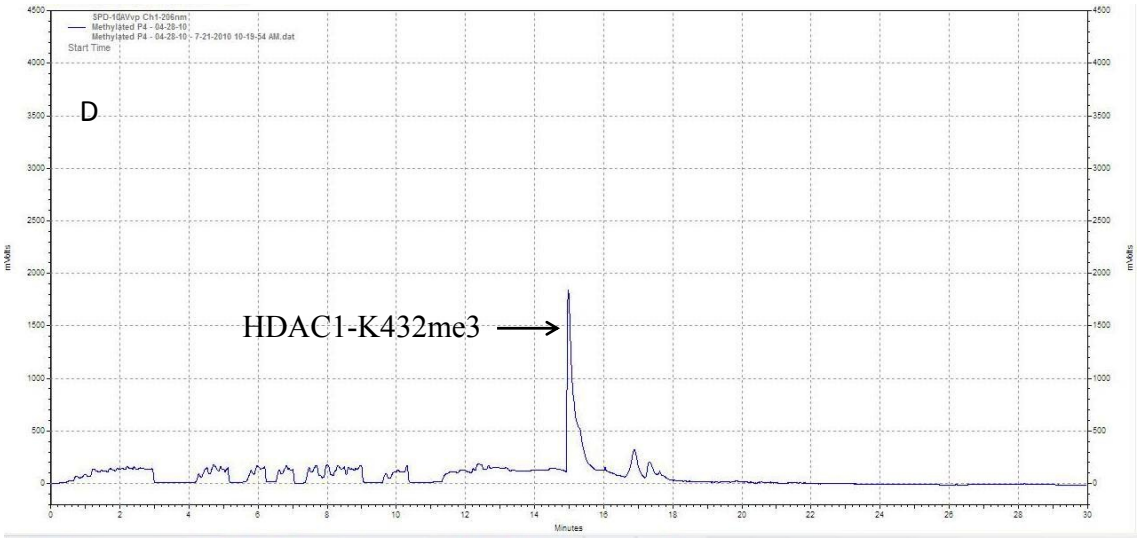
D
HDAC1-K432me3
mVolts
Minutes

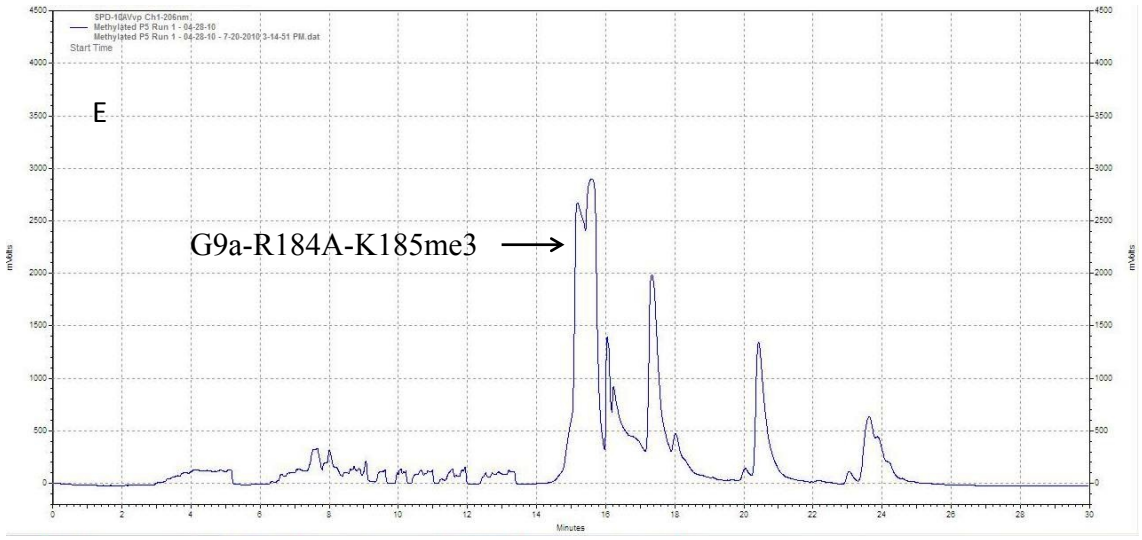
SPD-10AVvp Ch1-206nm:
Methylated P5 Run 1 - 04-28-10
Methylated P5 Run 1 - 04-28-10 - 7-20-2010 3-14-51 PM.dat
Start Time
E
G9a-R184A-K185me3
mVolts
Minutes

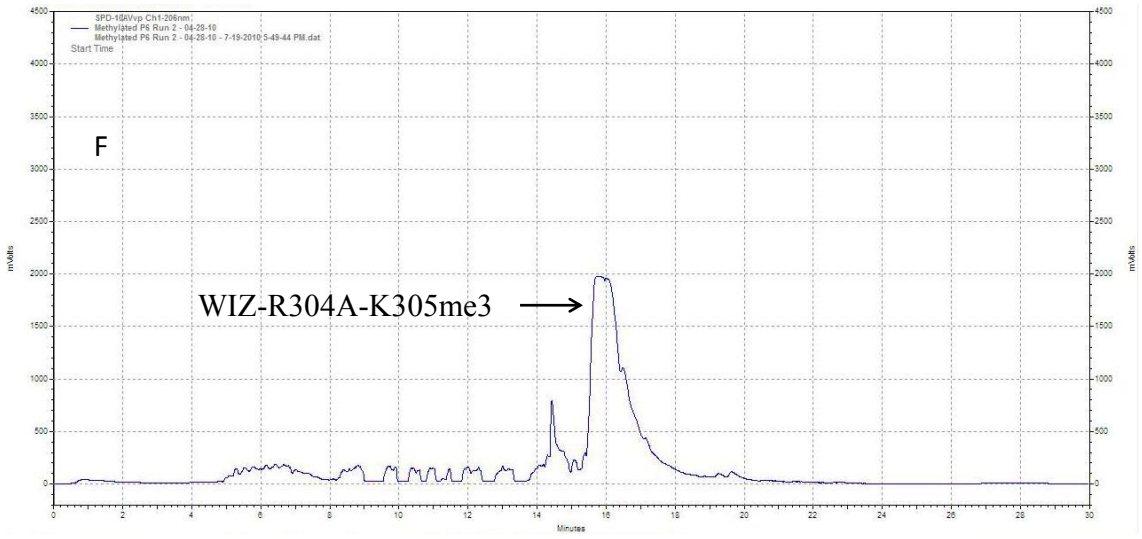
SPD-10AVvp Ch1-206nm:
Methylated P6 Run 2 - 04-28-10
Methylated P6 Run 2 - 04-28-10 - 7-19-2010 5-49-44 PM.dat
Start Time
F
WIZ-R304A-K305me3
mVolts
Minutes

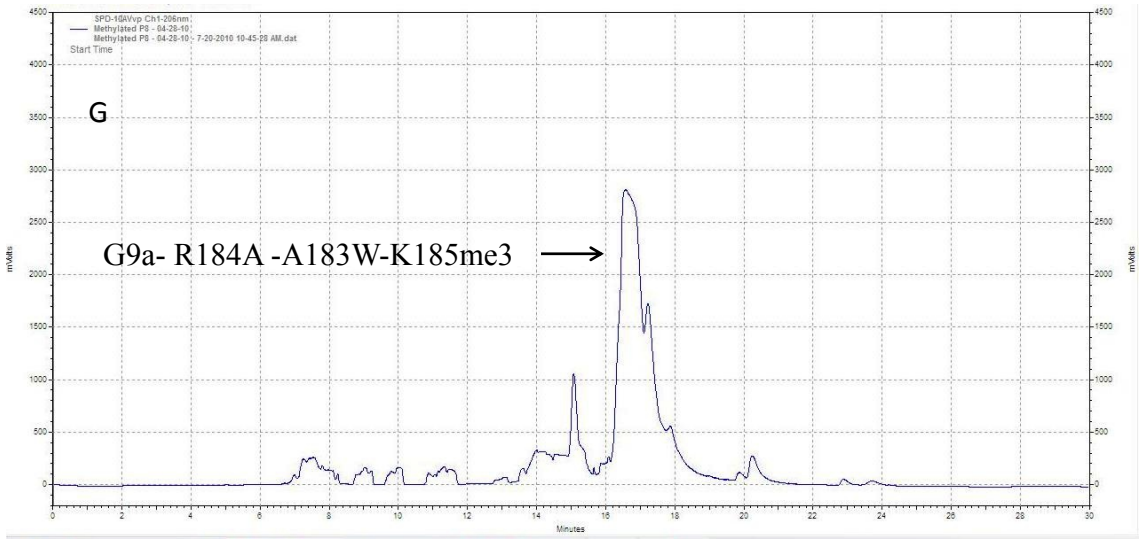
G
G9a- R184A -A183W-K185me3
mVolts
Minutes

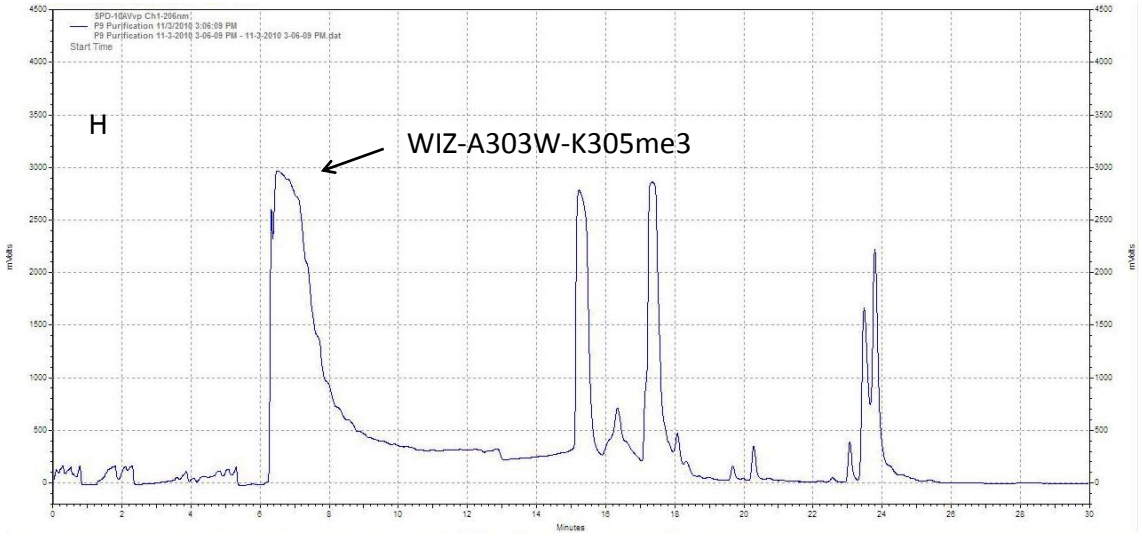
H
WIZ-A303W-K305me3
mVolts
Minutes

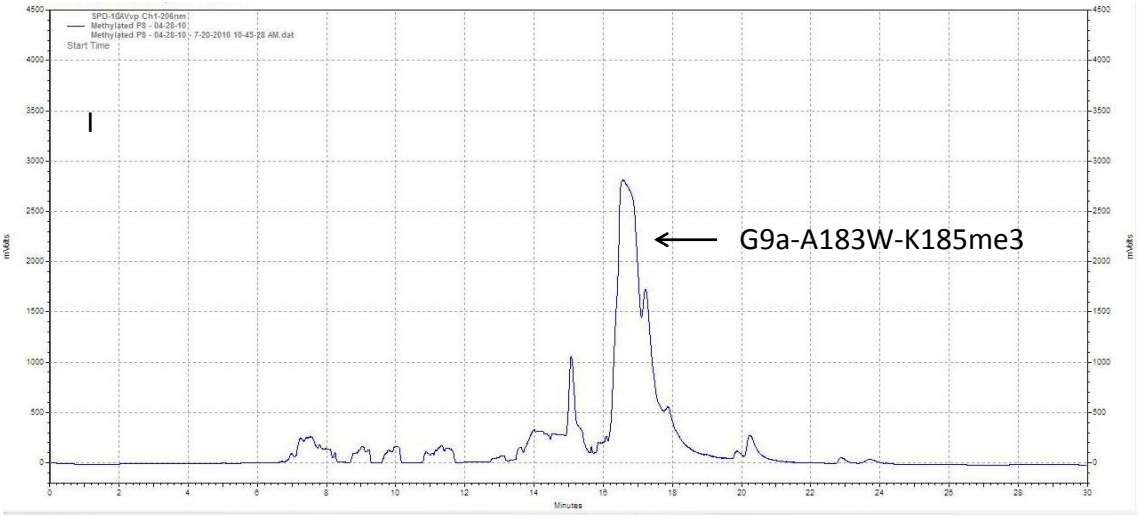

Figure 13: LC-MS analysis of all the peptides used in the study: A) H3-K9me3, B) WIZ-K305me3, C) CDYL1-K135me3, D) CSB-K170me3, E) CSB-K297me3, F) CSB-K448me3, G) CSB-K1054me3, H) G9a-K185me3, I) Dnmt1-K70me3, J) KLF12-K313me3, K) ACINUS-K654me3, L) HDAC1-K432me3, M) G9a-R184A-K185me3, N) WIZ-R304A-K305me3, O) G9a-R184A-A183W-K185me3, and P) WIZ-A303W-K305me3.

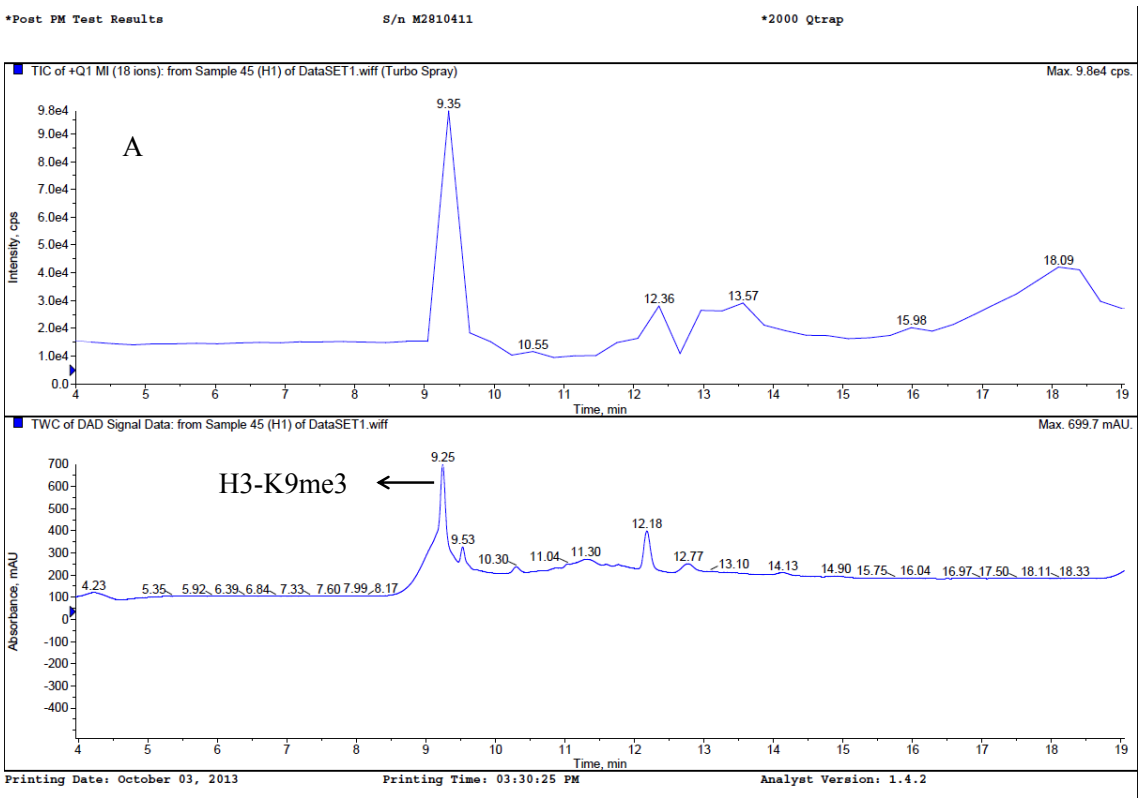
*Post PM Test Results
S/n M2810411
*2000 Qtrap
TIC of +Q1 MI (18 ions): from Sample 45 (H1) of DataSET1.wiff (Turbo Spray)
Max. 9.8e4 cps.
A
Intensity, cps
Time, min
9.35
10.55
12.36
13.57
15.98
18.09
TWC of DAD Signal Data: from Sample 45 (H1) of DataSET1.wiff
Max. 699.7 mAU.
H3-K9me3
Absorbance, mAU
9.25
9.53
10.30
11.04
11.30
12.18
12.77
13.10
14.13
14.90
15.75
16.04
16.97
17.50
18.11
18.33
4.23
5.35
5.92
6.39
6.84
7.33
7.60
7.99
8.17
Printing Date: October 03, 2013
Printing Time: 03:30:25 PM
Analyst Version: 1.4.2

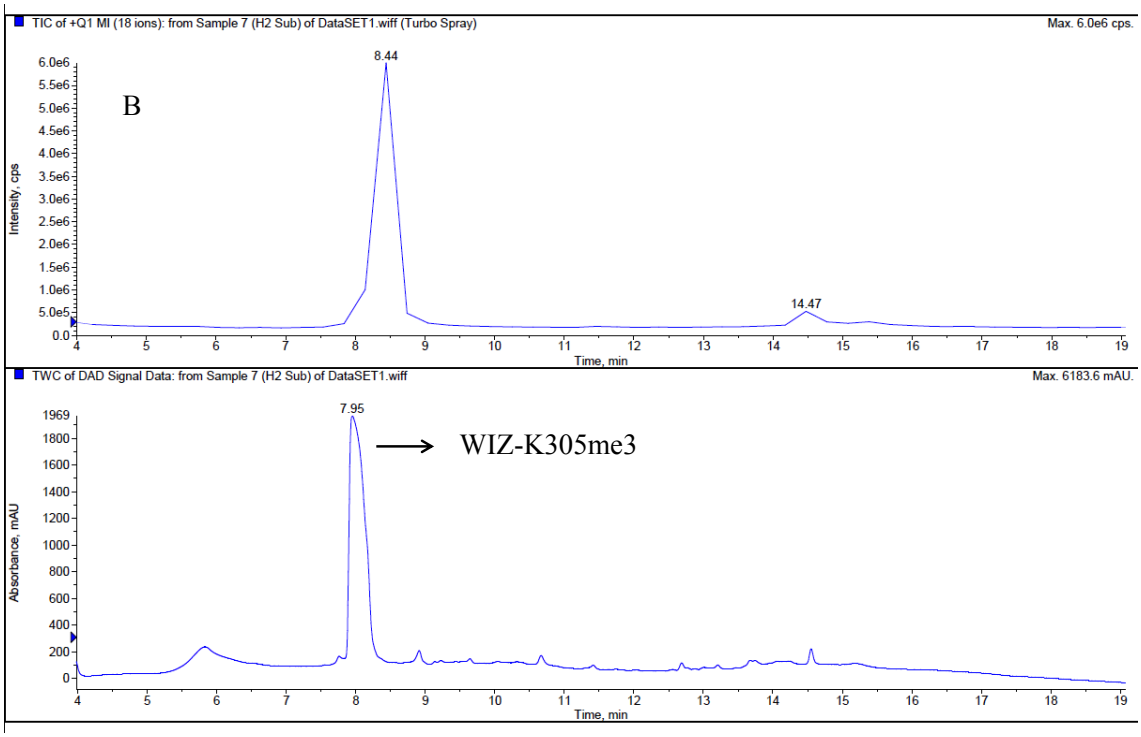
TIC of +Q1 MI (18 ions): from Sample 7 (H2 Sub) of DataSET1.wiff (Turbo Spray)
Max. 6.0e6 cps.
B
Intensity, cps
Time, min
8.44
14.47
TWC of DAD Signal Data: from Sample 7 (H2 Sub) of DataSET1.wiff
Max. 6183.6 mAU.
WIZ-K305me3
Absorbance, mAU
7.95

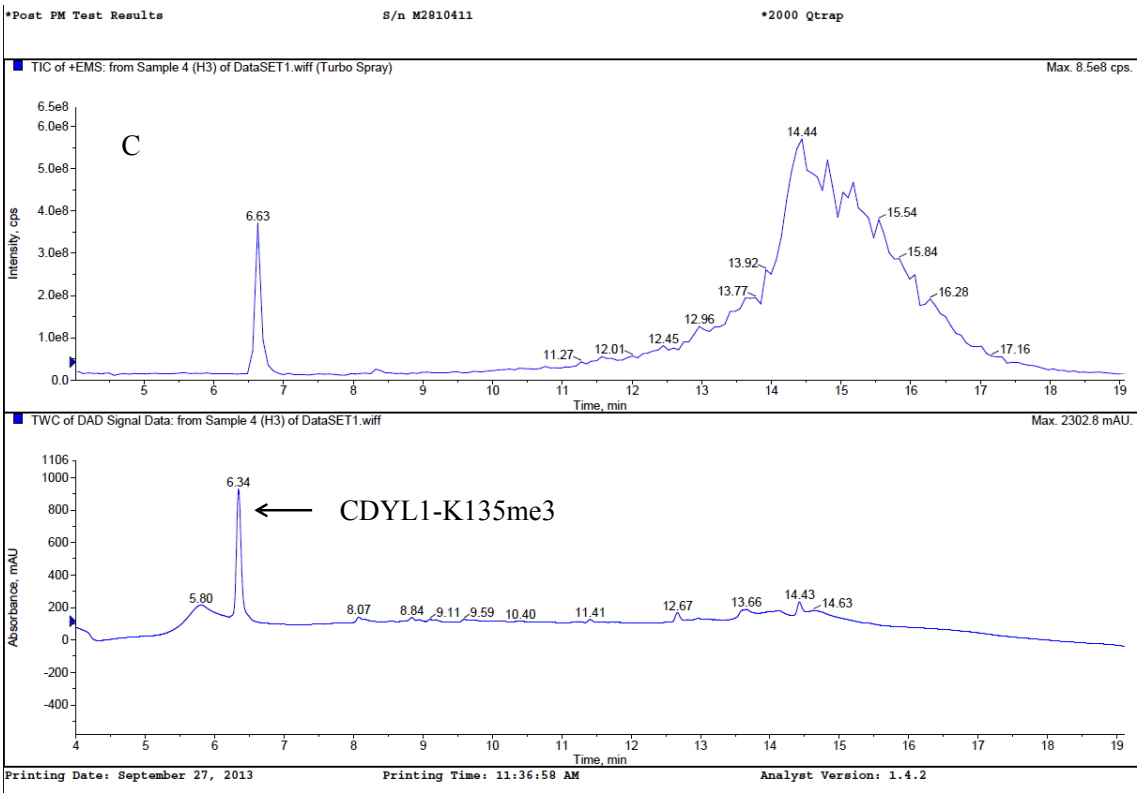
*Post PM Test Results
S/n M2810411
*2000 Qtrap
TIC of +EMS: from Sample 4 (H3) of DataSET1.wiff (Turbo Spray)
Max. 8.5e8 cps.
C
Intensity, cps
Time, min
TWC of DAD Signal Data: from Sample 4 (H3) of DataSET1.wiff
Max. 2302.8 mAU.
CDYL1-K135me3
Absorbance, mAU
Time, min
Printing Date: September 27, 2013
Printing Time: 11:36:58 AM
Analyst Version: 1.4.2

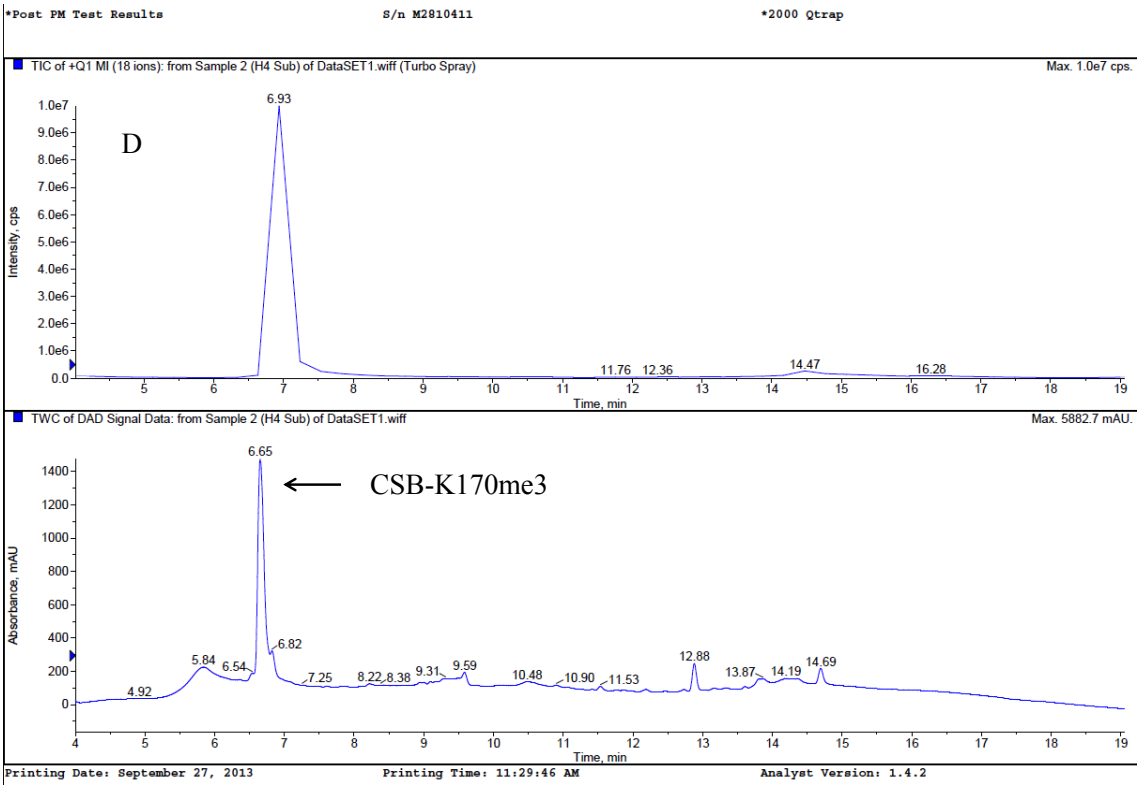
*Post PM Test Results
S/n M2810411
*2000 Qtrap
TIC of +Q1 MI (18 ions): from Sample 2 (H4 Sub) of DataSET1.wiff (Turbo Spray)
Max. 1.0e7 cps.
D
Intensity, cps
Time, min
TWC of DAD Signal Data: from Sample 2 (H4 Sub) of DataSET1.wiff
Max. 5882.7 mAU.
CSB-K170me3
Absorbance, mAU
Time, min
Printing Date: September 27, 2013
Printing Time: 11:29:46 AM
Analyst Version: 1.4.2

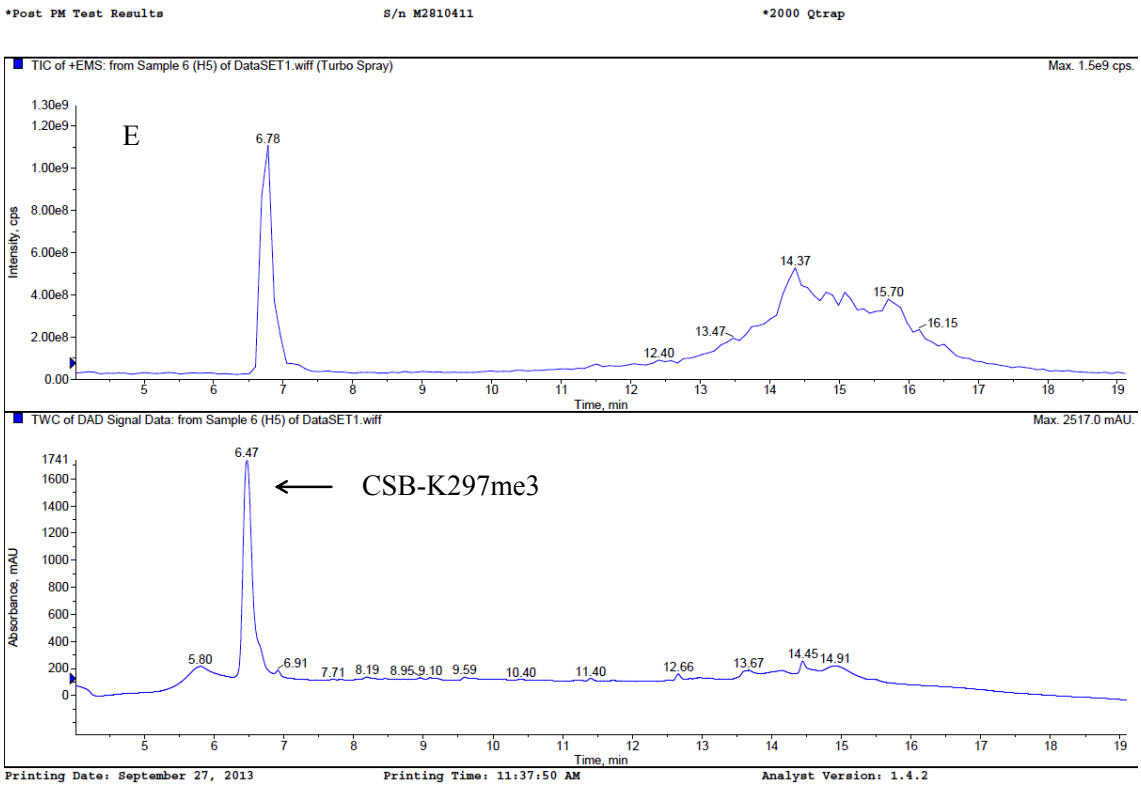
*Post PM Test Results
S/n M2810411
*2000 Qtrap
TIC of +EMS: from Sample 6 (H5) of DataSET1.wiff (Turbo Spray)
Max. 1.5e9 cps.
E
6.78
14.37
15.70
16.15
13.47
12.40
Intensity, cps
Time, min
TWC of DAD Signal Data: from Sample 6 (H5) of DataSET1.wiff
Max. 2517.0 mAU.
6.47
CSB-K297me3
5.80
6.91
7.71
8.19
8.95
9.10
9.59
10.40
11.40
12.66
13.67
14.45
14.91
Absorbance, mAU
Time, min
Printing Date: September 27, 2013
Printing Time: 11:37:50 AM
Analyst Version: 1.4.2

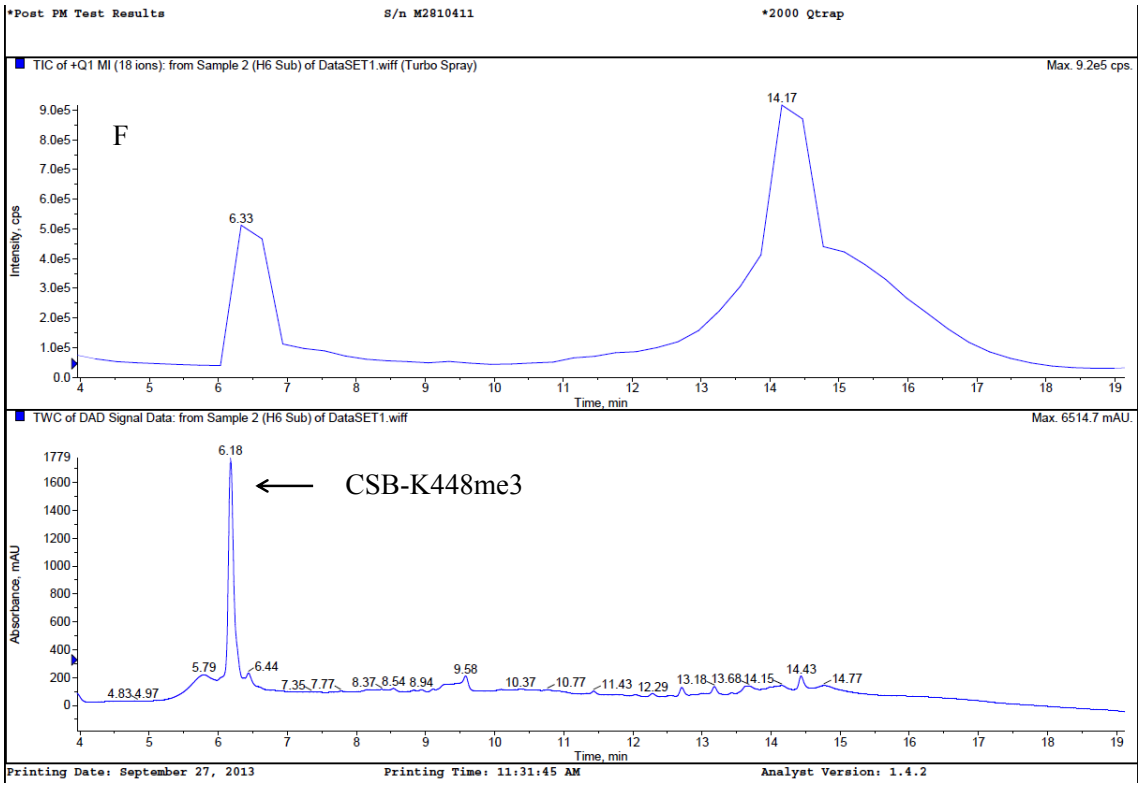
*Post PM Test Results
S/n M2810411
*2000 Qtrap
TIC of +Q1 MI (18 ions): from Sample 2 (H6 Sub) of DataSET1.wiff (Turbo Spray)
Max. 9.2e5 cps.
F
14.17
6.33
Intensity, cps
Time, min
TWC of DAD Signal Data: from Sample 2 (H6 Sub) of DataSET1.wiff
Max. 6514.7 mAU.
6.18
CSB-K448me3
5.79
6.44
9.58
14.43
14.77
4.83
4.97
7.35
7.77
8.37
8.54
8.94
10.37
10.77
11.43
12.29
13.18
13.68
14.15
Absorbance, mAU
Time, min
Printing Date: September 27, 2013
Printing Time: 11:31:45 AM
Analyst Version: 1.4.2

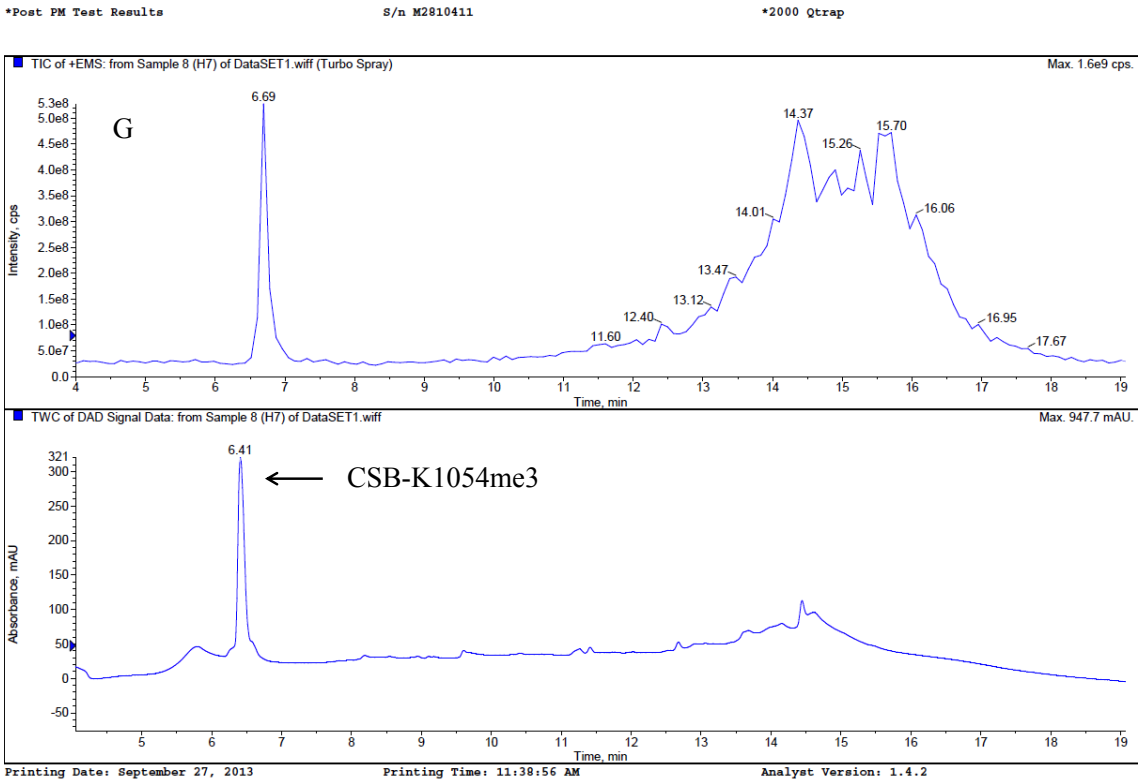
*Post PM Test Results
S/n M2810411
*2000 Qtrap
TIC of +EMS: from Sample 8 (H7) of DataSET1.wiff (Turbo Spray)
Max. 1.6e9 cps.
G
Intensity, cps
Time, min
6.69
11.60
12.40
13.12
13.47
14.01
14.37
15.26
15.70
16.06
16.95
17.67
TWC of DAD Signal Data: from Sample 8 (H7) of DataSET1.wiff
Max. 947.7 mAU.
Absorbance, mAU
6.41
CSB-K1054me3
Printing Date: September 27, 2013
Printing Time: 11:38:56 AM
Analyst Version: 1.4.2

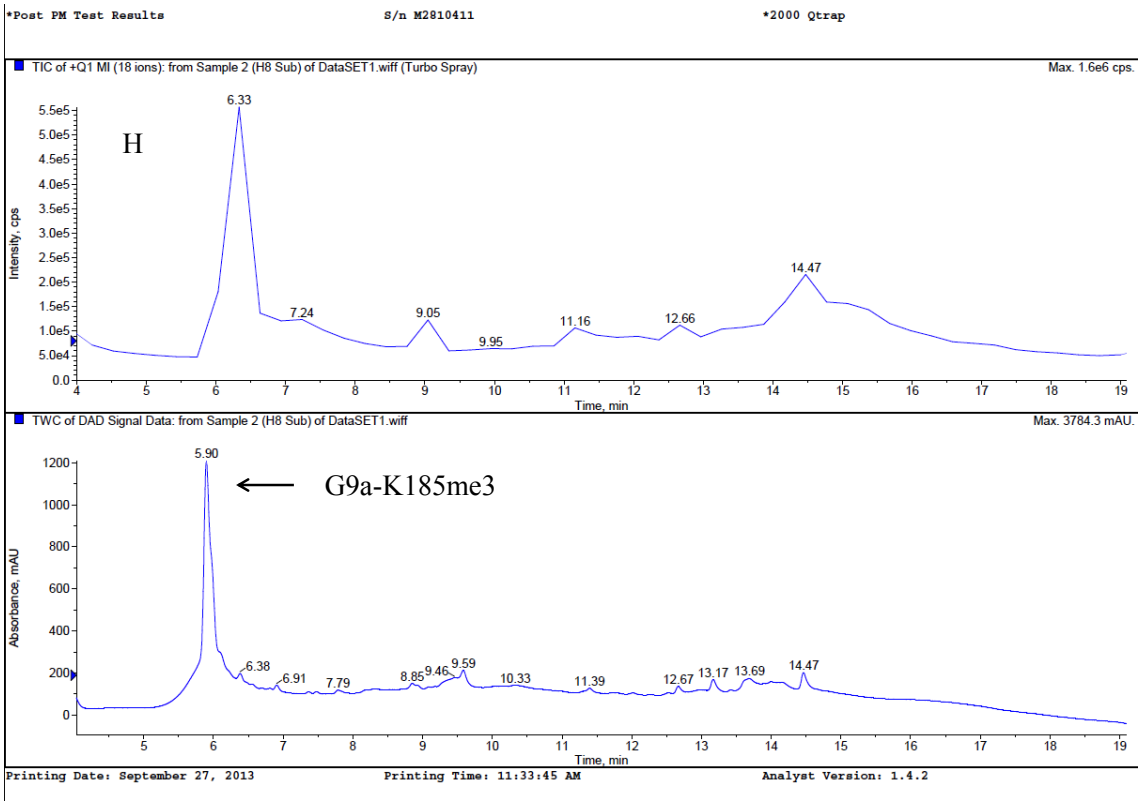
*Post PM Test Results
S/n M2810411
*2000 Qtrap
TIC of +Q1 MI (18 ions): from Sample 2 (H8 Sub) of DataSET1.wiff (Turbo Spray)
Max. 1.6e6 cps.
H
Intensity, cps
Time, min
6.33
7.24
9.05
9.95
11.16
12.66
14.47
TWC of DAD Signal Data: from Sample 2 (H8 Sub) of DataSET1.wiff
Max. 3784.3 mAU.
Absorbance, mAU
5.90
G9a-K185me3
6.38
6.91
7.79
8.85
9.46
9.59
10.33
11.39
12.67
13.17
13.69
14.47
Printing Date: September 27, 2013
Printing Time: 11:33:45 AM
Analyst Version: 1.4.2

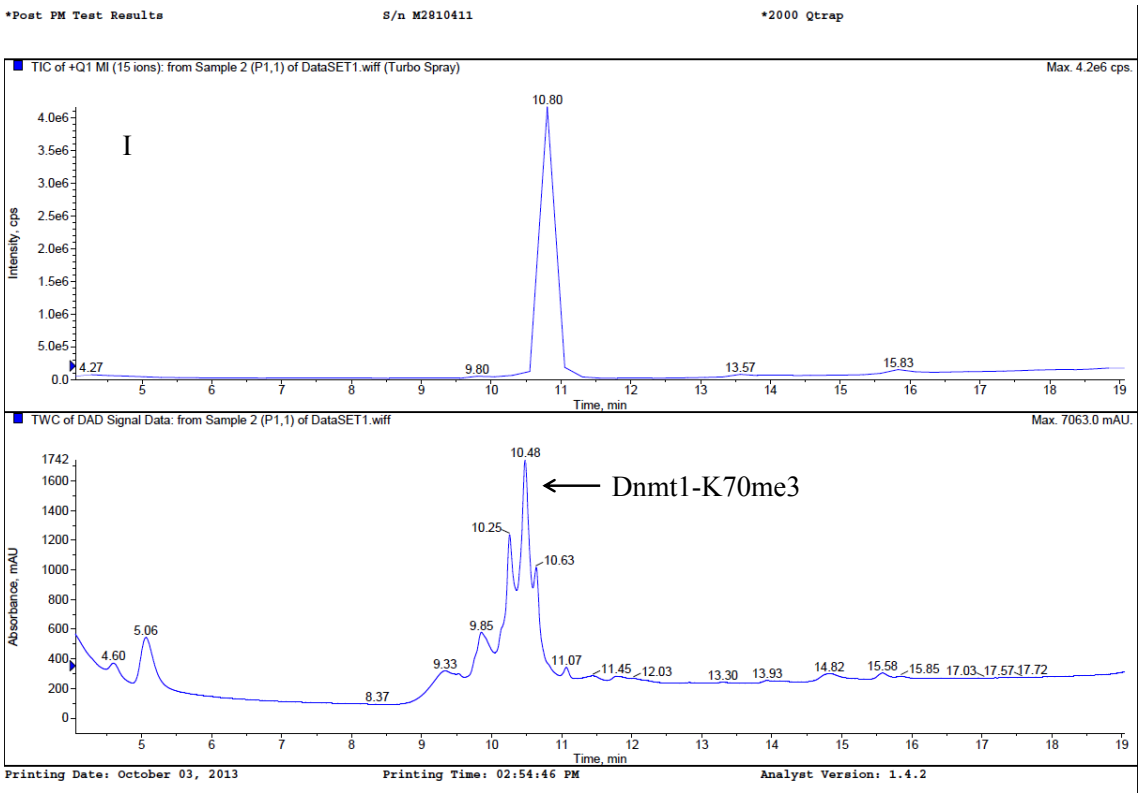
*Post PM Test Results
S/n M2810411
*2000 Qtrap
TIC of +Q1 MI (15 ions): from Sample 2 (P1,1) of DataSET1.wiff (Turbo Spray)
Max. 4.2e6 cps.
I
Intensity, cps
Time, min
4.27
9.80
10.80
13.57
15.83
TWC of DAD Signal Data: from Sample 2 (P1,1) of DataSET1.wiff
Max. 7063.0 mAU.
Absorbance, mAU
Dnmt1-K70me3
4.60
5.06
8.37
9.33
9.85
10.25
10.48
10.63
11.07
11.45
12.03
13.30
13.93
14.82
15.58
15.85
17.03
17.57
17.72
Printing Date: October 03, 2013
Printing Time: 02:54:46 PM
Analyst Version: 1.4.2

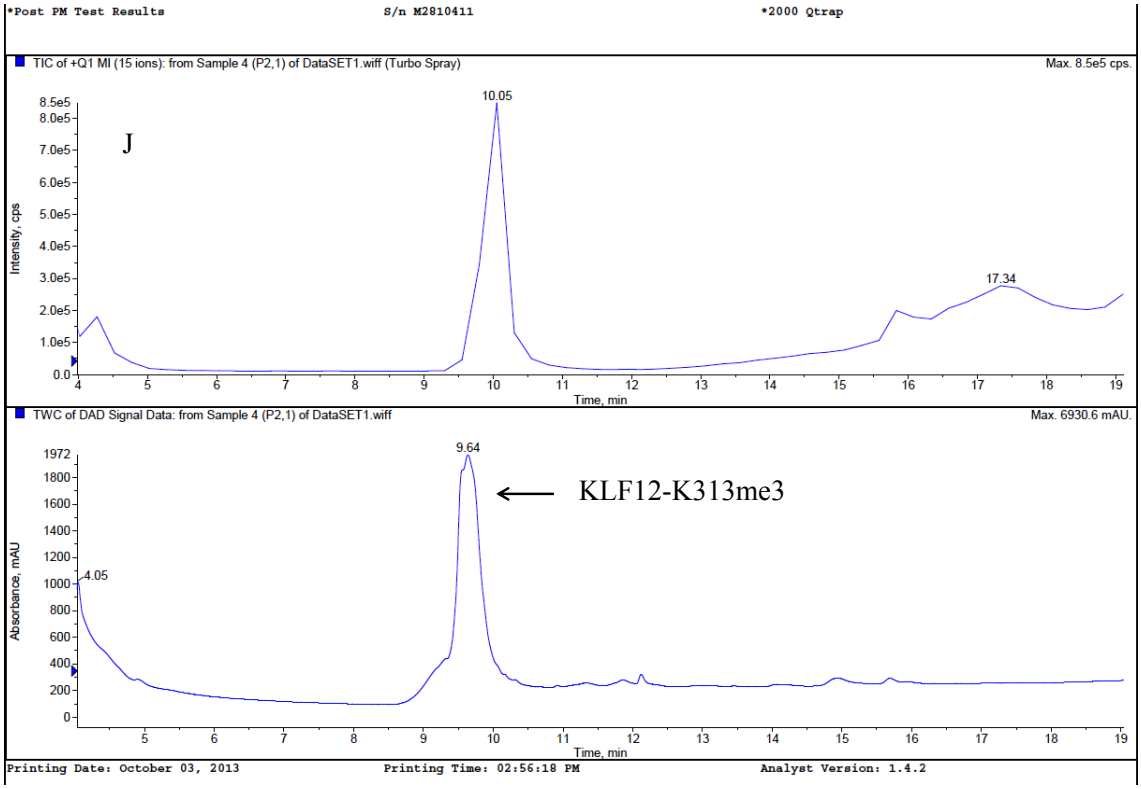
*Post PM Test Results
S/n M2810411
*2000 Qtrap
TIC of +Q1 MI (15 ions): from Sample 4 (P2,1) of DataSET1.wiff (Turbo Spray)
Max. 8.5e5 cps.
J
Intensity, cps
Time, min
10.05
17.34
TWC of DAD Signal Data: from Sample 4 (P2,1) of DataSET1.wiff
Max. 6930.6 mAU.
Absorbance, mAU
KLF12-K313me3
4.05
9.64
Printing Date: October 03, 2013
Printing Time: 02:56:18 PM
Analyst Version: 1.4.2

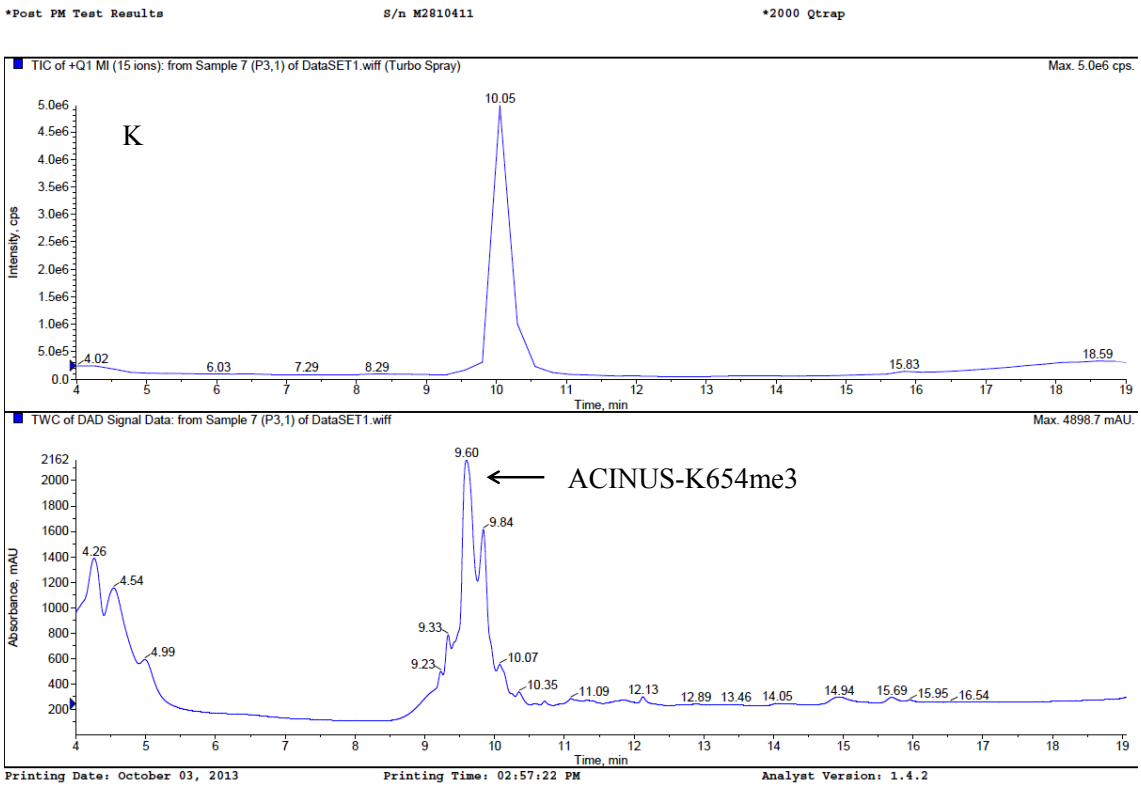
*Post PM Test Results
S/n M2810411
*2000 Qtrap
TIC of +Q1 MI (15 ions): from Sample 7 (P3,1) of DataSET1.wiff (Turbo Spray)
Max. 5.0e6 cps.
K
Intensity, cps
Time, min
TWC of DAD Signal Data: from Sample 7 (P3,1) of DataSET1.wiff
Max. 4898.7 mAU.
ACINUS-K654me3
Absorbance, mAU
Time, min
Printing Date: October 03, 2013
Printing Time: 02:57:22 PM
Analyst Version: 1.4.2

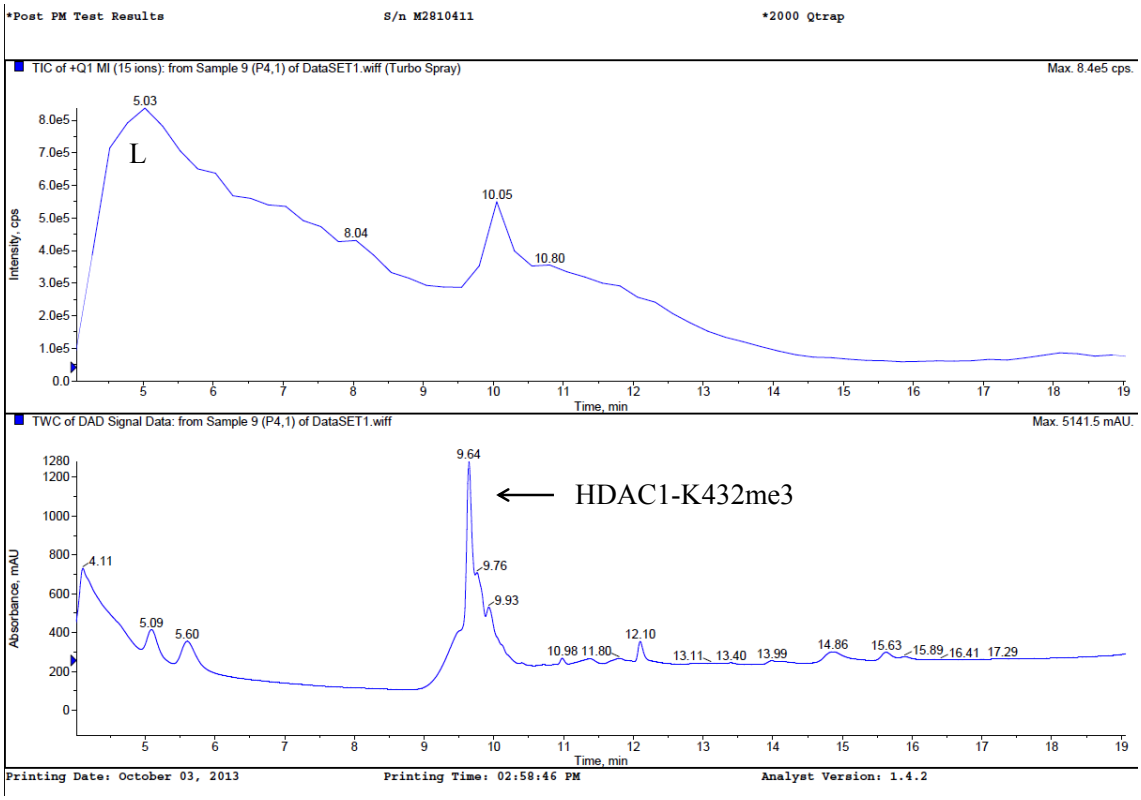
*Post PM Test Results
S/n M2810411
*2000 Qtrap
TIC of +Q1 MI (15 ions): from Sample 9 (P4,1) of DataSET1.wiff (Turbo Spray)
Max. 8.4e5 cps.
L
Intensity, cps
Time, min
TWC of DAD Signal Data: from Sample 9 (P4,1) of DataSET1.wiff
Max. 5141.5 mAU.
HDAC1-K432me3
Absorbance, mAU
Time, min
Printing Date: October 03, 2013
Printing Time: 02:58:46 PM
Analyst Version: 1.4.2

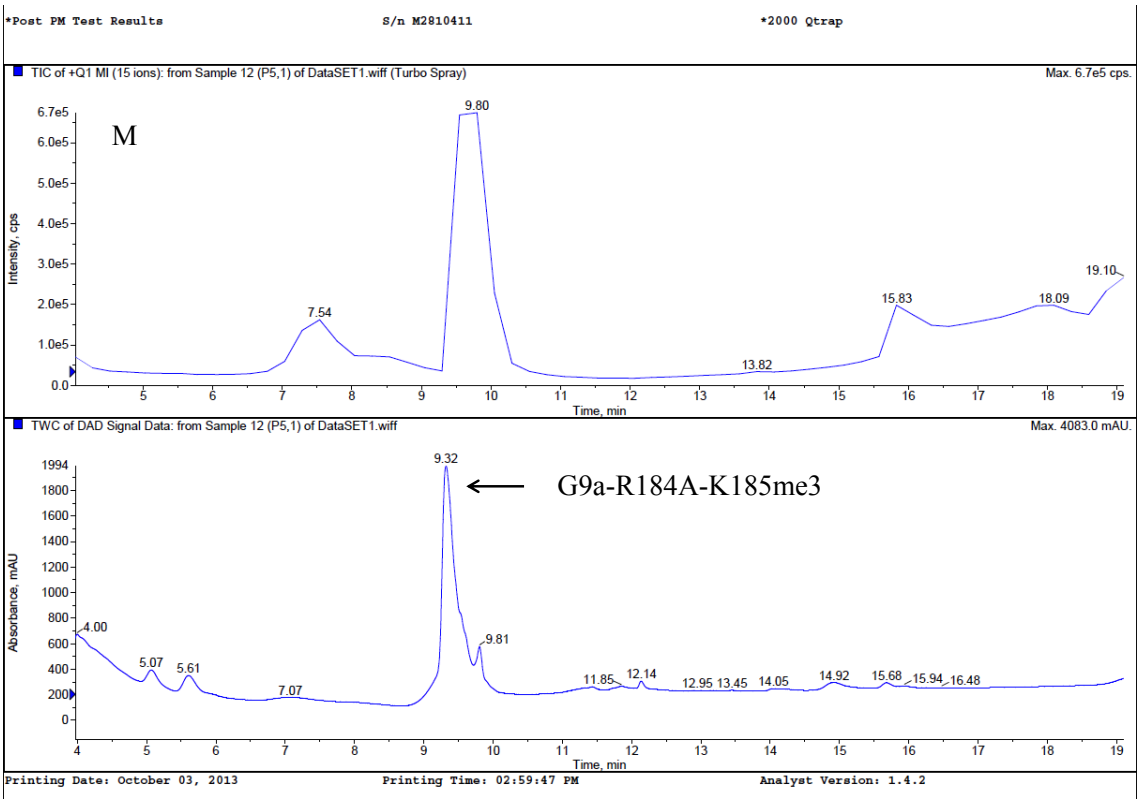
*Post PM Test Results
S/n M2810411
*2000 Qtrap
TIC of +Q1 MI (15 ions): from Sample 12 (P5,1) of DataSET1.wiff (Turbo Spray)
Max. 6.7e5 cps.
M
Intensity, cps
Time, min
TWC of DAD Signal Data: from Sample 12 (P5,1) of DataSET1.wiff
Max. 4083.0 mAU.
G9a-R184A-K185me3
Absorbance, mAU
Printing Date: October 03, 2013
Printing Time: 02:59:47 PM
Analyst Version: 1.4.2

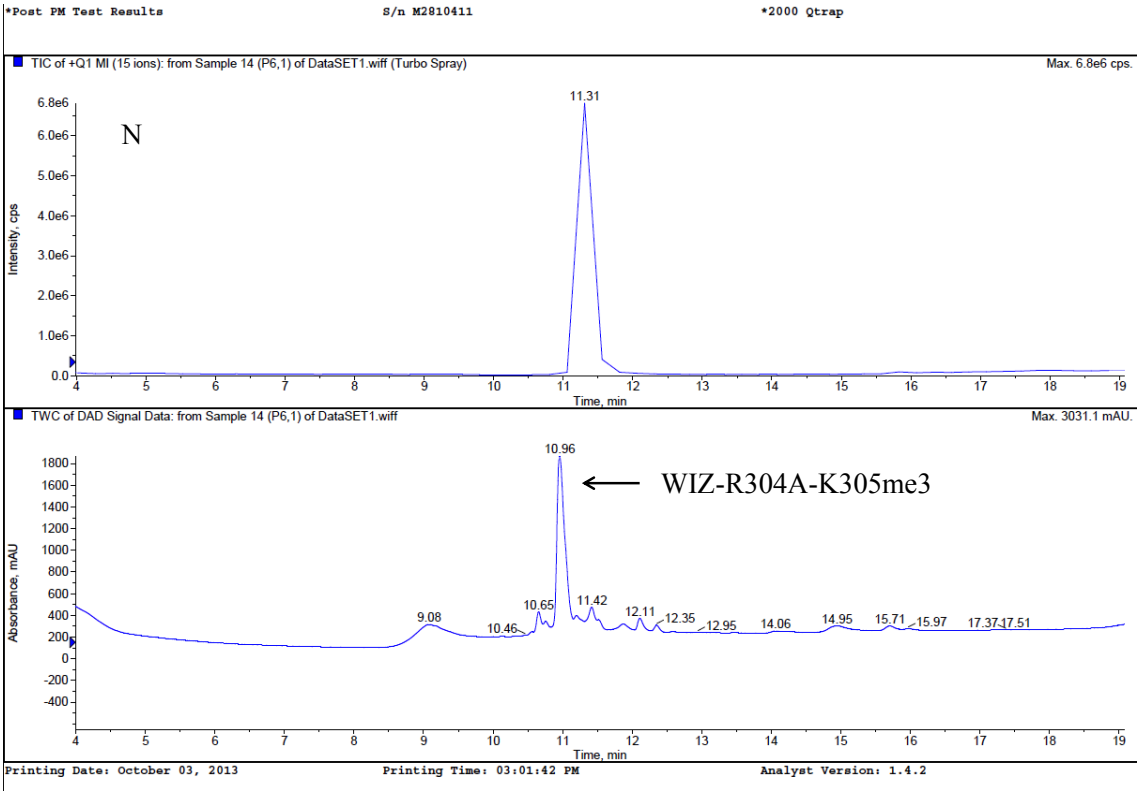
*Post PM Test Results
S/n M2810411
*2000 Qtrap
TIC of +Q1 MI (15 ions): from Sample 14 (P6,1) of DataSET1.wiff (Turbo Spray)
Max. 6.8e6 cps.
N
Intensity, cps
Time, min
TWC of DAD Signal Data: from Sample 14 (P6,1) of DataSET1.wiff
Max. 3031.1 mAU.
WIZ-R304A-K305me3
Absorbance, mAU
Printing Date: October 03, 2013
Printing Time: 03:01:42 PM
Analyst Version: 1.4.2

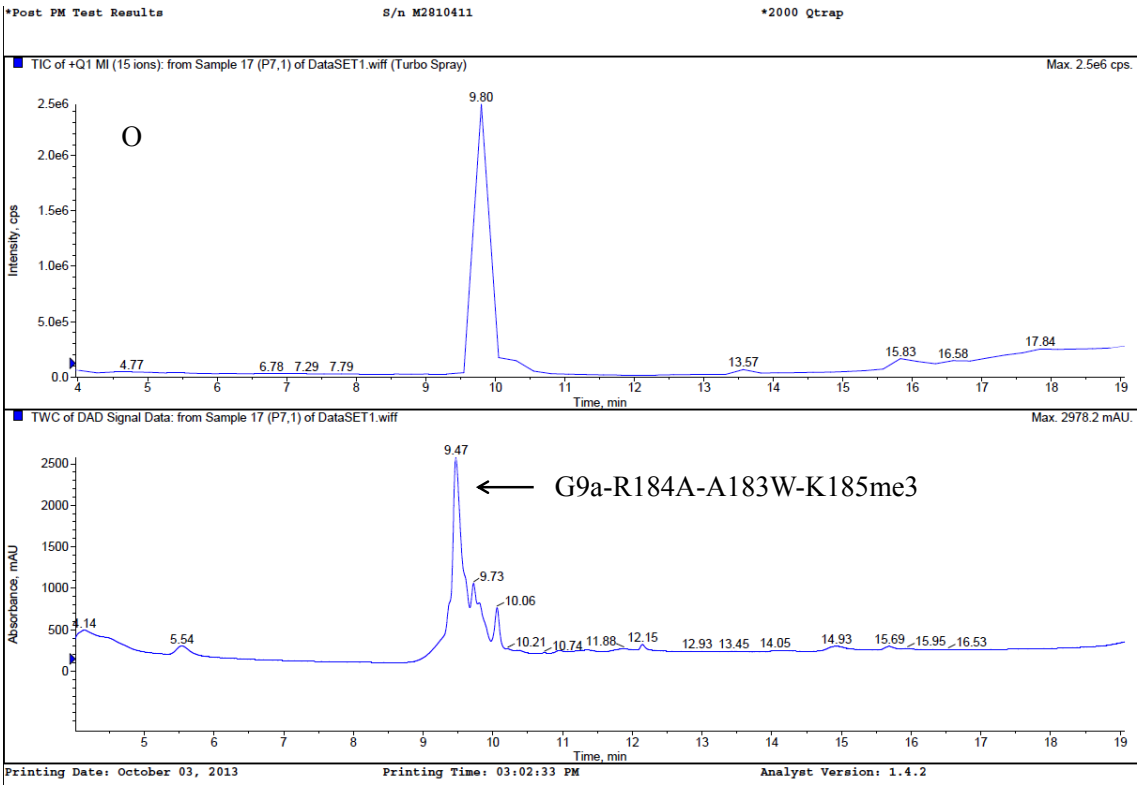
*Post PM Test Results
S/n M2810411
*2000 Qtrap
TIC of +Q1 MI (15 ions): from Sample 17 (P7,1) of DataSET1.wiff (Turbo Spray)
Max. 2.5e6 cps.
O
Intensity, cps
Time, min
TWC of DAD Signal Data: from Sample 17 (P7,1) of DataSET1.wiff
Max. 2978.2 mAU.
G9a-R184A-A183W-K185me3
Absorbance, mAU
Time, min
Printing Date: October 03, 2013
Printing Time: 03:02:33 PM
Analyst Version: 1.4.2

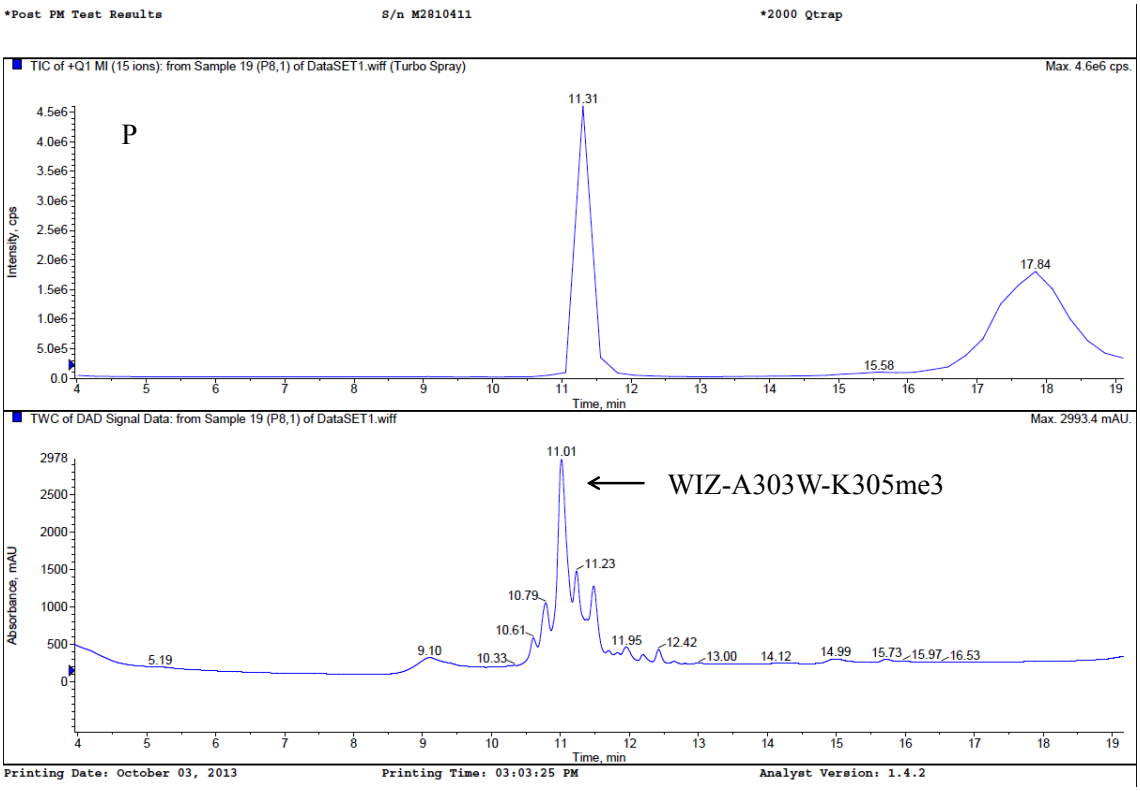
*Post PM Test Results
S/n M2810411
*2000 Qtrap
TIC of +Q1 MI (15 ions): from Sample 19 (P8,1) of DataSET1.wiff (Turbo Spray)
Max. 4.6e6 cps.
P
Intensity, cps
Time, min
TWC of DAD Signal Data: from Sample 19 (P8,1) of DataSET1.wiff
Max. 2993.4 mAU.
WIZ-A303W-K305me3
Absorbance, mAU
Time, min
Printing Date: October 03, 2013
Printing Time: 03:03:25 PM
Analyst Version: 1.4.2

LCMS-based demethylase assay development

The non-histone trimethylated peptides from widely interspaced zinc finger motifs protein (WIZ), chromodomain Y-like protein (CDYL1), Cockayne syndrome group B protein (CSB, four peptides) and G9a were custom synthesized (Table **1**). In addition, a second set of peptides were synthesized and purified (Table **2**). H3-K9me3 peptide was used as a positive control. Next, a liquid chromatography (LC) method was developed using an Agilent Zorbax Eclipse XDB-C18 column (2.1 x 150 mm, 3.5 μm particles). This allowed separation and quantification of the substrate (H3-K9me3, eluted at 9.3 min) and the products (H3-K9me2, eluted at 11.6 min and H3-K9me1, eluted at 14.5 min). This LC method was used to identify optimized cofactor concentrations (500 μM FeSO4, 4 mM 2OG and 10 mM ascorbate). A time course experiment (0-4 hrs) was performed and assay duration was fixed to 4 hrs.

Kinetic properties of JMJD2A-C with H3-K9me3 as substrate

For uniformity the specific activities of JMJD2A-C were determined by reduction of substrate peak area because more than one product (di- and/or monomethylated products, ratios of which varied among different substrates and enzyme isoforms) was formed in the assay reactions. Specific activities, determined by the reduction of substrate peak area, were linear during the course of the reaction (Figure 14, Figure 15).

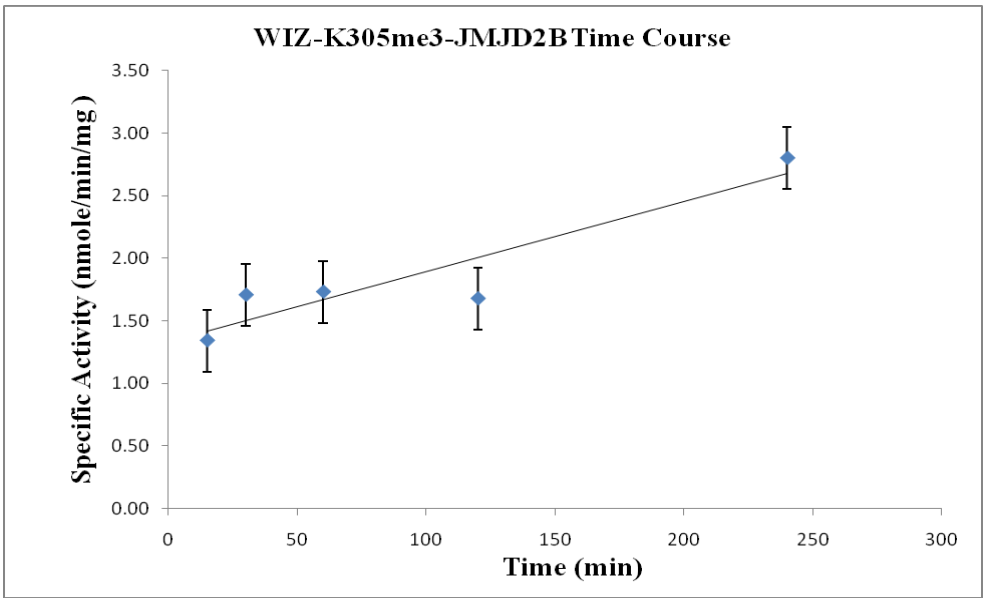

Figure 14 Plot of specific activity (nmole/min/mg) vs time (min) for JMJD2B with WIZ-K305me3. Note that WIZ-K305me3 showed linearity being the best substrate for JMJD2B.

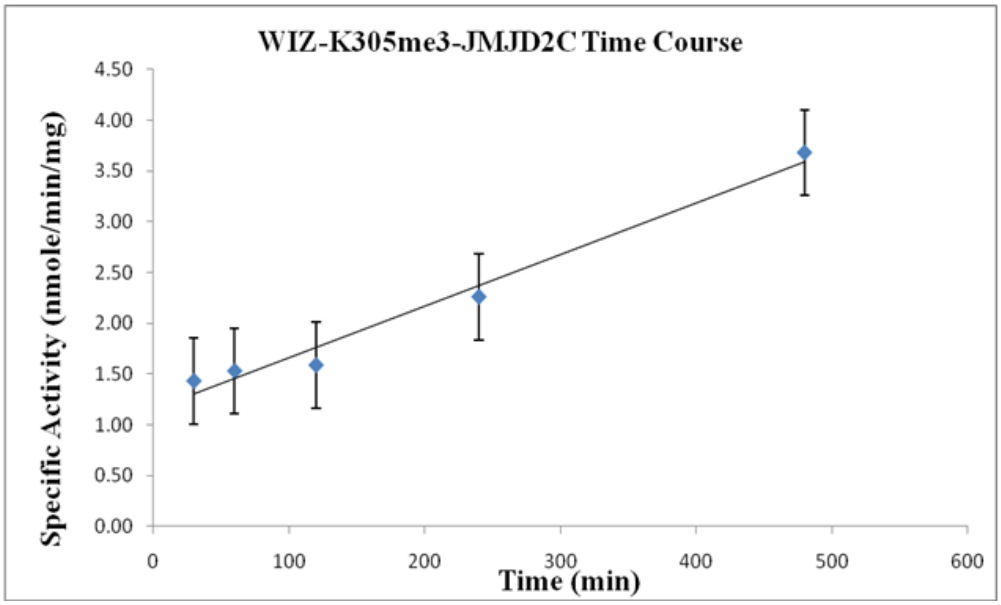

Figure 15: Plot of specific activity (nmole/min/mg) vs time (min) for JMJD2C with WIZ-K305me3. Note that WIZ-K305me3 showed linearity being the second best substrate for JMJD2B.

Although, JMJD2A, B and C isoforms share high sequence homology (Figure 16), we observed differences in their specific activities with JMJD2A being the most active isoform (1.0 ±0.5 nmole min^{-1} mg^{-1}) followed by JMJD2C (0.5 ±0.5 nmole min^{-1} mg^{-1}), while JMJD2B was the least active isoform (0.29 ±0.13 nmole min^{-1} mg^{-1}) k_{cat}/K_M). The k_{cat}/K_M values were determined by dividing the specific activity (velocity, nmole min^{-1} mg^{-1}) with total enzyme added (15 nmoles) and substrate (50 nmole/µl) and were found to be 1.1 $M^{-1}s^{-1}$for JMJD2A, 0.56 $M^{-1}s^{-1}$ for JMJD2C and 0.33 $M^{-1}s^{-1}$for JMJD2B. The observed specific activities are relatively low, which is not surprising given the drastic effect these enzymes exert on transcription [93, 94].

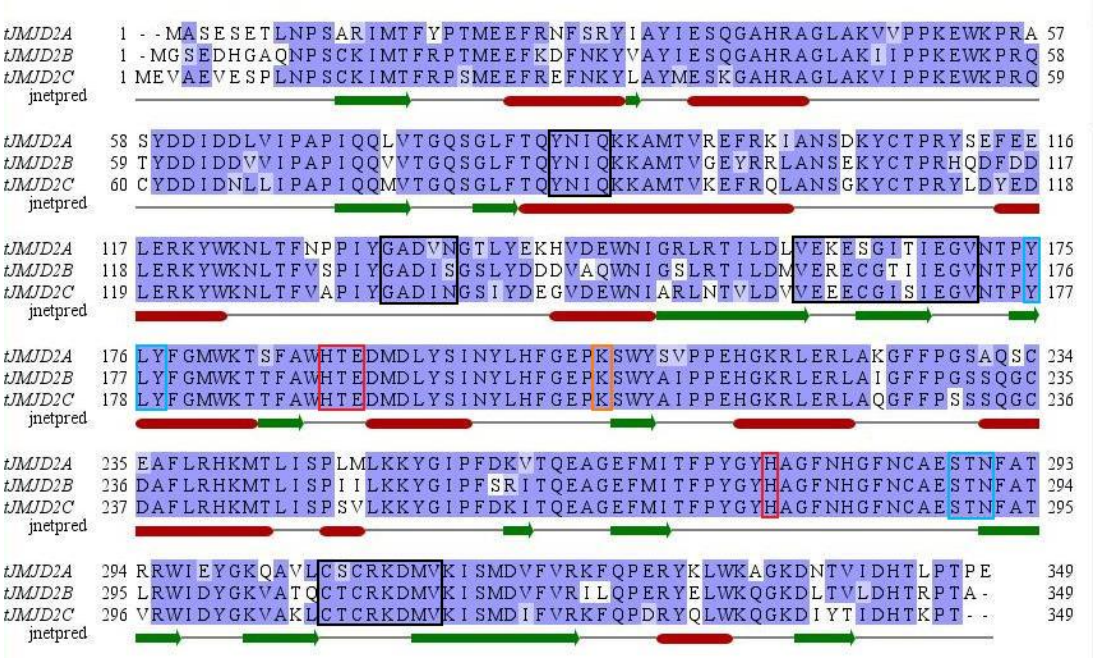

Figure 16: Multiple sequence alignment of tJMJD2A-C proteins. Initial alignment was done using ClustalW and then manually adjusted for secondary structure prediction using Jnet server. Substrate (peptide backbone) binding domains are boxed in black, while methylated lysyl side-chain environment is in blue. The residues binding the catalytic iron(II) are in red and 2OG in orange. Predicted secondary structure elements are given below the alignment.

Identification of non-histone substrates:

Next, we checked if JMJD2A-C can accept peptides from non-histone proteins as substrates. The trimethylated non-histone peptides from WIZ, CDYL1, CSB and G9a proteins were incubated with optimized cofactors in the presence and absence of JMJD2A-C. LC assays clearly showed appearance of a new peak consistent with the retention time of dimethylated peptide in the presence of enzyme (Figure 17).

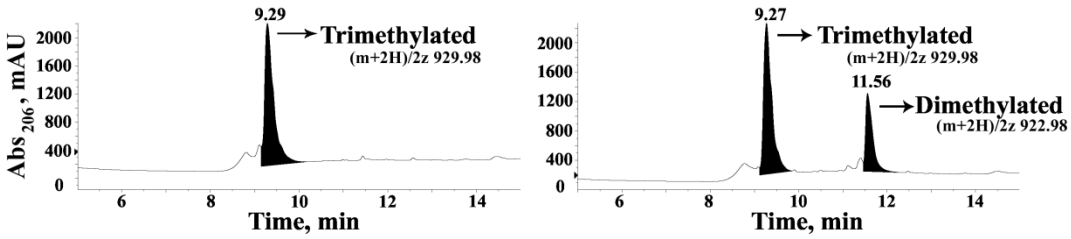

Figure 17: Liquid chromatography method used to characterize JMJD2 family KDMs. The left panel shows HPLC profile of CSB-K170me3 peptide in the absence of enzyme (negative control), while the right panel shows HPLC profile of CSB-K170me3 peptide in the presence of JMJD2A (assay reaction).

Mass spectrometry analysis confirmed that the new peak was indeed of dimethylated peptide products (Figure 18). For some substrates peaks corresponding to monomethylated peptides were also detected in the presence of enzymes (Table 3). Interestingly, JMJD2A-C KDMs showed better activities with a number of non-histone substrates compared to its only known substrate, H3-K9me3 (Table 4).

Table 3: Identification of monomethylated products by LCMS method formed by demethylation of the corresponding trimethylated peptide substrates. A "+" indicates presence while "–" indicates absence of monomethylated peptide.

Isoforms	H3-K9me3	WIZ-K305me3	CDYL1-K135me3	CSB-K170me3	CSB-K297me3	CSB-K448me3	CSB-K1054me3	G9a-K185me3
tJMJD2A	+	–	+	–	–	+	–	–
tJMJD2B	–	+	+	–	–	+	+	–
tJMJD2C	–	+	+	–	–	+	–	–

Table 4: Specific activity of GST-tJMJD2A-C KDMs for histone (H3-K9me3) and non-histone substrates. All values are nmole min-1 mg-1

Isoforms	H3-K9me3	WIZ-K305me3	CDYL1-K135me3	CSB-K170me3	CSB-K297me3	CSB-K448me3	CSB-K1054me3	G9a-K185me3
tJMJD2A	1.0 ±0.5	1.88 ±0.13	1.00 ±0.12	1.1 ±0.2	0.64 ±0.12	0.6 ±0.2	1.9 ±0.2	2.6 ±0.2
tJMJD2B	0.29 ±0.13	3.5 ±0.4	0.95 ±0.07	2.0 ±0.4	0.4 ±0.3	2.5 ±1.1	1.43 ±0.13	2.4 ±0.6
tJMJD2C	0.5 ±0.5	3.1 ±0.4	3.40 ±0.01	1.9 ±0.2	1.5 ±0.3	2.32 ±0.10	1.63 ±0.05	2.12 ±0.03

JMJD2A, JMJD2B and JMJD2C showed the best specific activities with G9a-K185me3 (2.6 ±0.2 nmole min^{-1} mg^{-1}), WIZ-K305me3 (3.5 ±0.4 nmole min^{-1} mg^{-1}) and CDYL1-K135me3 (3.40 ±0.01 nmole min^{-1} mg^{-1}), respectively. In general WIZ-K305me3 was the best substrate and showed linear specific activities over the course of reaction (Figure 14, Figure 15). The activity pattern (JMJD2A>JMJD2C>JMJD2B) of only CSB-K1054me3 was similar to H3-K9me3. JMJD2B and 2C isoforms showed better activities than JMJD2A towards WIZ-K305me3, CSB-K170me3 and CSB-

K448me3. While all three isoforms showed similar activities with G9a automethylation site (G9a-K185me3).

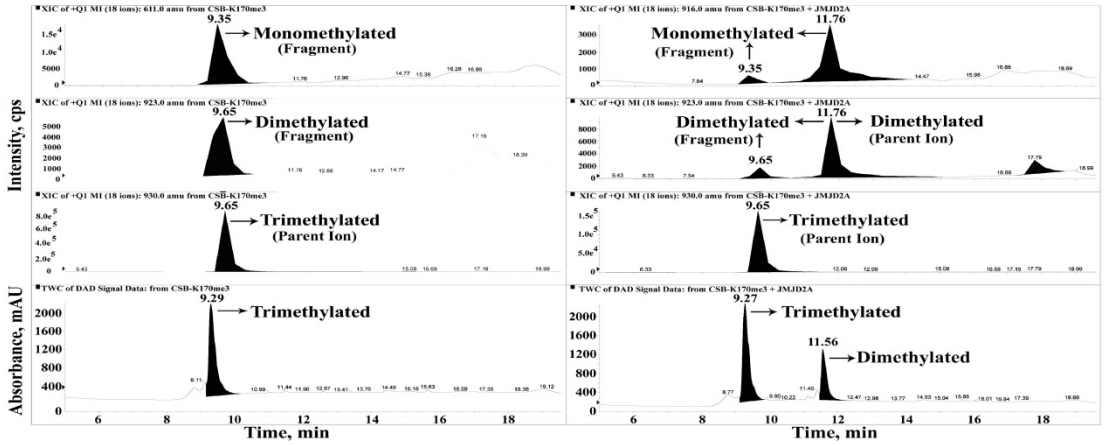

Figure 18: Liquid chromatography method used to characterize JMJD2 family KDMEs. The bottom left panel shows HPLC profile of CSB-K170me3 peptide in the absence of enzyme (negative control), while the bottom right panel shows HPLC profile of CSB-K170me3 peptide in the presence of JMJD2A (assay reaction). The upper three panels in both the negative control and assay reaction show mass scan for tri-, di- and monomethylated CSB-1 peptides. The assay reaction shows appearance of dimethylated product peak at 11.56 mins in LC with a corresponding MS peak at 11.76 mins. Peaks for di- and monomethylated peptides in the mass scans for negative control are due to fragmentation of the trimethylated peptide in MS. Similarly, dimethylated product lost one methyl group and was detected in the mass scan for monomethylated peptide in assay reaction.

Importance of Arginine at –1 position for substrate recognition by JMJD2 KDMs

Based on the identification of seven non-histone peptide substrates (WIZ-K305me3, CDYL1-K135me3, CSB-K170me3, CSB-K297me3, CSB-K448me3, CSB-K1054me3 and G9a-K185me3) from four different proteins (WIZ, CDYL1, CSB and G9a) as substrates for JMJD2a-c KDMs, we wanted to evaluate the substrate specificity of JMJD2A-C KDMs [92]. In order to determine essential amino acids required for substrate recognition by the Jmjd2a-c KDMs, we searched for consensus motifs in these eight peptides (one histone and seven non-histones). These studies suggested conservation of Arg at the –1 position. However, the conserved Arg at the –1 position may be due to G9a PKMT substrate specificity rather than Jmjd2 KDMs because all the non-histone substrates examined were G9a substrates [92]. Site-directed mutagenesis studies by Rathert et al. showed preference of Arg at –1 position for G9a substrate recognition [91]. Therefore, to study the role of Arg at –1 position for Jmjd2 substrate recognition we mutated –1 Arg to Ala in two most efficient non-histone substrates (WIZ and G9a) and performed demethylation assays with JMJD2a-c. While G9a-R184A-K185me3 mutant showed ~60% reduction in the activity (*e.g.* the specific activity of GST-tJMJD2a was 1.54±0.3 nmoles min^{-1} mg^{-1} using G9a-K185me3 as substrate compared to 0.5±0.12 nmoles min^{-1} mg^{-1} for the G9a-R184A-K185me3 mutant), there was a complete loss in the activity with WIZ-R304A-K305me3 mutant as substrate for all three isoforms of JMJD2 (Table 5, Figure 19,Figure 20, Figure 21). These experiments clearly demonstrate a critical role for Arg at –1 position in substrate recognition by JMJD2 family KDMs.

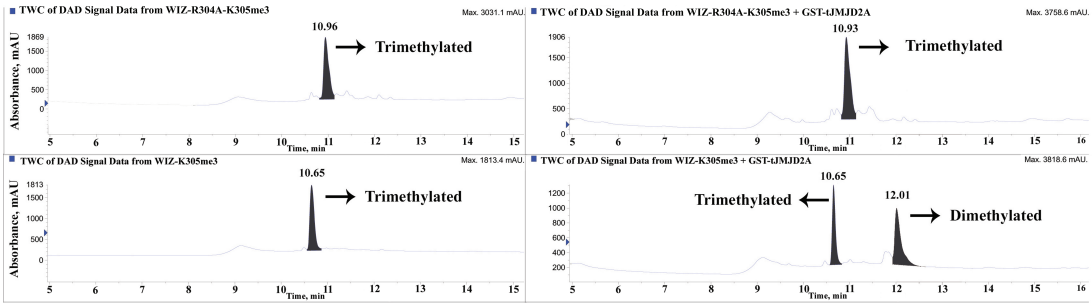

Figure 19: LCMS analysis showing the importance of Arg at –1 position in Jmjd2A substrates. The bottom left panel shows HPLC profile of WIZ-K305me3 peptide in the absence of enzyme (negative control), while the bottom right panel shows HPLC profile of WIZ-K305me3 peptide in the presence of JMJD2A (assay reaction). The top left panel shows HPLC profile of WIZ-R304A-K305me3 peptide in the absence of enzyme (negative control), while the top right panel shows HPLC profile of WIZ-R304A-K305me3 peptide in the presence of JMJD2A (assay reaction). Note the absence of product in WIZ-R304A-K305me3 mutant.

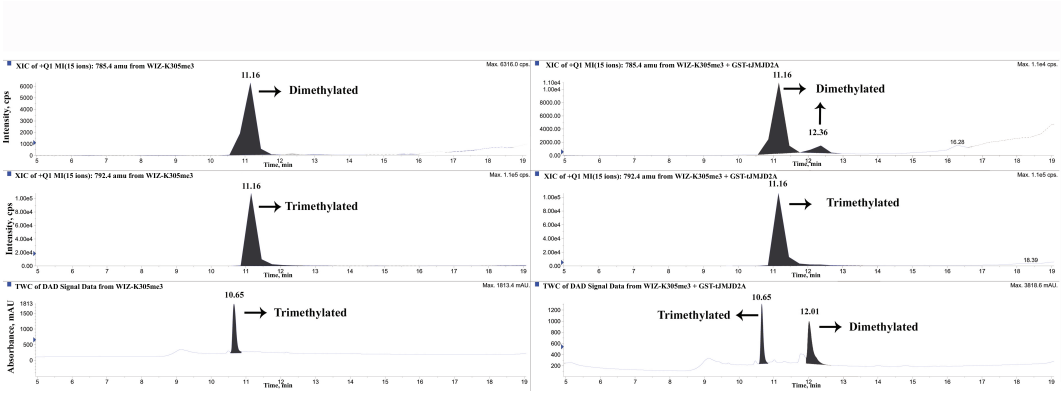

Figure 20: Liquid chromatography method used to characterize JMJD2A-C KDMs. The bottom left panel shows HPLC profile of WIZ-K305me3 peptide in the absence of enzyme (negative control), while the bottom right panel shows HPLC profile of WIZ-K305me3 peptide in the presence of JMJD2A (assay reaction). The upper two panels in both the negative control and assay reaction show mass scan for tri- and dimethylated WIZ-K305me3 peptides. The assay reaction shows appearance of dimethylated product peak at 12.01 min in LC with a corresponding MS peak at 12.36 min. Peaks for dimethylated peptides in the mass scans for negative control are due to fragmentation of the trimethylated peptide in MS.

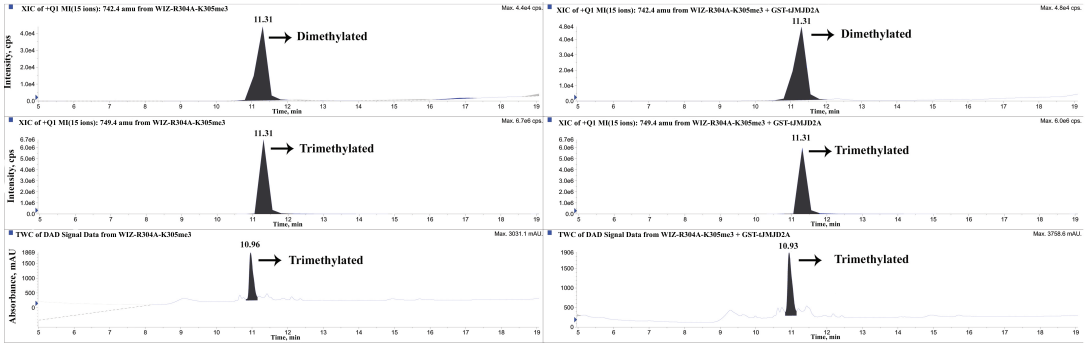

Figure 21: Liquid chromatography method used to characterize JMJD2A-C KDMs. The bottom left panel shows HPLC profile of WIZ-R304A-K305me3 peptide in the absence of enzyme (negative control), while the bottom right panel shows HPLC profile of WIZ-R304A-K305me3 peptide in the presence of JMJD2A (assay reaction). The upper two panels in both the negative control and assay reaction show mass scan for tri- and dimethylated WIZ-R304A-K305me3 peptides. The assay reaction shows no dimethylated product peak in LC and no corresponding MS peak. Peaks for dimethylated peptides in the mass scans for negative control are due to fragmentation of the trimethylated peptide in MS.

Table 5 Specific activities of GST-tJMJD2A-C KDMs for H3-K9me3 and non-histone substrates (nmoles min^{-1} mg^{-1} ± SE).

Peptide	tJMJD2A	tJMJD2B	tJMJD2C
H3-K9me3	2.32±0.23	1.98±0.19	2.32±0.42
WIZ-K305me3	2.5±0.31	2.5±0.44	2.5±0.5
WIZ-R304A-K305me3	0.06±0.01	-0.01±0.04	-0.09±0.04
WIZ-A303W-K305me3	1.09±0.23	1.30±0.44	1.52±0.21
G9a-K185me3	1.54±0.3	1.2±0.64	1.9±0.24
G9a-R184A-K185me3	0.5±0.12	0.8±0.24	0.70±0.31
G9a-A183W-K185me3	0.82±0.14	0.62±0.1	0.90±0.13
G9a-A183W-R184A-K185me3	0.43±0.13	0.15±0.1	0.08±0.09
Dnmt1-K70me3	0.2±0.06	0.24±0.12	0.11±0.08
KLF12-K313me3	0.14±0.1	0.10±0.08	0.14±0.1
ACINUS-K654me3	0.3±0.11	0.11±0.06	0.3±0.07
HDAC1-K432me3	0.3±0.14	0.23±0.12	0.51±0.21

Preference of smaller amino acids at –2 position for substrate recognition by JMJD2 KDMs

Our motif search also suggested a preference for a smaller amino acid at the –2 position. Ng et al. also suggested propensity for smaller amino acids at –2 position by aligning the sequences of H3-K9me3 and H3-K36me3 peptides (Ala-7 in H3-K9 and Gly-34 in H3-K36) [50]. To evaluate the role of smaller amino acids at –2 position, we synthesized WIZ and G9a peptides with an Ala to Trp substitution at –2 position. The demethylation assays with G9a-A183W-K185me3 and WIZ-A303W-K305me3 mutants showed up to 50% reduction in the specific activities for all three isoforms of JMJD2 (2.5±0.31 for WIZ-K305me3 to 1.09±0.23 nmoles min^{-1} mg^{-1} for WIZ-A303W-K305me3 mutant and 1.54±0.3 for G9a-K185me3 to 0.82±0.14 nmoles min^{-1} mg^{-1} for G9a-A183W-K185me3 mutant using GST-tJMJD2A KDM) (Table 5, Figure 22, Figure 23, Figure 24). These results demonstrate that a smaller amino acid at –2 position is one of the important determining factors for substrate specificity by JMJD2 family KDMs. We also went ahead and synthesized a G9a peptide with mutations incorporated at -1 (Arg to Ala) and -2 (Ala to Trp) positions. This resulted in further reduction in specific activity from 1.54±0.30 to 0.43±0.13 nmoles min^{-1} mg^{-1} for JMJD2A, 1.2±0.64 to 0.15±0.1 nmoles min^{-1} mg^{-1} for JMJD2B and 1.9±0.24 to 0.08±0.09 nmoles min^{-1} mg^{-1} for Jmjd2C.

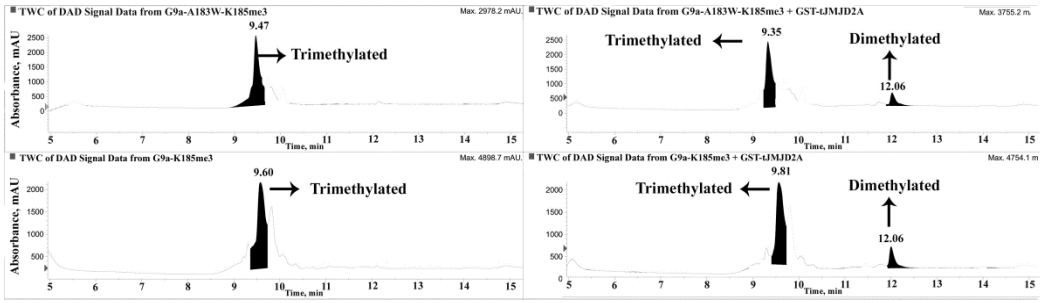

Figure 22: LCMS analysis showing the importance of smaller amino acid at –2 position in JMJD2A substrates. The bottom left panel shows HPLC profile of G9a-K185me3 peptide in the absence of enzyme (negative control), while the bottom right panel shows HPLC profile of G9a-K185me3 peptide in the presence of Jmjd2a (assay reaction). The top left panel shows HPLC profile of G9a-A183W-K185me3 peptide in the absence of enzyme (negative control), while the top right panel shows HPLC profile of G9a-A183W-K185me3 peptide in the presence of Jmjd2a (assay reaction).

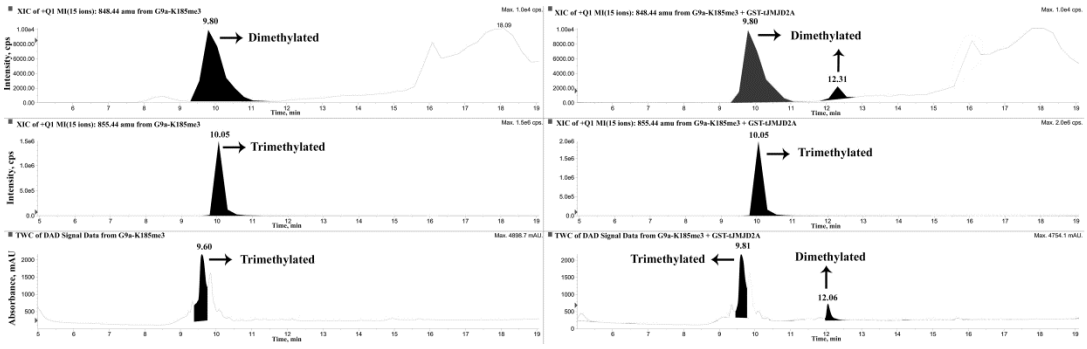

Figure 23: Liquid chromatography method used to characterize JMJD2A-C KDMs. The bottom left panel shows HPLC profile of G9a-K185me3 peptide in the absence of enzyme (negative control), while the bottom right panel shows HPLC profile of G9a-K185me3 peptide in the presence of JMJD2A (assay reaction). The upper two panels in both the negative control and assay reaction show mass scan for tri- and dimethylated G9a-K185me3 peptides. The assay reaction shows appearance of dimethylated product peak at 12.06 min in LC with a corresponding MS peak at 12.31 min. Peaks for dimethylated peptides in the mass scans for negative control are due to fragmentation of the trimethylated peptide in MS.

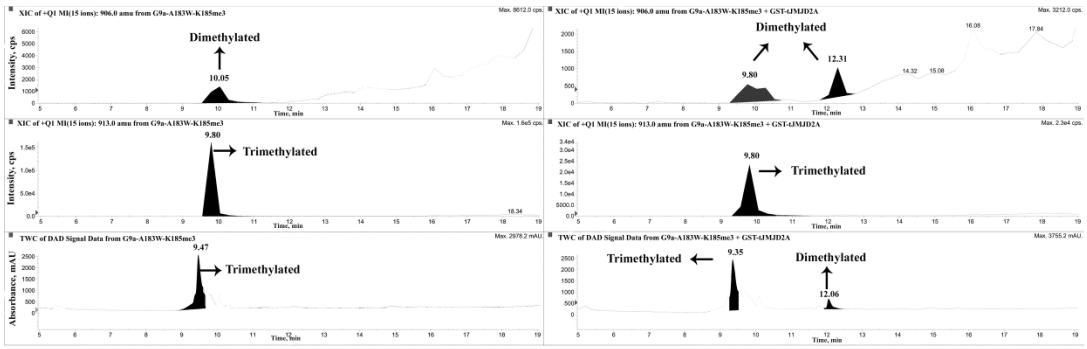

Figure 24: Liquid chromatography method used to characterize JMJD2A-C KDMs. The bottom left panel shows HPLC profile of G9a-A183W-K185me3 peptide in the absence of enzyme (negative control), while the bottom right panel shows HPLC profile of G9a-A183W-K185me3 peptide in the presence of JMJD2A (assay reaction). The upper two panels in both the negative control and assay reaction show mass scan for tri- and dimethylated G9a-A183W-K185me3 peptides. The assay reaction shows appearance of dimethylated product peak at 12.06 min in LC with a corresponding MS peak at 12.31 min. Peaks for dimethylated peptides in the mass scans for negative control are due to fragmentation of the trimethylated peptide in MS. There is a clear reduction in product peak with G9a-A183W-K185me3 peptide compared to G9a-K185me3 wild type peptide.

Similarity in substrate specificities of G9a methyltransferase and Jmjd2 demethylases

To gain further insight into substrate specificity of JMJD2 KDMs, four new non-histone methylated peptides from Dnmt1, KLF12, ACINUS and HDAC1 were synthesized. A previous study identified these peptides as poor substrates of G9a PKMT [91]. Interestingly, these non-histone methylated peptides also showed poor activity with all three isoforms of JMJD2 KDMs (Table 5) compared to the ones identified in Ponnaluri et al [92]. Among these newly synthesized non-histone substrates HDAC1-K432me3 showed the highest activity (0.51±0.21 nmoles min^{-1} mg^{-1}) compared to ACINUS-K654me3, KLF12-K313me3 and Dnmt1-K70me3 (0.3±0.07, 0.14±0.1 and 0.11±0.08 nmoles min^{-1} mg^{-1}, respectively, using GST-tJMJD2C). Interestingly, along with Arg at –1 position, only HDAC1-K432me3 has a smaller amino acid (Gly) at –2 position; while ACINUS-K654me3, KLF12-K313me3 and Dnmt1-K70me3 have Leu, Ser and Asn, respectively, all larger amino acids (Table **2**). These results further show that JMJD2A-C KDMs prefer a smaller amino acid at –2 position for substrate selectivity.

G9a methylates histones and some non-histone proteins [91, 95]. Rathert et al. showed strong preference for Arg at –1 position for methylation by G9a [91]. This result correlates well with the crystallographic data [96], which identified interactions between the guanidino group of –1 Arg and the carboxyl groups of Asp1145, Asp1135, Asp1131 of G9a-like-protein (G9a-like-protein and G9a share >80% identity in their SET domain). These interactions help orient the substrate in the active site of G9a-like-protein. Our results demonstrate that JMJD2A-C KDMs, which catalyze the opposite

reaction, also prefers Arg at –1 position. A closer examination of tJmjd2a structure, co-crystallized with H3-K9me3 substrate [50], identified similar interactions between the guanidino group of –1 Arg from the substrate with the carboxyl group of Glu169 of tJmjd2a.

The structures of a number of PKMTs have been reported [97-102]. These structures collectively highlight a remarkable plasticity in the substrate / peptide binding site and lack of clear structural motifs that correlate with sequence selectivity. Similarly, the crystal structure of JMJD2A revealed that the binding of the methylated peptide substrates to the active site are achieved by few polar side chain interactions [50]. This provides a degree of plasticity in substrate recognition by JMJD2 family KDMs, an unusual feature for sequence specific enzymes. Taken together, these results suggest that lysine methylating and demethylating enzymes are generally very non-specific with only a few amino acids (Arg at –1 position and a small amino acid –2 position) determining their substrate selectivity. This is very surprising considering these enzymes catalyze opposing reactions, have completely different structures and reaction mechanisms (supplementary text). A recent proteomics study identified 1750 proteins with 3600 unique acetylation sites [103] which are in good comparison to the number of phosphorylation sites found in the cell [104, 105]. Considering lax substrate specificities of protein lysine methylases and demethylases it is likely that, like acetylation and phosphorylation, methylation is a more prevalent post translational modification of cellular proteins than what is currently known.

Discussion

JMJD2A-C KDMs demethylate trimethylated histone H3-lysine-9 (H3-K9me3), and also H3-K9me2 and H3-K36me3 albeit at lower rates. In the current study we expressed and purified JMJD2A-C isoforms to homogeneity. An LCMS method was developed to separate and quantify both substrate (trimethylated) and products (di- and/or monomethylated peptides). This method was used to determine the kinetics of the enzymes for both histone and non-histone substrates. We demonstrated for the first time that in addition to its only known substrate, H3-K9me3, JMJD2A-C can demethylate non-histone peptides from WIZ, CDYL1, CSB and G9a proteins. Interestingly, JMJD2A-C showed better activities with non-histone substrates identified in this study, suggesting they may have additional demethylation roles *in vivo* (Table 4).

The crystal structure of JMJD2A in complex with H3-K9me3 and H3-K36me3 peptides showed that the binding of these two substrates were achieved by distinct conformations, yet orientation of trimethylated lysine toward the active site were superimposable [50]. The preference of H3-K9me3 over H3-K36me3 by JMJD2A was due to intra-substrate hydrogen bonding and presence of a Gly-Gly motif at the +3 position. However, a Gly-Gly motif was absent in WIZ-K305me3, CSB-K1054me3, and G9a-K185me3 peptides, which were significantly better substrates than H3-K9me3, suggesting a sequence specific requirement of this motif only in H3-K9me3 peptide for catalysis by JMJD2A. All the substrates examined in this study contain an Arg at –1 position. This may be due to the candidate-based approached taken during this study. Since all the substrates examined in this study were substrates of G9a, preference of

Arg at –1 position could be due to G9a methyltransferase rather than JMJD2 demethylases. Indeed, in H3-K36me3 peptide, which is also a substrate of JMJD2A, Arg is absent at –1 position suggesting lack of absolute requirement of this residue in the JMJD2A substrates. Ng et al. [50] suggested propensity for smaller amino acids in the –2 position by sequence alignment of H3-K9me3 and H3-K36me3 peptides (Ala-7 in H3-K9 and Gly-34 in H3-K36). Consistently, in this study five of the seven non-histone substrates carried either an Ala or a Gly residue at the –2 position. Taken together, these results suggest remarkable flexibility in the substrate recognition by JMJD2-family KDMs.

Conclusion

Crystal structure of JMJD2A revealed that the binding of the methylated peptide substrates is achieved by few polar side chain interactions providing some degree of plasticity in substrate recognition [50]. JMJD2 family KDMs contains many protein-protein interacting domains like PHD and Tudor domain. These domains are mainly found in nuclear proteins which are associated with transcriptional regulation. JMJD2 family KDMs, which are overexpressed in a number of cancers, were believed to reverse the methylation marks on the lysine residue of histone tail. In prostate cancer, JMJD2-family KDMs are involved in androgen receptor (AR)-mediated upregulation of AR-response genes by reversion of the repressive H3-K9me3 mark [93, 94]. It is interesting to note that repressive heterochromatin formation is initiated by a complex consisting of G9a, WIZ, CtBP, GLP, and CDYL1 proteins. During this process WIZ stabilizes G9a/GLP heterodimer [106] and mediates its interaction with CtBP, allowing methylation of H3-K9 by G9a [107]. H3-K9me3 is recognized by chromodomain (methylated lysine binding domain) of CDYL1, initiating formation of local repressive chromatin structure [107] (Figure 25).

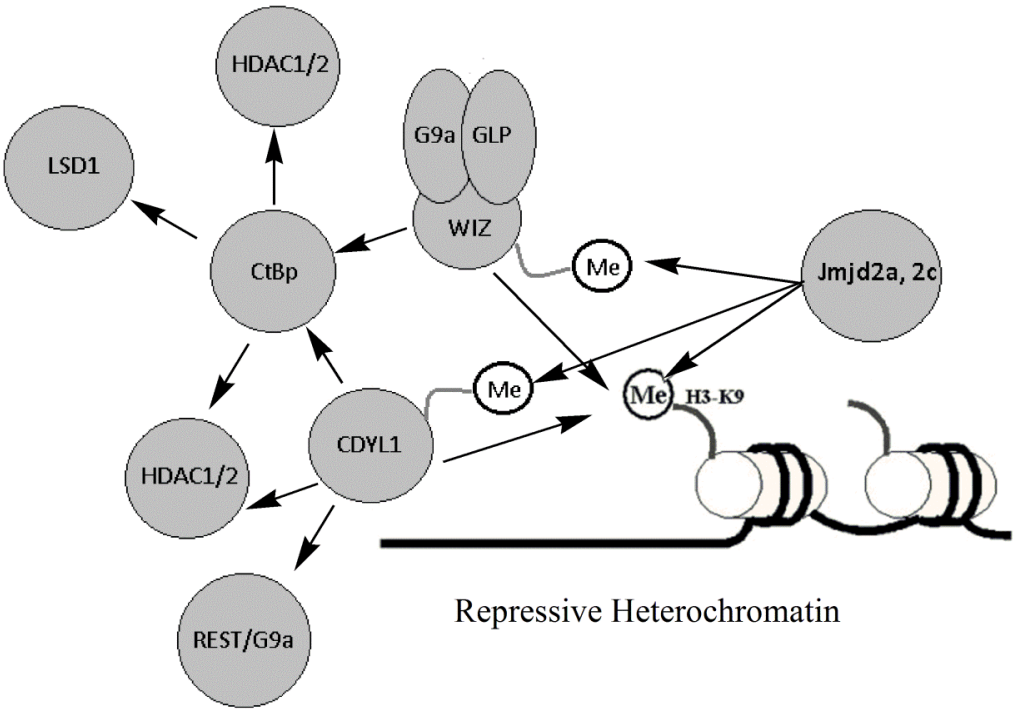

Figure 25: Model depicting the interaction observed in the transcription machinery associated with formation of the repressive heterochromatin.

All the non-histone substrates identified in this study are involved in transcriptional regulation. Therefore, reversion of methylation marks on H3-K9 and G9a interacting proteins, as identified in this study, may allow upregulation of transcription by JMJD2 family KDMs during cancer development. Thus identification of these non-histone substrates for JMJD2A-C KDMs suggests presence of a new layer of epigenetic regulation. We also identified the importance of Arg at –1 position and a smaller amino acid at –2 position in the substrate specificity of Jmjd2 family KDMs. Although G9a PKMT and JMJD2A-C KDMs catalyze opposing reactions and have

completely different structures and reaction mechanisms, we found similarities in their substrate specificities. Based on our results and lax substrate specificities of methylases and demethylases, we believe that methylation is a much more prevalent post translational modification than currently known.

CHAPTER III

EVALUATING THE ROLE OF HISTONE DEMETHYLASES IN OXYGEN MEDIATED PATHOPHYSIOLOGICAL CONDITIONS

Introduction

Oxygen plays a critical role as the electron acceptor during oxidative phosphorylation, a key process in cellular energy generation. In addition, oxygen also plays important roles in apoptosis, membrane transport [108], and gene expression [109]. Thus, it is essential to maintain oxygen homeostasis in cells. If the oxygen tension in our body drops below the threshold levels, cells experience hypoxia. Hypoxia is observed in both physiological as well as pathological conditions. Physiological processes where hypoxia is experienced include wound healing, embryonic development, and adaptation to higher altitudes. Pathological conditions include ischemic heart diseases, neovascularization in cancer and retinal diseases [110].

Hypoxia inducible factor (HIF) is a central molecule that plays a vital role in eliciting the effect of oxygen tension at the cellular level by modulating gene expression [61]. HIF is a member of PAS family of basic helix-loop-helix heterodimeric transcription factors, consisting of α subunits (HIF-1α, -2α, and -3α) and HIF-1β/ARNT subunit. Normally, hydroxylation of the conserved proline residues (Pro402 and Pro564 in human HIF-1α) by the oxygen-dependent HIF prolyl hydroxylases/dioxygenases (PHD1-3) under normoxic conditions allows the binding of HIF-α isoforms to the wild-type (wt)-pVHL. This binding of hydroxylated HIF-α to pVHL, the substrate recognition subunit of an E3 ubiquitin ligase, allows rapid proteosomal degradation of

HIF-α under normoxia [111, 112]. When the oxygen level drops, PHDs become inactive resulting in lower HIF-α prolyl-hydroxylation, allowing it to escape proteosomal degradation. Following this process, HIF-α translocates to the nucleus and dimerizes with HIF-β. Thus during hypoxia HIF-α/β heterodimer accumulates in the nucleus, recruits several transcriptional co-activators, and binds to hypoxia response element (HRE) of target genes causing overexpression of VEGF and other pro-angiogenic factors.

HIF pathway is intimately associated with the pathobiology of a number of oxygen-dependent retinal diseases such as VHL, proliferative diabetic retinopathy, glaucoma, and retinopathy of prematurity [113]. In all these conditions hypoxia-induced neovascularization is the central cause of pathogenesis. Little is known about the epigenetic regulation during HIF-mediated transcription activation of pro-angiogenic genes in oxygen-dependent retinal diseases. However, transcriptional adaptations mediated by hypoxia and HIFs (HIF-1α, HIF-2α, HIF3α and HIF-1β/ARNT) suggest changes in the epigenetic histone modifications [114]. A number of recent studies have identified a role of histone methylation in HIF-mediated hypoxia adaptation in cancer cell [69-71]. The HIF pathway upregulates, in addition to many known proteins that facilitate metabolic adaptation to hypoxia, transcription of 17 out of the 22 Jumonji-C (Jmj) domain containing iron (II), 2-oxoglutarate (2OG)-dependent histone lysine demethylases (KDMs) in the hypoxic cancer cells [69]. Of these 17, four Jmj KDMs (*JMJD1A, JMJD2B, JMJD2C* and *JARID1B*) were direct transcription targets of HIF as HIF-α/β bound to the HRE present in the promoter regions of these genes [69].

JMJD1A regulates the expression of some pro-angiogenic hypoxia-inducible genes (*ADM* and *GDF15*) by decreasing histone methylation at their promoters and knock-down of JMJD1A reduces tumor growth [69, 72]. Based on these observations we investigated the role of KDMs in oxygen-dependent retinal diseases.

Hemangioblastomas (also known as the blood vessel tumor or VHL disease) are multisystem tumor syndromes, where mutations in the VHL protein (pVHL) lead to constitutive activation of the HIF pathway. In patients with mutated pVHL, even though HIF-α gets hydroxylated at the proline residues under normoxia, it is not bound by mutated pVHL, allowing it to escape proteosomal degradation. Subsequently, HIF-α translocates to the nucleus, dimerizes with the HIF-1β subunit, and recruits transcriptional co-activators. The active HIF-α/β heterodimer binds to a core DNA sequence (G/ACGTG) in the hypoxia-response-element (HRE) present in the promoters of target genes, causing overexpression of hypoxia response genes, which includes a number of pro-angiogenic factors [*e.g.* vascular endothelial growth factor (VEGF), erythropoietin (EPO), platelet-derived growth factor (PDGF) etc.]. As a result, hemangioblastomas of retina, central nervous system (CNS), and kidney are highly vascular in nature [115].

In addition to these vascular cells, hemangioblastomas are composed of 'stromal cells'. However, the cytological origin of these neoplastic stromal cells remains unknown. A number of studies have shown coexistence of pro-angiogenic and stem cell markers in tumorlet-like stromal cells in the retinal and optic nerve hemangioblastomas [116, 117], leading to the suggestion that hemangioblastomas originate from

developmentally arrested stem cells or embryonic progenitors [116-119]. Failure to specify the histological origin of stromal cells in hemangioblastomas has precluded the development of nonsurgical therapies for these multisystem blood vessel tumor syndromes.

All current therapies for hemangioblastomas and oxygen-dependent retinal diseases have significant limitations and side-effects; while anti-VEGF therapies (*e.g.* Macugen, Lucentis, etc.) had minimal detectable beneficial effects [120, 121]. This lack of efficacy of anti-VEGF therapies is possibly due to overexpression of other pro-angiogenic factors (*e.g.* EPO, PDGF, etc.). Hence, blocking of a master regulator like HIF pathway could be a viable alternate strategy for treating pathological conditions like hemangioblastomas and oxygen dependent retinal diseases.

In the first part of the study we evaluated the response to hypoxia in human retinal pigment epithelial cells. We also determined the levels of induction of a panel of histone demethylases in these RPE cells along with known HIF target genes. Further using a generic KDM inhibitor like DMOG resulted in inhibition of JMJD1A target gene expression, suggesting the possible use of KDM inhibitors to block amplification of HIF pathway.

Screening for inhibitors of the HIF pathway was performed as a collaborative project with Divya Teja Vavilala. We identified honokiol, a biphenolic phytochemical extracted from the *Magnolia* genus (which has been used for thousands of years in the traditional Japanese and Chinese medicine) as a potent inhibitor of the HIF pathway. We also observed inhibition of the hypoxia-induced expression of histone lysine

demethylases in a number of cancer and retinal pigment epithelial cell lines when treated with honokiol [122], thus providing an evidence-based scientific explanation of honokiol's therapeutic benefits.

In the second part of the study we evaluated the expression of cancer stem cell markers in VHL deficient renal cell carcinoma cell lines associated with VHL disease. Also, we determined the induction of these CSM markers in RPE cells under hypoxic conditions mimicking VHL loss. Further, the efficacy of honokiol's inhibition of HIF mediated induction of CSM markers was compared with digoxin and doxorubicin (known HIF inhibitors).

Materials and Methods

Chemicals and reagents

All chemicals were supplied by the Sigma-Aldrich Chemical Co. (Saint Louis, MO) unless otherwise stated, and were of analytical grade or higher. Honokiol was purchased from the Stanford Chemicals (Irvine, CA), while digoxin and doxorubicin were ordered from Carbosynth LLC (San Diego, CA).

Cell Culture:

Human retinal pigment epithelial cell lines (D407 and ARPE19) and renal cell carcinoma derived cell lines (RCC4, RCC4-T314, PRC3, and WT8) were used for these studies. RCC4 and PRC3 cells lack a functional *VHL* gene, whereas RCC4-T314 and WT8 cells have a wt-*VHL* incorporated into them. The RCC4, RCC4-T314, PRC3, and WT8 cell lines were generously provided by Dr. M. Celeste Simon (University of Pennsylvania Cancer Center), while D407 cell line was generously gifted by Dr. Richard Hunt (University of South Carolina). DMEM medium, supplemented with 10% heat inactivated FBS, 100 µg/ml of streptomycin, and 100 U/ml of penicillin (media components were purchased from Corning), was used to grow D407, ARPE19, RCC4, and T314. PRC3 and WT8 were maintained in the above mentioned media supplemented with 1 mg/ml G418. Cells were cultured in a CO_2 incubator that was maintained at 37°C, 5% CO_2, and 90% relative humidity.

Treatment of cells with HIF inhibitors

Digoxin, Doxorubicin, and Honokiol used for the study were prepared in DMSO. Dimethyloxalylglycine (DMOG), a general 2OG-dependent dioxygenase inhibitor, was prepared in water. The inhibition studies were carried out by adding 1mM DMOG or 1 μM of digoxin or 1 μM of doxorubicin or 20 μM of honokiol in to the media in a flask containing ≈70% confluent cells. In the control samples 0.1% of DMSO, corresponding to the DMSO concentration in the cells treated with highest inhibitor concentration, was added.

Hypoxia treatment

Cells were subjected to hypoxic condition using an artificial gas mix of 1% O_2, 5% CO_2, and 94% N_2 in a Bactron Anaerobic Chamber. Prior to the treatment the system was purged to generate the hypoxic atmosphere inside the chamber according to the manufacturer's instructions. Once the cells were ready for treatment (~70% confluent), they were aseptically transferred into the chamber through the airlocks to maintain hypoxic conditions inside the chamber and incubated for 12 hrs or time indicated at 37°C. Cell lysis for RNA extraction was performed after exposure to hypoxia for 12 h in the hypoxic chamber to avoid equilibration of the cells to normoxic conditions. RCC4, T314, PRC3 and WT8 cell lines were treated in a similar way, albeit under normoxic conditions due to absence of wt-pVHL in RCC4 and PRC3, which mimic hypoxic conditions with respect to the HIF pathway.

RNA Extraction from Cells

Cells grown under normoxic or hypoxic conditions were lysed in TRI® reagent and the lysate was collected into a micro centrifuge tube. Following phase separation with chloroform, the aqueous phase containing RNA was separated. To this aqueous layer, 100% isopropanol was added to precipitate RNA. The RNA pellet obtained was washed twice with 75% ethanol and dissolved in DNase/RNase-free water. The concentration of RNA was determined using Nanodrop (Thermo Fisher Scientific, Wilmington, DE, USA). RNA was reverse transcribed using M-MLV reverse transcriptase (Promega). The reverse transcription was initiated by denaturation for 5 minutes at 70°C followed by reverse transcription for 1 hour at 42°C and final extension for 5 minutes at 72°C.

Quantitative Real time PCR Analysis

The primers for all the genes analyzed by quantitative real time PCR were designed with the primer design tool of Genscript. Two sets of primer pairs from different regions were manually selected for each gene. The oligonucleotides were synthesized by Integrated DNA Technologies and are listed in Table 6. All the quantitative real time PCR reactions were set up in biological triplicates and experimental duplicates. Each quantitative real time PCR reaction contained 80 ng of cDNA, 2.5 units of Taq polymerase, 0.25mM dNTP, 1X SYBR green and 1.5 µM of forward and reverse primers in 20 µl of total reaction volume. The reactions were set in a 96 well qPCR plates in a Roche LightCycler 480II qPCR instrument. The reactions were carried out with initial denaturation at 95°C for 5 minutes, followed by 45 cycles

of denaturation at 95°C for 10 seconds, annealing at 55°C for 10 seconds and extension at 72°C for 10 seconds. Ribosomal protein L32 was used as an internal control to normalize the sample to obtain ΔC_t value. $2^{-\Delta\Delta Ct}$ method was used to analyze the relative gene expression levels.

Table 6: Sequences of primes used for qPCR analysis for the complete panel of KDMs and JMJD1A target genes.

S.No.	Gene - Primer Name	Primer Sequence
1	FBXL10-qPCR-F1	ATGTCCCAGTTTGTGCGTTA
2	FBXL10-qPCR-R1	TGGTGTGGCTGAACTCTAGG
3	FBXL10-qPCR-F2	AAGACACGGTGGAAGAGGAG
4	FBXL10-qPCR-R2	GGTGGATGATTTCATTGCAG
5	FBXL11-qPCR-F1	TGAAGGAAAGCCAGACTGAA
6	FBXL11-qPCR-R1	CACCAAAGTCCACATGGAAG
7	FBXL11-qPCR-F2	CCTGTGTGCAAGGAGAGTGT
8	FBXL11-qPCR-R2	GACTGAGTGAGGCAGTCTGG
9	HR-qPCR-F1	AACCTGGGTTGTTTGGCTTA
10	HR-qPCR-R1	ATCTCTCCATCCCTCTGGTG
11	HR-qPCR-F2	CTGATGCTGACCCAGTTTGT
12	HR-qPCR-R2	CGGATATCAAACTTGACCCA
13	JARID1A-qPCR-F1	AGATGAGGTCACCCGAAGAC
14	JARID1A-qPCR-R1	AGAGAGTGCCTTTCCGTTGT

S.No.	Gene - Primer Name	Primer Sequence
15	JARID1A-qPCR-F2	AGGACTCGGACCAAACTGAC
16	JARID1A-qPCR-R2	GCTGATGACACACGGAAGAC
17	JARID1C-qPCR-F1	TGGAGTCAACATCGCCTAAG
18	JARID1C-qPCR-R1	CAATAAACTGGGCATTGCTG
19	JARID1C-qPCR-F2	TGCTGGAGAAGGGTATCACA
20	JARID1C-qPCR-R2	CTTGATACACTGGCGCTCAT
21	JARID1D-qPCR-F1	TTCTGTGATGGCTGTGATGA
22	JARID1D-qPCR-R1	CTGTTTACACTCCGCCAAGA
23	JARID1D-qPCR-F2	ACACTCCACAGCTGACCTTG
24	JARID1D-qPCR-R2	CTTGATAGGCCTCCACCTGT
25	JARID2-qPCR-F1	TTCTCTGCCTTCGAGGTTCT
26	JARID2-qPCR-R1	CTGGCATGAAGATGAAGCAT
27	JARID2-qPCR-F2	CAAGGTGGACACCAACACTC
28	JARID2-qPCR-R2	ATGGACCCTGTGTTATTGGG
29	JHDM1A-qPCR-F1	TGAGCGTGAAAGGTTGTTTC
30	JHDM1A-qPCR-R1	CATGGTACCAAACGGAAGTG
31	JHDM1A-qPCR-F2	TGCTCAAGGAGCAGAAGATG
32	JHDM1A-qPCR-R2	GCCTCCTCACACTCACTCCT
33	JHDM1D-qPCR-F1	GCTCTCGAGTCTTCCCAAGT
34	JHDM1D-qPCR-R1	TAGGTGAAGGGAGCCTGAGT
35	JHDM1D-qPCR-F2	TTCGAGCAATAGAGGAGGAAA

S.No.	Gene - Primer Name	Primer Sequence
36	JHDM1D-qPCR-R2	CATCTTTCTTCGGGAATGGT
37	JHDM2A-qPCR-F1	AATTGTACAGTGGCCTGCAA
38	JHDM2A-qPCR-R1	ATCTCCCAGAAAGCGAACAG
39	JHDM2A-qPCR-F2	CAGCCAGCACATCTCCTCTA
40	JHDM2A-qPCR-R2	GGATTTGCTTAAAGGTGGGA
41	JHDM2B-qPCR-F1	CATTCGAGTCTCCATTGCAC
42	JHDM2B-qPCR-R1	TGAAACAGATGCAACCCATT
43	JHDM2B-qPCR-F2	TCTCACTGGATGAACGAAGC
44	JHDM2B-qPCR-R2	CAGCTGCTCCTCAGAGTCAC
45	JMJD1A-qPCR-F1	TCTGAGGCCTCTCCCAGTAT
46	JMJD1A-qPCR-R1	ACTTTGCTGTCTTGGGTCCT
47	JMJD1A-qPCR-F2	CAGCCAGCACATCTCCTCTA
48	JMJD1A-qPCR-R2	GGATTTGCTTAAAGGTGGGA
49	JMJD1B-qPCR-F1	CATTCGAGTCTCCATTGCAC
50	JMJD1B-qPCR-R1	TGAAACAGATGCAACCCATT
51	JMJD1B-qPCR-F2	CAGACAGTTCGGCATCAAAT
52	JMJD1B-qPCR-R2	TTGCTAAATCTGCCAACCAG
53	JMJD1C-qPCR-F1	TGTAAGCGACCTCGAGAGAA
54	JMJD1C-qPCR-R1	CGCTCTTTGTCATCAGCACT
55	JMJD1C-qPCR-F2	GCAAGTGAGCTCAGAAATGC
56	JMJD1C-qPCR-R2	TCAGAAATCCACAACAAGGC

S.No.	Gene - Primer Name	Primer Sequence
57	JMJD2A-qPCR-F1	ATCACCATTGAGGGTGTGAA
58	JMJD2A-qPCR-R1	ATGTCTTCAGTGTGCCAAGC
59	JMJD2A-qPCR-F2	AGGAAGAGGCTGAGGAGACA
60	JMJD2A-qPCR-R2	ATACAGACAGCGCAGTGAGG
61	JMJD2D-qPCR-F1	AAATCCAACGACTCCTGCTT
62	JMJD2D-qPCR-R1	TTGTAAAGATCGTGGTTGCC
63	JMJD2D-qPCR-F2	CACCGATTTATGGTGCTGAC
64	JMJD2D-qPCR-R2	TGACGCCTTCTATGACAACC
65	JMJD3-qPCR-F1	GGGCAACTGTACGAGTCAGA
66	JMJD3-qPCR-R1	GAAGCTTCCTCCGTATCGAA
67	JMJD3-qPCR-F2	GCCGAATTCAAGATCCTACC
68	JMJD3-qPCR-R2	CGTGTTGTTGCTGTTCCTCT
69	JMJD6-qPCR-F1	CCGGCACAACTACTACGAGA
70	JMJD6-qPCR-R1	CTTTCATACCGCTCCACAAA
71	JMJD6-qPCR-F2	GCCTGTTTCCTACCAGCACT
72	JMJD6-qPCR-R2	TAGCTTCGTCTTGCTGGTTC
73	PHF8-qPCR-F1	GGTTTCATGGCAGTTGTGTT
74	PHF8-qPCR-R1	GGGCAGTGGTAGAGGTCAAT
75	PHF8-qPCR-F2	GCCTTAACATCGAGATGCAG
76	PHF8-qPCR-R2	TCTGAAGAGGTCTGCTGTGC
77	PHF2-qPCR-F1	CCATCCTCGTCCCTAAGAAA

S.No.	Gene - Primer Name	Primer Sequence
78	PHF2-qPCR-R1	TCAGCTTCATCTTGCAGTCC
79	PHF2-qPCR-F2	TCTCACAAATCTGGGAAGCA
80	PHF2-qPCR-R2	GCTGTGAAGGTTTGAAGTGC
81	ADM1-qPCR-F1	CACTTCGGGCTTCTCACTG
82	ADM1-qPCR-R1	AAAGTCTCAGACGTCCCACTG
83	ADM1-qPCR-F2	GGTGTCTTCTAAGCCACAAGC
84	ADM1-qPCR-R2	CTCGGGAAGTCCTTCGTC
85	EDN2-qPCR-F1	CAGTTCTGTGTCCTCGCACT
86	EDN2-qPCR-R1	GCAGCCTCCAGATGAATGTA
87	EDN2-qPCR-F2	CTATGGTCTCCGTGCCTACC
88	EDN2-qPCR-R2	TTGGGCATGAGATGAGGAC
89	EDN1-qPCR-F1	TCATGATCCCAAGCTGAAAG
90	EDN1-qPCR-R1	AGGCTATGGCTTCAGACAGG
91	EDN1-qPCR-F2	GTTCAGTTTGAACGGGAGGT
92	EDN1-qPCR-R2	TGAGCTCAGCGCCTAAGAC
93	GDF15-qPCR-F1	GCTACGAGGACCTGCTAACC
94	GDF15-qPCR-R1	GAGGTCGGTGTTCGAATCTT
95	GDF15-qPCR-F2	CAAGAACTCAGGACGGTGAA
96	GDF15-qPCR-R2	ATCTGGAGTCTTCGGAGTGC
97	HMOX1-qPCR-F1	GGCTTTATGCCATGTGAATG
98	HMOX1-qPCR-R1	GTAAGGAAGCCAGCCAAGAG

S.No.	Gene - Primer Name	Primer Sequence
99	HMOX1-qPCR-F2	CATGCAGCGCTATGTGAAG
100	HMOX1-qPCR-R2	AGACAGGTCACCCAGGTAGC
101	SERPENB8-qPCR-F1	CCATTTCTCGTCTCATGCTC
102	SERPENB8-qPCR-R1	AGGGTTAAATCAGAGGGCAA
103	SERPENB8-qPCR-F2	CTCGCCGTGAAAGAGTGAT
104	SERPENB8-qPCR-R2	GGGAGCATGAGACGAGAAAT
105	SERPINE1-qPCR-F1	CACTGGAAAGGCAACATGAC
106	SERPINE1-qPCR-R1	TCGTGAAGTCAGCCTGAAAC
107	SERPINE1-qPCR-F2	GGATGAGATCAGCACCACAG
108	SERPINE1-qPCR-R2	GGAACAGCCTGAAGAAGTGG
109	VEGF-qPCR-F2	CTTGCCTTGCTGCTCTAC
110	VEGF-qPCR-R2	TGGCTTGAAGATGTACTCG
111	Glut1 – qPCR-F1	CGGGCCAAGAGTGTGCTAAA
112	Glut1 – qPCR-R1	TGACGATACCGGAGCCAATG
113	CD24 – F1	TGCTCCTACCCACGCAGATT
114	CD24 – R1	TCAGAGGAGTAGGAGAGAGGAAAC
115	CD44 – F1	TCAGAGGAGTAGGAGAGAGGAAAC
116	CD44 – R1	GAAAAGTCAAAGTAACAATAACAGTGG
117	NOTCH1 – F1	CACTGTGGGCGGGTCC
118	NOTCH – R1	GTTGTATTGGTTCGGCACCAT
119	CD34 – F1	TCCAGAGACAACCTTGAAGC

S.No.	Gene - Primer Name	Primer Sequence
120	CD34 – R1	CTTCTTAAACTCCGCACAGC
121	CD144 – F1	TTCATGACGTGAACGACAAC
122	CD144 – R1	TCCACCACGATCTCATACCT
123	SOX2 – F1	GTATCAGGAGTTGTCAAGGCAGAG
124	SOX – R1	TCCTAGTCTTAAAGAGGCAGCAAAC
125	NANOG – F1	TTTGGAAGCTGCTGGGGAAG
126	NANOG – R1	GATGGAGGGAGGGGAGAGGA
127	C-MYC – F1	CGGAACTCTTGTGCGTAAGG
128	C-MYC – R1	CTCAGCCAAGGTTGTGAGGT
129	KLF4 – F1	TATGACCCACACTGCCAGAA
130	KLF4 – R1	TGGGAACTTGACCATGATTG
131	CD133 – F1	TCCACAGAAATTTACCTACATTGG
132	CD133 – R1	CAGCAGAGAGCAGATGACCA
133	OCT3/4 – F1	ACATGTGTAAGCTGCGGCC
134	OCT3/4 – R1	GTTGTGCATAGTCGCTGCTTG
135	LGR5 – F1	CTTCCAACCTCAGCGTCTTC
136	LGR5 – R1	TTTCCCGCAAGACGTAACTC
137	LEF1 – F1	TCCTGAAATCCCCACCTTCT
138	LEF1 – R1	TGGGATAAACAGGCTGACCT
139	TCF7 – F1	CAGCTCCCCCATACTGTGAG
140	TCF7 – R1	TGCTGTCTATATCCGCAGGAA

Results and Discussions

Validation of qPCR primers

The RCC4 clear-cell renal cell carcinoma cell line lacks VHL, an ubiquitin ligase, responsible for targeting the hydroxylated HIF-α for proteosomal degradation. Hence this cell line has stable HIF-α protein even under normoxic conditions, and translocates to the nucleus to constitutively activate the HIF pathway similar to the hypoxic conditions. T314 cells were derived from RCC4 cells by stably transfecting VHL. These cells express normal levels of VHL, and thus, do not activate HIF pathway under normoxic conditions. Due to this established link between VHL loss and activation of HIF pathway, RCC4 and T314 cell lines are ideal cell-based systems for studying the HIF-mediated transcription phenomena [123].

The cDNA from RCC4 and T314 cells were synthesized and utilized to validate the primers used in this study. In cases where the C_t values (number of PCR cycles elapsed before threshold) for the two primer pairs for a same gene were apart by more than 0.5 cycles, additional primer pairs were designed to produce consistent results by two independent primer pairs for the same gene (data not shown). As expected these experiments demonstrated an upregulation of a number of Jmj domain containing iron (II), 2OG-dependent KDMs in RCC4 cells (Figure 26), which represents the constitutively active HIF pathway. These experiments also validated our qPCR primers and experimental conditions.

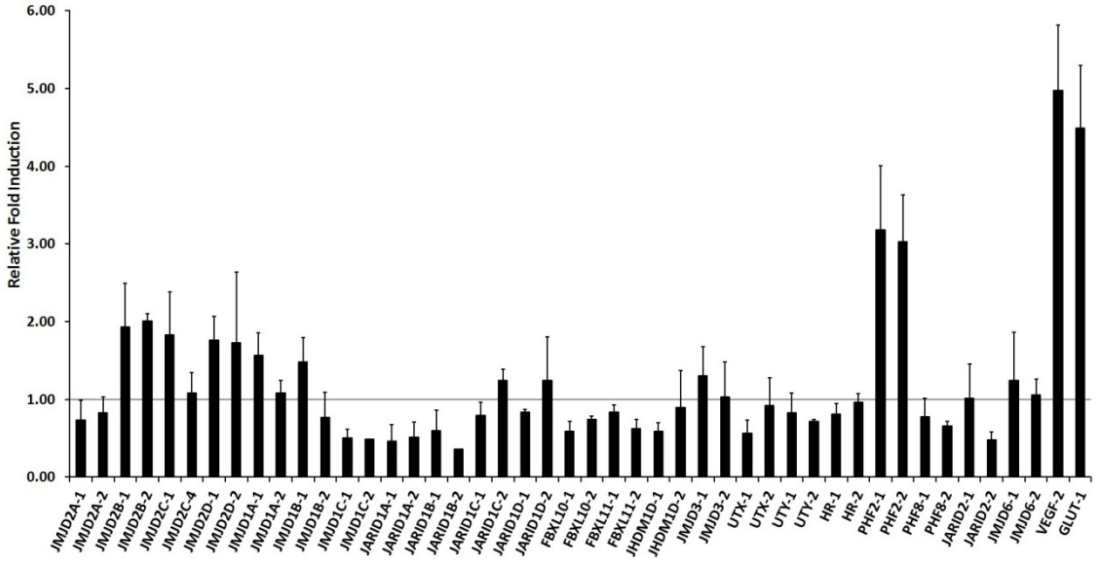

Figure 26: Expression of KDMs in RCC4 and T314 cells after 36 hours of culture under normoxic condition. RCC4 cells lack VHL, hence possess stable HIF-α protein even under normoxic condition and constitutively activate HIF pathway similar to the hypoxic conditions. By contrast, T314 cells have stably transfected VHL and hence do not activate HIF pathway under normoxic conditions.

Hypoxia induces expression of KDMs in retinal pigment epithelial cells

An activation of the HIF pathway leading to induction of pro-angiogenic genes such as *VEGF* is responsible for a number of hypoxia induced retinal diseases such as VHL, proliferative diabetic retinopathy, glaucoma, and retinopathy of prematurity [113]. Since retinal pigment epithelial cells are one of the major cell constituents and secretor of VEGF in the retina [124], a human retinal pigment epithelial cell line (D407) was selected for these studies [125, 126]. These cells are spontaneously transformed cells derived from the primary culture of human retinal pigment epithelial cells. Recent studies have shown that these cells exhibit high levels of *VEGF* induction at both mRNA and protein levels under hypoxic conditions, and hence serve as a good model for evaluating the response of *VEGF* and other hypoxia regulated genes [125].

For all further studies a time course experiment (3, 6, 12 and 24 hours) was performed with D407 cells to identify the point where hypoxia responsive genes demonstrate the highest induction. For these studies the expression of known hypoxia responsive genes (*GLUT1* and *VEGF*) and three KDMs (*JMJD2B*, *JMJD2C* and *JMJD1A*) that are direct transcriptional targets of HIF were chosen as markers. These experiments showed that the expression of the tested genes peaked after ~24 hours of hypoxic treatment (Figure 27).

Based on these results the expression of the entire panel of KDMs was compared under hypoxic (1% O_2) and normoxic (21% O_2) conditions after 24 hours. The C_t values were normalized with their respective internal control (ribosomal protein

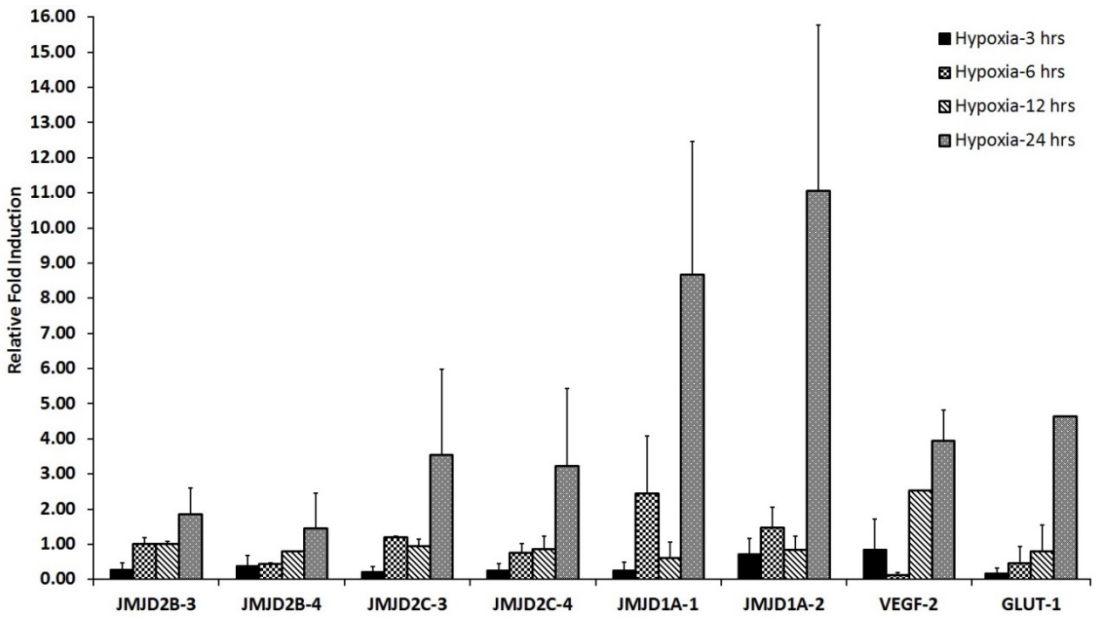

Figure 27: Time course experiment on D407 cells to determine an appropriate time for all further analysis. Three known KDM targets and known hypoxic response genes VEGF and GLUT1 were used as markers to determine the time point. Cells were harvested at 3, 6, 12 and 24 hrs followed by RNA extraction and qPCR reaction.

L32) and fold changes were calculated by comparing the hypoxia treated samples to their corresponding normoxia samples. *VEGF* and *GLUT1* genes, known hypoxic response genes, demonstrated ~6 and ~8 fold induction, respectively (Fig. 21). In addition, transcription of 14 out of the 20 Jmj domain containing iron (II), 2OG-dependent KDMs (*JMJD2B*, *JMJD1A*, *JMJD1B*, *JMJD1C*, *JARID1A*, *JARID1B*, *JARID1C*, *FBXL10*, *JHDM1D*, *JMJD3*, *UTX*, *HR*, *JARID2* and *JMJD6*) showed ≥1.5 fold induction with both primer pairs under hypoxic conditions (Figure 28).

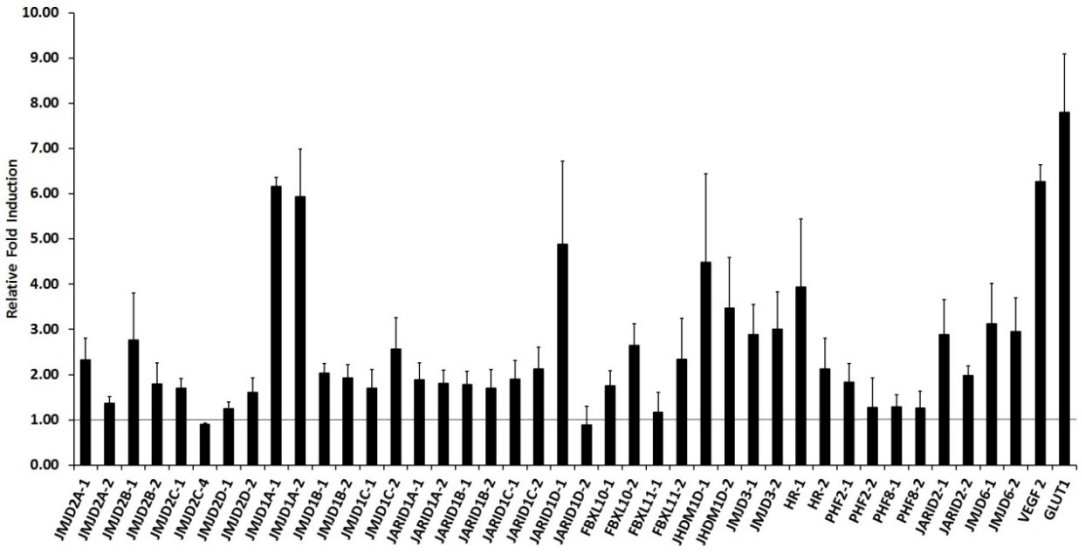

Figure 28: Expression of histone lysine demethylases in D407 cells with 24 hours hypoxia treatment. Ribosomal protein L32 was used as an internal control and all samples were normalized to their corresponding normoxia samples whose expression level was set to be 1.

Out of these 14 KDMs that are induced by hypoxia in retinal pigment epithelial cells, 13 were also induced in a number of cancer cell lines [127], suggesting an important role of these genes in hypoxic adaptation and neovascularization in cancer and retinal diseases. *JMJD1A* exhibited ~6 fold induction under hypoxia by the two independent primer pairs (Figure 28), similar to the levels observed for *VEGF* and *GLUT1*, suggesting a role in regulating the transcription of some important pro-angiogenic genes under hypoxic conditions.

Hypoxia induces expression of JMJD1A target genes in retinal pigment epithelial cells

Our studies have demonstrated that *JMJD1A* was one of the strongly induced KDMs under hypoxic condition. It is also a direct transcriptional target of HIF-α [69-71]. *JMJD1A* (also known as *KDM3A* or *JHDM2A*) acts as a coactivator for nuclear hormone receptors and regulates transcription by demethylating di- and mono-methylated histone-3 lysine-9 (H3K9-me2 and H3K9-me) into H3K9, respectively, at target promoters [128]. Recent studies have indicated that the expression of a subset of hypoxia induced genes (53 out of 821) is dependent on the expression of *JMJD1A* [69]. This subset included well known hypoxia induced genes such as *ADM*, *EDN1*, *EDN2*, *GDF15*, *HMOX1*, *SERPE1* and *SERPB8*. These genes play critical roles in vascular dilation (*ADM*) [129] and angiogenesis (*ADM*, *EDN1*, *SERPINE1*, and *HMOX1*) [130].

Therefore, to further investigate the role of *JMJD1A* in angiogenesis under hypoxic conditions in D407 cells, we evaluated the induction of *ADM*, *EDN1*, *EDN2*, *GDF15*, *HMOX1*, *SERPE1* and *SERPB8*, the known targets of *JMJD1A*. After 24 hours of hypoxia treatment, significant induction was noted for these downstream targets of

JMJD1A compared to normoxic conditions (Figure 29). These results also confirm a role of *JMJD1A* in hypoxia-mediated transcription.

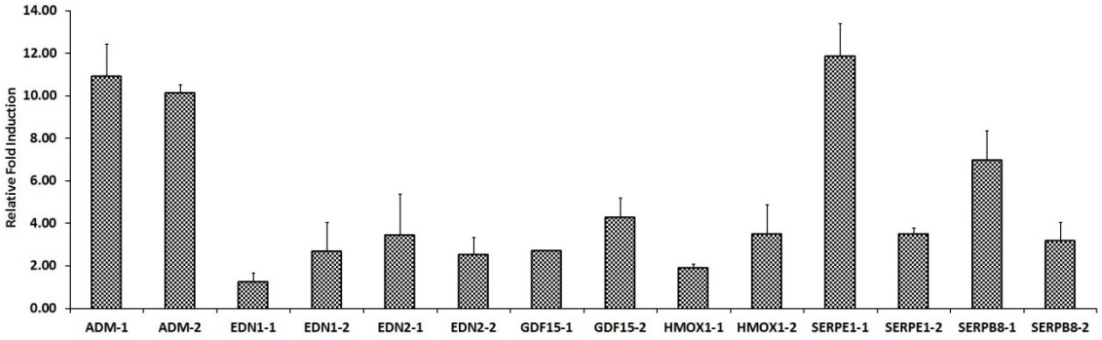

Figure 29: Expression of JMJD1A target genes in D407 cells under hypoxia. Ribosomal protein L32 was used as an internal control and all samples were normalized to their corresponding normoxia samples whose expression level was set to be 1.

Effect of dimethyloxalylglycine on JMJD1A-mediated pro-angiogenic gene expression

The downregulation of HIF pathway can inhibit neovascularization observed in cancer and retinal diseases. Since the HIF pathway induces the expression of a number of Jmj domain containing iron (II), 2OG-dependent KDMs and other pro-angiogenic genes whose expression is dependent on KDMs (such as *JMJD1A*), we explored if a general KDM inhibitor such as dimethyloxalylglycine (DMOG, a 2OG analog; Figure 30) can inhibit HIF pathway-mediated expression of pro-angiogenic genes.

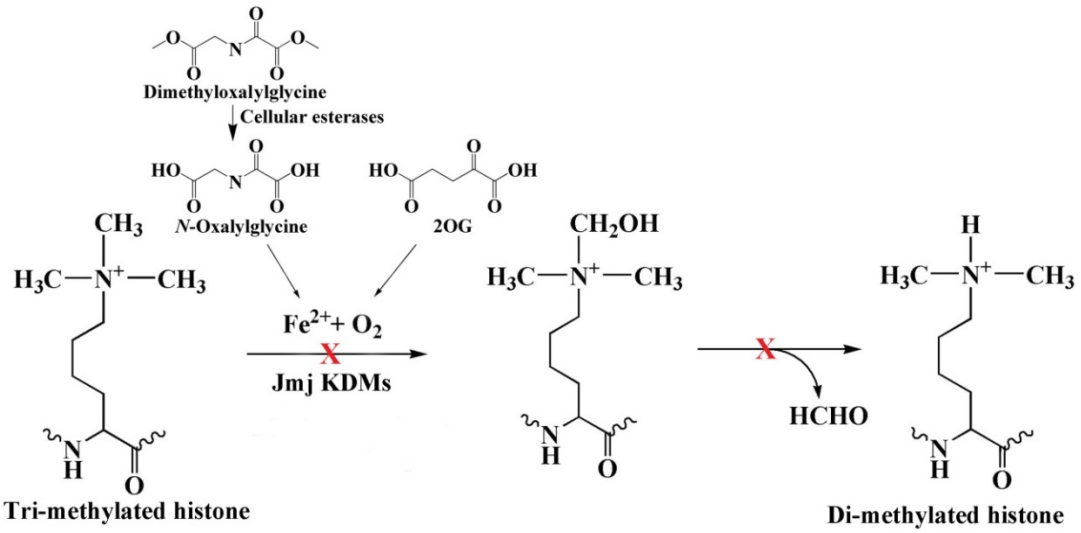

Figure 30: Schematic representation of biochemical reaction carried by iron(II), 2OG-dependent Jmj histone lysine demethylases (KDMs). Dimethyloxalylglycine (DMOG), which gets converted into *N*-oxalylglycine by cellular esterases, act as a competitive inhibitor for 2OG due to structural similarity.

To evaluate such effect of this general inhibitor on the expression of these KDMs and genes regulated by *JMJD1A*, both normoxic and hypoxic cells were treated with 1mM DMOG for 24 hours. These experiments also revealed an overall consistent level of KDMs' induction in DMOG-treated hypoxic cells compared to DMOG-treated normoxic cells (Figure 31). Some KDMs showed slightly lower induction in DMOG-treated hypoxic cells compared to untreated hypoxic cells suggesting a role for other iron (II), 2OG-dependent dioxygenases, e.g. *AlkB* family DNA demethylases (a recent paper showed that *AlkB5* is also a direct HIF target) in hypoxia-mediated KDMs' transcription [131].

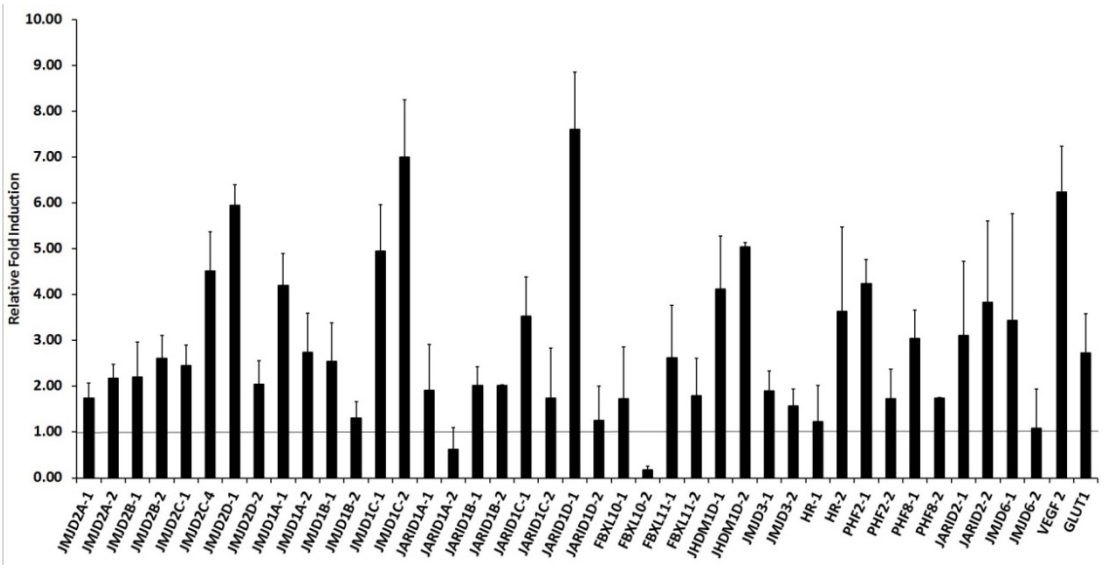

Figure 31: Expression of histone lysine demethylases in D407 cells with 24 hours of 1mM DMOG treatment under hypoxia and normoxia. Ribosomal protein L32 was used as an internal control and all samples were normalized to their corresponding normoxia samples whose expression level was set to be 1.

Importantly, treatment of retinal pigment epithelial cells with DMOG exhibited statistically significant inhibition of expression of five (*ADM*, *GDF15*, *HMOX1*, *SERPE1* and *SERPB8*) out of the seven (*ADM*, *EDN1*, *EDN2*, *GDF15*, *HMOX1*, *SERPE1* and *SERPB8*) tested pro-angiogenic JMJD1A target genes (Figure 32). These five inhibited genes included both of the known direct transcriptional targets of *JMJD1A* (*JMJD1A* induces expression of *ADM* and *GDF15* by directly demethylating H3K9-me2 and H3K9-me into H3K9 at their promoters) [69].

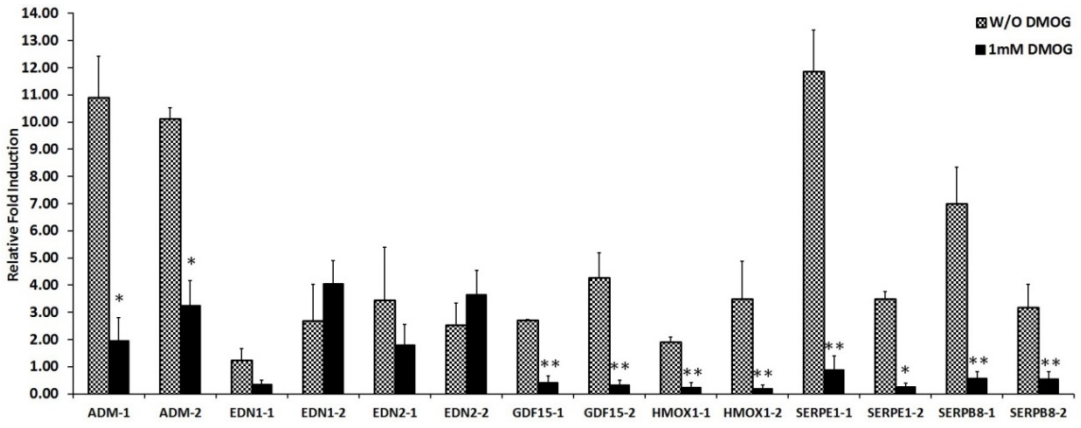

Figure 32: Expression of JMJD1A target genes in untreated vs 1mM DMOG treated D407 cells under 24 hours hypoxic condition. Ribosomal protein L32 was used as an internal control and all samples were normalized to their corresponding normoxia samples whose expression level was set to be 1. Student t-test was performed for all the samples to determine the statistical significance. * represents P <= 0.05 and ** represents P<= 0.001 as compared to untreated samples.

Thus, our results identify a new layer of epigenetic transcription regulation under hypoxia (Figure 33), and suggest that use of specific inhibitors of KDMs such as JMJD1A can be a new therapeutic approach to treat a number of diseases caused by the hypoxia induced neovascularization.

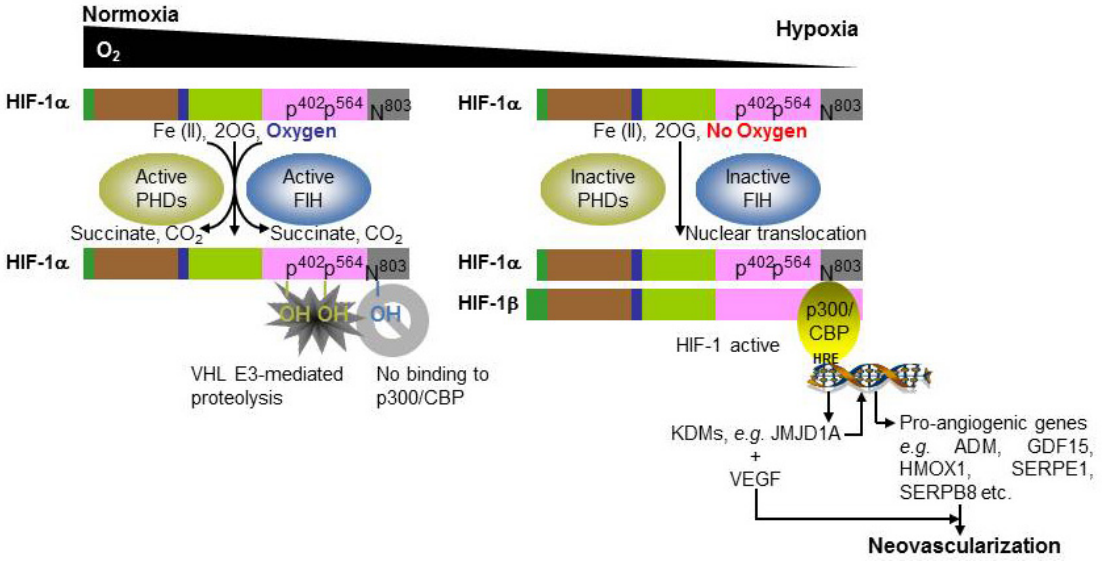

Figure 33: Control of HIF-α by the proline and aspartate hydroxylases. Under normoxic conditions (left panel), PHDs and FIH hydroxylate HIF-α on proline (P402/564) and aspartate (N803) residues, respectively, leading to ubiquitin ligase VHL E3-mediated destruction or inhibition of interaction with the transcription co-activator p300/CBP. However, under hypoxic conditions (right panel), these oxygen-sensitive hydroxylases become less active, allowing stabilization of HIF-α and its dimerization with HIF-α/β leading to transcription of hypoxia response genes, which includes a number of KDMs. The expressions of some pro-angiogenic genes are dependent on KDM expression. The fragment colors of HIF subunits represent different protein domains.

HIF-mediated expression of pro-angiogenic genes in renal cell carcinoma and retinal pigment epithelial cell lines

The human RCC4 cell line lacks wt-pVHL and hence has a constitutively active HIF pathway. RCC4-T314 cells were derived from the RCC4 cells by stably transfecting wt-*VHL*, and thus, these cells do not activate the HIF pathway under normoxia. Under hypoxia, HIF-α isoforms are stabilized in RCC4-T314 cells leading to activation of the HIF pathway [123]; By contrast, 786-O cells, another renal cell carcinoma cell line that is also *VHL*–/–, expresses only HIF-2α [132, 133]. Unlike *VHL*–/– RCC4 cells [123], HIF-1α is not detectable in *VHL*–/– 786-O cells [133]. The loss of HIF-1α expression in some *VHL*–/– RCC cells confers an *in vivo* growth advantage [134], possible due to the role of HIF-1α in apoptosis [108]. Reintroduction of wt-*VHL* in 786-O cells leads to downregulation of HIF-2α protein levels, restores normal oxygen-dependent regulation of HIF-2α subunit and transcription of pro-angiogenic genes which, in turn, suppresses tumor formation in mouse xenografts [132, 133, 135]. Importantly, a HIF-2α variant, which lacks pVHL-binding sites, prevents tumor suppression by exogenously introduced wt-*VHL* in *VHL*–/– cells [134, 136]. Conversely, downregulation of HIF-2α in *VHL*–/– cells, similar to the effects observed with the reintroduction of wt-*VHL* in these cells [132, 135], serves to inhibit expression of pro-angiogenic genes, inhibits the proliferation of vascular endothelial cells, and to suppress tumor growth by *VHL*–/– cells [137]. Further, HIF-α inactivation abolishes the cellular response to hypoxia *in vitro*, indicating that HIF-α is the only pVHL target required for this response, and the tumor forming ability of *VHL*–/– 786-O cells is

dependent on the constitutive activation of the HIF pathway. Due to this established link between VHL loss and activation of the HIF pathway, RCC4 and PRC3 (*i.e.* 786-O cells with empty vector) cell lines with their *VHL*+/+ counterparts (RCC4-T314 and WT8) are ideal cell-based system for determining the HIF-mediated transcription phenomena.

The cDNA from RCC4, RCC4-T314, PRC3, and WT8 cells were synthesized under normoxic conditions and the level of expressions of pro-angiogenic genes were compared. These experiments demonstrated a significant upregulation of a number of HIF-dependent pro-angiogenic genes in RCC4 and PRC3 cells compared to RCC4-T314 and WT8 cells (Figure 34A and Figure 34B), respectively, representing the constitutively active HIF pathway in these cells. Our studies also demonstrated that Jmj-domain containing protein 1A (JMJD1A) was one of the strongly induced histone lysine demethylases in *VHL*–/– renal cell carcinomas cell lines (Figure 26). Recent studies in renal cell carcinomas have revealed that higher levels of JMJD1A are present around the blood vessels, suggesting its role in angiogenesis [138]. JMJD1A regulates the expression of adrenomedullin (ADM) and growth differentiation factor 15 (GDF15) by directly binding to their promoters and demethylating dimethylated histone-3 lysine-9 [69]. These genes play critical roles in HIF-dependent signaling and angiogenesis [139, 140]. Therefore, we further investigated the expression of these two JMJD1A targets and observed significant induction in *VHL*–/– renal cell carcinoma cell lines compared to their *VHL*+/+ counterparts. Further, since a retinal cell line similar to RCC4 and PRC3 cells with respect to VHL inactivation is not available, we determined that

treating the human retinal pigment epithelial cell lines (D407 and ARPE-19) with hypoxia induces the expression of these pro-angiogenic genes. Similar to the renal cell carcinoma cells, our results demonstrated that hypoxia indeed induced the expression of pro-angiogenic genes, JMJD1A, and its target genes in these retinal pigment epithelial cell lines (Figure 34C and Figure 34D). Overexpression of some of these markers was also confirmed at protein levels by western blots (data not shown).

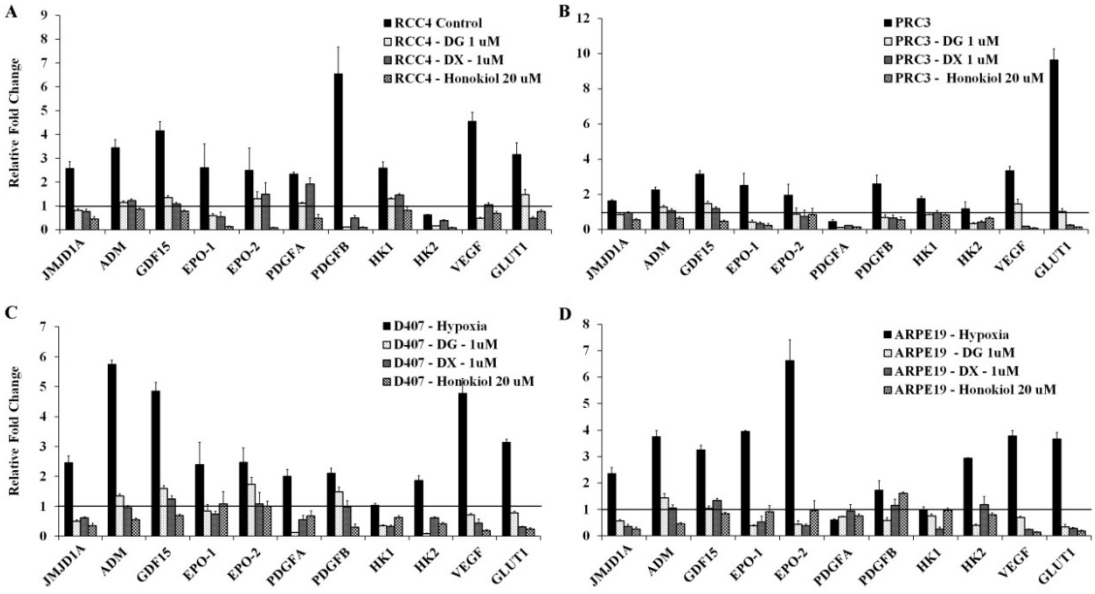

Figure 34: Relative fold change in the mRNA levels of indicated pro-angiogenic genes in: RCC4 (Panel A), PRC3 (Panel B), D407 under hypoxia (Panel C), and ARPE19 under hypoxia (Panel D) in the presence or absence of 1 μM digoxin (DG), 1 μM doxorubicin (DX), and 20 μM honokiol. Solid, beveled, grey, and checked bars represent relative mRNA fold change ± standard error for control, 1 μM DG, 1 μM DX, and 20 μM honokiol treatments, respectively. Normoxic levels are represented by the horizontal line.

HIF-mediated expression of stem cell markers in renal cell carcinoma and retinal pigment epithelial cell lines

A number of studies have shown a coexistence of pro-angiogenic and stem cell markers in hemangioblastomas [116, 117]. Therefore, it has been suggested that hemangioblastomas originate from developmentally arrested stem cells or embryonic progenitors [116-119]. However, recent studies have shown that the HIF pathway also plays a role in the expression of stem cell markers in cancer cells [141, 142]. Therefore, we evaluated the extent to which these markers are induced under normoxic conditions in *VHL–/–* RCC4 and PRC3 cells compared to RCC4-T314 and WT8 cells, respectively, and under hypoxic conditions in noncancerous retinal pigment epithelial cells (D407 and ARPE19).

For these studies, markers from different pathways downstream to the HIF pathway were selected. These markers play important roles in stem cell maintenance/differentiation [143], and can be classified into: (i) Wnt pathway markers [Lymphoid enhancer-binding factor 1 (*LEF1*), Leucine-rich repeat-containing G protein-coupled receptor 5 (*LGR5*) and Transcription Factor 7 (*TCF7*)]; (ii) drug resistance proteins [Multi-drug resistance 1(*MDR1*, also known as P-glycoprotein 1 or P-gp), Multidrug resistance-associated protein 2 (*MRP2*) and Breast cancer resistance protein (*BCRP*)]; (iii) Yamanaka factors [Octamer-binding transcription factor 4 (*OCT3/4*), Kruppel-like factor 4 (*KLF4*), c-myc, and Sex determining region Y-box 2 (*SOX2*)]; and (iv) cancer stem cell-associated markers [Aldehyde Dehydrogenase 1

(*ALDH1*), Cluster of differentiation 24 (*CD24*), Cluster of differentiation 34 (*CD34*), Cluster of differentiation 44 (*CD44*), Cluster of differentiation 133 (*CD133*), Cluster of differentiation 144 (*CD144*, also known as VE-cadherin), *NANOG*, and *NOTCH1*].

Upon activation of the HIF pathway, either due to the loss of functional pVHL or due to hypoxia, we detected overexpression of 2 out of 3 Wnt pathway markers (*i.e. LEF1*, *LGR5*), 1 out of 3 drug resistance proteins (*i.e. MDR1*/*P-GP*), and 4 out of 8 other stem cell/cancer stem cell markers (*i.e. CD133*, *CD144*, *NANOG*, and *NOTCH1*) in most of the cell lines (Figure 35 and Figure 36). In general, over expression of target genes was more pronounced when the HIF pathway was activated by the exposure of cells to hypoxic condition. Taken together, these results show that mutations in the *VHL* gene leads to the activation of the HIF pathway. This activated pathway induces the expression of stem cell/cancer stem cell markers, in addition to overexpression of pro-angiogenic factors. Thus our results suggest a possible mechanism for the origin of neoplastic stromal cells in hemangioblastomas.

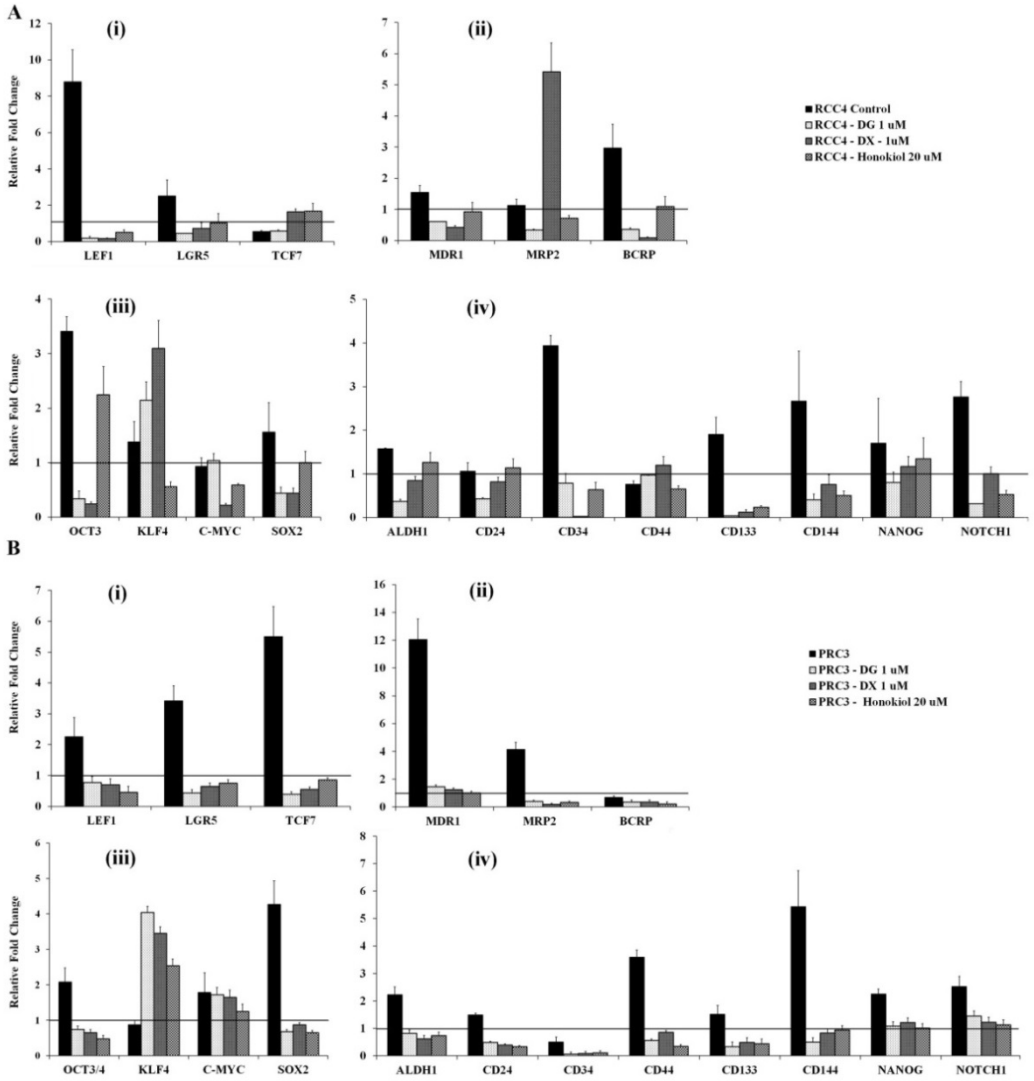

Figure 35: Relative fold change in the mRNA levels of indicated stem cell/cancer stem cell markers in: RCC4 (Panel A) and PRC3 (Panel B) in the presence or absence of 1 μM digoxin (DG), 1 μM doxorubicin (DX), and 20 μM honokiol. In both panels (i) represents Wnt pathway genes, (ii) represents drug resistance genes, (iii) represents Yamanaka factors, and (iv) represents cancer stem cell-associated markers. Solid, beveled, grey, and checked bars represent relative mRNA fold change ± standard error

for control, 1 μM DG, 1 μM DX, and 20 μM honokiol treatments respectively. Normoxic levels are represented by the horizontal line.

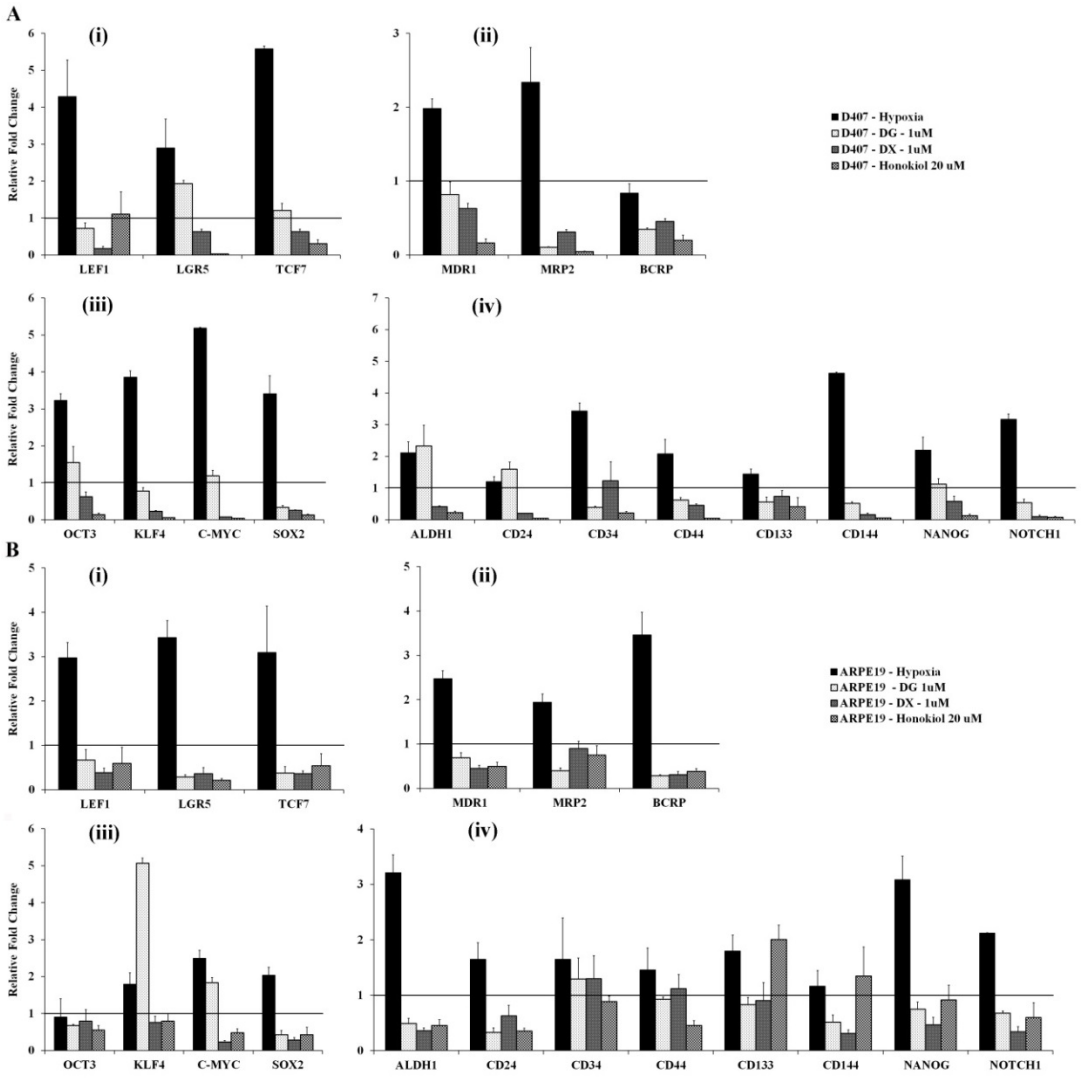

Figure 36: Relative fold change in the mRNA levels of indicated stem cell/cancer stem cell markers in: D407 (Panel A) and ARPE-19 (Panel B) in the presence or absence of 1 μM digoxin (DG), 1 μM doxorubicin (DX), and 20 μM honokiol under hypoxia. In both panels (i) represents Wnt pathway genes, (ii) represents drug resistance genes, (iii) represents Yamanaka factors, and (iv) represents cancer stem cell-associated markers.

Solid, beveled, grey, and checked bars represent relative mRNA fold change ± standard error for control, 1 μM DG, 1 μM DX, and 20 μM honokiol treatments respectively. Normoxic levels are represented by the horizontal line.

Inhibitors of the HIF pathway down-regulates the expression of stem cell marker

In order to conclusively prove that the transcription of pro-angiogenic and stem cell markers is due to the HIF pathway, we evaluated the effectiveness of digoxin, doxorubicin, and honokiol, three recently identified HIF inhibitors from natural sources, to suppress the transcription of selected markers. We found that all the three HIF inhibitors strongly (≈50-90% for most genes) inhibited the expression of HIF-dependent transcription of selected markers in the retinal pigment epithelial cell lines (D407 and ARPE-19) under hypoxia, and *VHL*–/– renal cell carcinoma cells under normoxic conditions (Figure 34, Figure 35, Figure 36). These results confirm that the inhibition of the HIF pathway by digoxin, doxorubicin, and honokiol, is conserved across multiple cell lines without any noticeable cytotoxicity under both hypoxic and normoxic conditions. Importantly, no significant change in the transcription of HIF independent housekeeping genes (ribosomal protein L32, actin and GAPDH) was noted (data not shown). These results suggest that digoxin, doxorubicin, and honokiol are not general transcription inhibitors, but rather are specific inhibitors for the HIF pathway.

The treatment of RCC4, RCC4-T314, APRE-19 and D407 cells with honokiol under normoxia or hypoxia did not alter their proliferation in cell culture (data not shown). These results are consistent with a number of cell-based studies showing that the inhibition of the HIF pathway in *VHL*–/– RCC cells, by reintroduction of wt-*VHL* in

VHL–/– cells, does not inhibit their proliferation in cell culture [134, 136, 137]. However, such inhibition of the HIF pathway abolishes the tumor forming ability of *VHL*–/– 786-O cells in mouse models [134, 136, 137]. Therefore, the inhibitors of the HIF pathway evaluated in this study, all of which are used by humans for other conditions, can be used for the treatment of pVHL-associated hemangioblastomas.

VHL disease is an autosomal dominant tumor syndrome with a predilection for the retina, CNS, and kidney. The incidence of VHL disease is ≈1 in 36,000, and it is estimated that there are ≈7,000 patients with VHL disease in the U.S. alone. The VHL disease is associated with significant mortality with an average life-expectancy of patients is ≈50 years. The mean age at diagnosis of hemangioblastomas in VHL disease is ≈25 years. Ocular hemangioblastoma is observed in up to 85% patients with VHL disease and is the earliest manifestation of the disease. The VHL-associated ocular hemangioblastomas can cause massive exudation, subretinal edema, inflammation, retinal detachment, or glaucoma, resulting in loss of vision. Current treatment with laser photocoagulation or cryotherapy can cause subretinal and vitreous hemorrhage. Further, using such methods, it is difficult to specifically target and treat optic disc lesions. Anti-VEGF therapies have been largely ineffective [120, 121], possibly due to contribution of other pro-angiogenic factors, such as EPO, PDGF, etc. in hemangioblastomas. Thus, there remains an unmet medical need to develop more effective treatments for hemangioblastomas. Based on our studies, we propose a model where mutations in the *VHL* gene lead to activation of the HIF pathway in patients with hemangioblastomas. This results in the expression of stem cell/cancer stem cell markers, in addition to

overexpression of pro-angiogenic factors, in neoplastic stromal cells (Figure 37). Finally, the current study evaluates the use of HIF inhibitors as an effective therapeutic agent for the treatment of hemangioblastomas, for which limited treatment options are currently available.

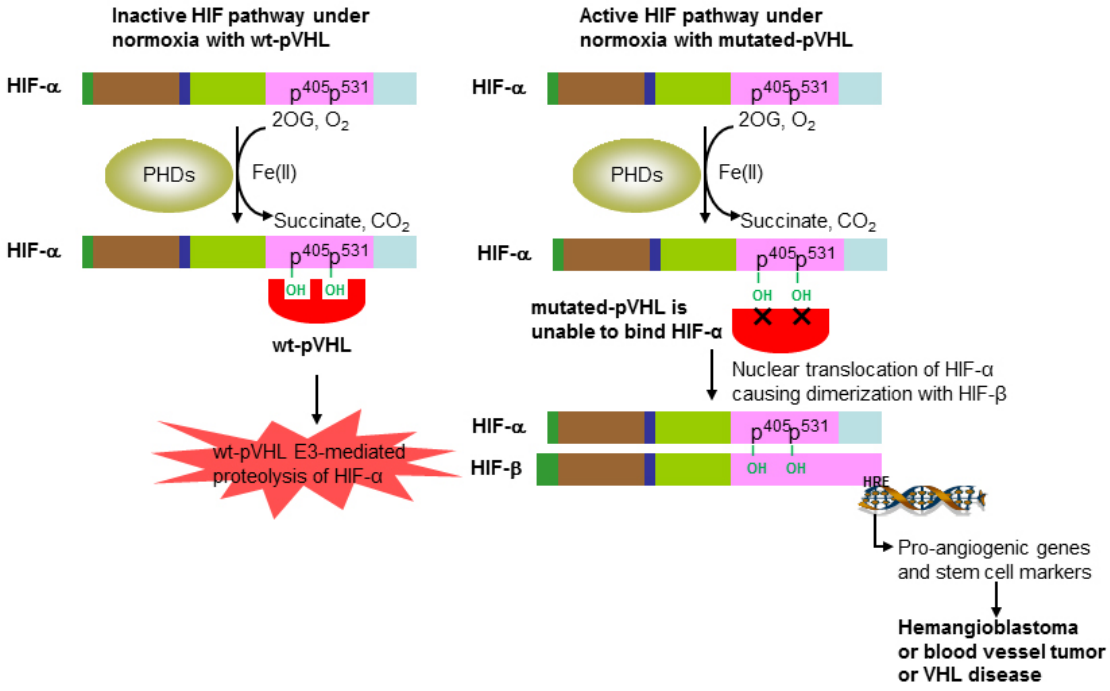

Figure 37: A model showing modulation of the HIF pathway by pVHL under normal conditions or in hemangioblastomas. Under normal normoxic conditions (left panel), PHDs hydroxylate HIF-α on proline (P405/531) residues, leading to ubiquitin ligase pVHL E3-mediated destruction of HIF-α. However, in patients with mutations in pVHL, although HIF-α gets hydroxylated at the proline residues, it escapes proteosomal degradation, allowing its translocation and dimerization with HIF-β in the nucleus leading to transcription of hypoxia response genes even under normoxic conditions, which includes a number of pro-angiogenic and stem cell markers in neoplastic stromal cells in hemangioblastomas (right panel). The fragment colors of HIF subunits represent different protein domains.

CHAPTER IV

DEVELOPMENT OF A HPLC BASED METHOD FOR EVALUATING THE CATALYSIS BY TET2 DNA DEMETHYLASE

Introduction

Cytosine methylation at carbon-5 is an important covalent modification of mammalian DNA. Methylation of DNA at cytosine carbon-5 in the CpG dinucleotides is carried by DNA methyltransferases [144] . Due to the critical role played by the human DNA methyltransferases in normal development and disease states, numerous studies were directed toward the identification of 5mC demethylases. Ultimately, using sophisticated bioinformatics tools three putative DNA modifying enzymes, TET1-3, were identified in the mammalian genomes [28]. Biochemical characterization of the newly identified putative DNA modifying enzymes showed that TET1 hydroxylates 5mCs into 5-hydroxymethylcytosines (5hmCs) both *in vitro* and in mammalian cells [24]. A significant genomic presence of 5hmC (~0.6% of all Cs; accounting for ~40% of all 5mCs) was also observed in Purkinje cells from the mouse cerebellum [26]. TET1 is highly expressed in embryonic stem cells (ESCs), and several studies have used high quality TET1 antibodies to characterize TET protein binding and 5hmC deposition across the mESC genomes using parallel DNA sequencing technology [145-148]. These studies have shown that TET1 binds predominantly to CpG islands and TET1-bound promoters show significantly lower levels of 5mC marks, possibly due to TET1-mediated demethylation. Surprisingly, given the established role of 5mC in gene

repression, all these studies have shown that the knockdown of TET1 causes more genes to be de-repressed than de-activated.

The *TET1* gene was initially identified as a fusion partner of the MLL (myeloid/lymphoid or mixed lineage leukemia) gene in acute myeloid leukemia (AML) [149]. Using cytogenetics and single nucleotide polymorphism arrays, we and others have shown that *TET2* is one of the most frequently mutated genes in myelodysplastic syndromes (MDS) [150-152]. The *TET2* mutations are also prevalent in a number of myeloid malignancies such as MDS-myeloproliferative neoplasms (MDS-MPN) and acute myeloid leukemia derived from MDS and MDS-MPN (sAML) [152]. Patients with *TET2* mutations show low levels of genomic 5hmC in the marrow compared to those with wild-type *TET2* [150].

Role of TET2 oxygenase in hematopoiesis

In order to determine the function of TET2 in normal hematopoiesis and myeloid transformation, a number of groups have generated TET2-knockout mouse models [153-156]. These studies showed that TET2 was highly expressed in hematopoietic stem cell (HSC) and other progenitor cells, and that ablation of TET2 dramatically diminished the levels of genomic 5hmC in bone marrow cells. Importantly, in contrast to TET1-knockout mouse model [157], which shows some reduction in the cellular 5hmC levels but are viable, fertile and appear to develop normally, TET2-knockout mice developed diverse myeloid malignancies. Although TET2-knockout mice are viable and grossly normal, as they age, they start dying from different hematopoietic malignancies.

Results from studies of TET2-knockout mice suggest that wild-type TET2 promotes hematopoietic differentiation. TET2 loss resulted in an expansion of the HSC and other myeloid progenitor cell numbers. TET2-deficient HSC and progenitor cells also showed progressively diminished hematopoiesis. $TET2^{-/-}$ and $TET2^{+/-}$ HSCs had a higher ability to self-renew, providing a competitive advantage to these cells compared to wild-type HSCs for repopulating hematopoietic lineages. Further, consistent with a high percentage of patients with heterozygous TET2 alterations, heterozygous cells from $TET2^{+/-}$ mice behaved similar to $TET2^{-/-}$ cells and developed diverse myeloid malignancies. $TET2^{+/-}$ cells also exhibited a competitive advantage over wild-type TET2 cells in transplantation assays, although this occurred over a longer period compared to $TET2^{-/-}$ cells. These results suggest that TET2 haploinsufficiency is sufficient to change the properties of HSCs leading to induction of myeloid malignancies.

Other genes also play a role in the maintenance of 5hmC levels in cells (Figure 38). For example, the normal function of isocitrate dehydrogenases (IDH1/2) is to convert isocitrate into 2-oxoglutarate (2OG). In some AML and glioblastoma patients mutations in IDH-1/2 create neomorphic variants of the enzymes, which produce 2-hydroxyglutarate (2HG) instead of 2OG [158]. Due to the structural similarity with 2OG, 2HG binds in the 2OG binding pocket in the active site of dioxygenases, which impairs their function. Thus, 2HG acts as a competitive inhibitor for a number of 2OG-dependent dioxygenases like histone lysine demethylases (KDMs), prolyl hydroxylases,

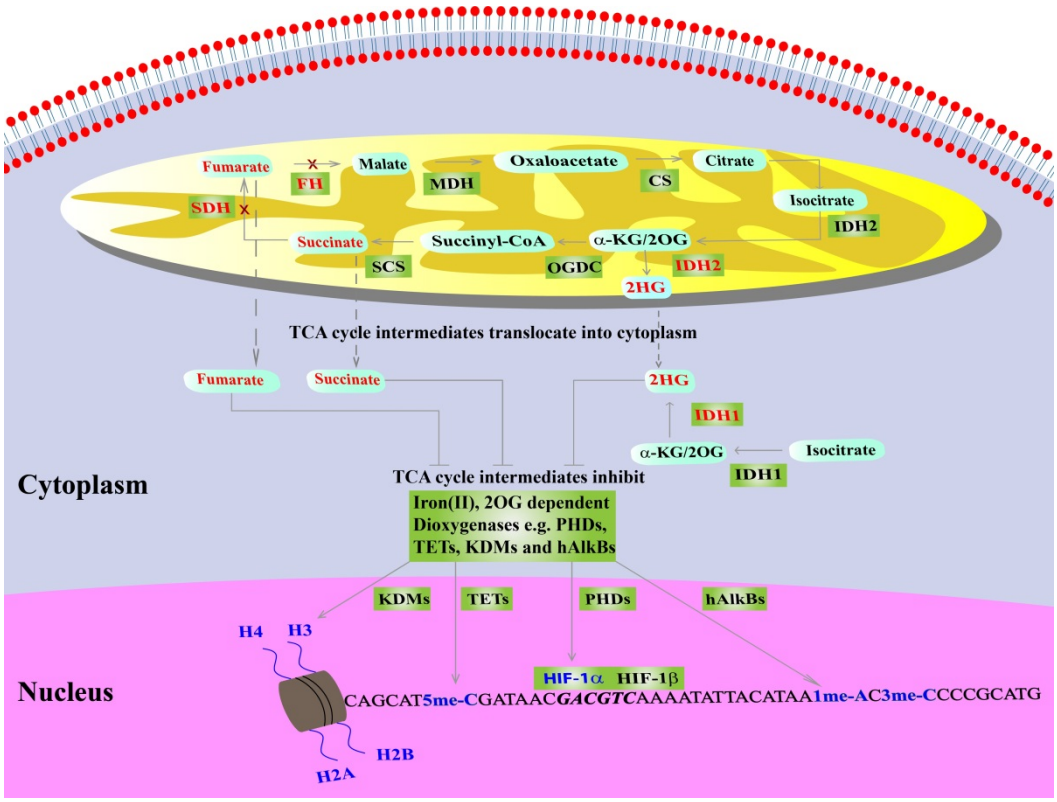

Figure 38: Mutations in the enzymes of TCA cycle can influence the activity of Fe(II), 2OG-dependent dioxygenases involved in epigenetics causing cancers. Normally IDH1/2 converts isocitrate to 2OG, while in subsequent steps succinate is converted to fumarate by succinate dehydrogenase (SDH) and fumarate to malate by fumarate hydratase (FH). Mutations in the SDH and FH genes lead to accumulation of succinate and fumarate, respectively, while mutations in IDH1/2 gene allow neomorphic enzymes to convert isocitrate in to 2HG. Accumulated succinate, fumarate or 2HG, due to structural similarity with 2OG, act as competitive inhibitors of 2OG-dependent dioxygenases leading to changes in the epigenetic landscape. Mutated enzymes and

their altered substrates or products are represented in red font. The substrates of Fe(II), 2OG-dependent dioxygenases involved in epigenetics are shown in bold blue font.

and DNA demethylases like TET2 [159, 160]. Inhibition of dioxygenases such as KDMs and TET2 leads to an increase in the histone lysine methylation and a decrease in the 5-hydroxymethylcytosine levels in cells. Thus, clinical features of some IDH1/2 gain-of-function mutations are similar to TET2 mutations in AML patients.

Other key TCA cycle enzymes (*e.g.* succinate dehydrogenase, SDH, and fumarate hydratase, FH) are also mutated in various cancers [161, 162]. Mutations in these enzymes lead to cellular accumulation of succinate and fumarate, respectively. Due to structural similarity with 2OG, these TCA cycle intermediates inhibit the activity of dioxygenases like prolyl-hydroxylase-domains (PHDs) resulting in pseudo-hypoxic environment and activation of hypoxia-inducible-factor (HIF) pathway leading to aberrant cellular proliferation [163] (Figure 38). It would be interesting to check the status of these enzymes in leukemia patients and evaluate their effects on TET dioxygenases.

Three-dimensional topology of TET dioxygenases

A comparison of primary sequences of a number of Fe(II), 2OG-dependent dioxygenases reveals some conserved motifs (*e.g.* iron and 2OG binding), but with little primary sequence similarity among different subfamilies [164]. Yet, the reported crystal structures of Fe(II), 2OG-dependent dioxygenases have demonstrated an emergence of a common structural platform among different subfamilies. The results from these

studies have revealed a β-strand core containing eight anti-parallel β-strands folded into a "Jelly-roll" motif. This characteristic motif harbors the dioxygenase active site consisting of three residues (two histidine and one aspartate or glutamate residues known as the "2-His-1-carboxylate triad") occupying one side of the Fe(II) coordination sphere [52]. The residues which constitute the 2-His-1-carboxylate triad are generally present on or near the relatively rigid β-strand core, indicating a divergent evolution within the 2OG-dependent dioxygenase subfamilies.

Bioinformatics analyses followed by secondary structure predictions suggest the existence of a similar Jelly-roll motif containing the 2-His-1-carboxylate triad (His-1672×Asp-1674…His-2028 in TET1; His-1382×Asp-1384…His-1881 in TET2; His-942×Asp-944…His-1538 in TET3) in the active site of TET dioxygenases (Figure 39). This 2-His-1-carboxylate triad forms a common Fe(II) binding platform, which allows dioxygenases to carry out a range of oxidation reactions [164]. The Fe(II) metal center, locked in the 2-His-1-carboxylate triad, binds three exogenous ligands (*i.e.* 2OG and O_2) on the other side. Thus, oxygen binds to the metal center *trans* to any residue constituting the 2-His-1-carboxylate triad. The remaining two Fe(II) coordinates are occupied by the carboxyl and keto oxygen atoms of 2OG (**Figure 3**). The 5-carboxylate group of 2OG binds to either an arginine (present on the eighth β-sheet of the Jelly-roll) or a lysine (present on the fourth β-sheet of the Jelly-roll) residue from the enzyme. Thus, based on the binding of 5-carboxylate group of 2OG two subfamilies of Fe(II), 2OG-dependent dioxygenases have been identified. In TET dioxygenases, the 5-carboxylate group of 2OG binds an Arg residue. In some dioxygenases where the 5-

carboxylate group of 2OG binds an Arg residue, a characteristic Arg×Ser motif is found where the Ser residue forms an additional hydrogen bond with the 5-carboxylate group of 2OG (Arg-2043×Ser-2045 in TET1, Arg-1896×Ser-1898 in TET2, Arg-1553×Ser-1555 in TET3).

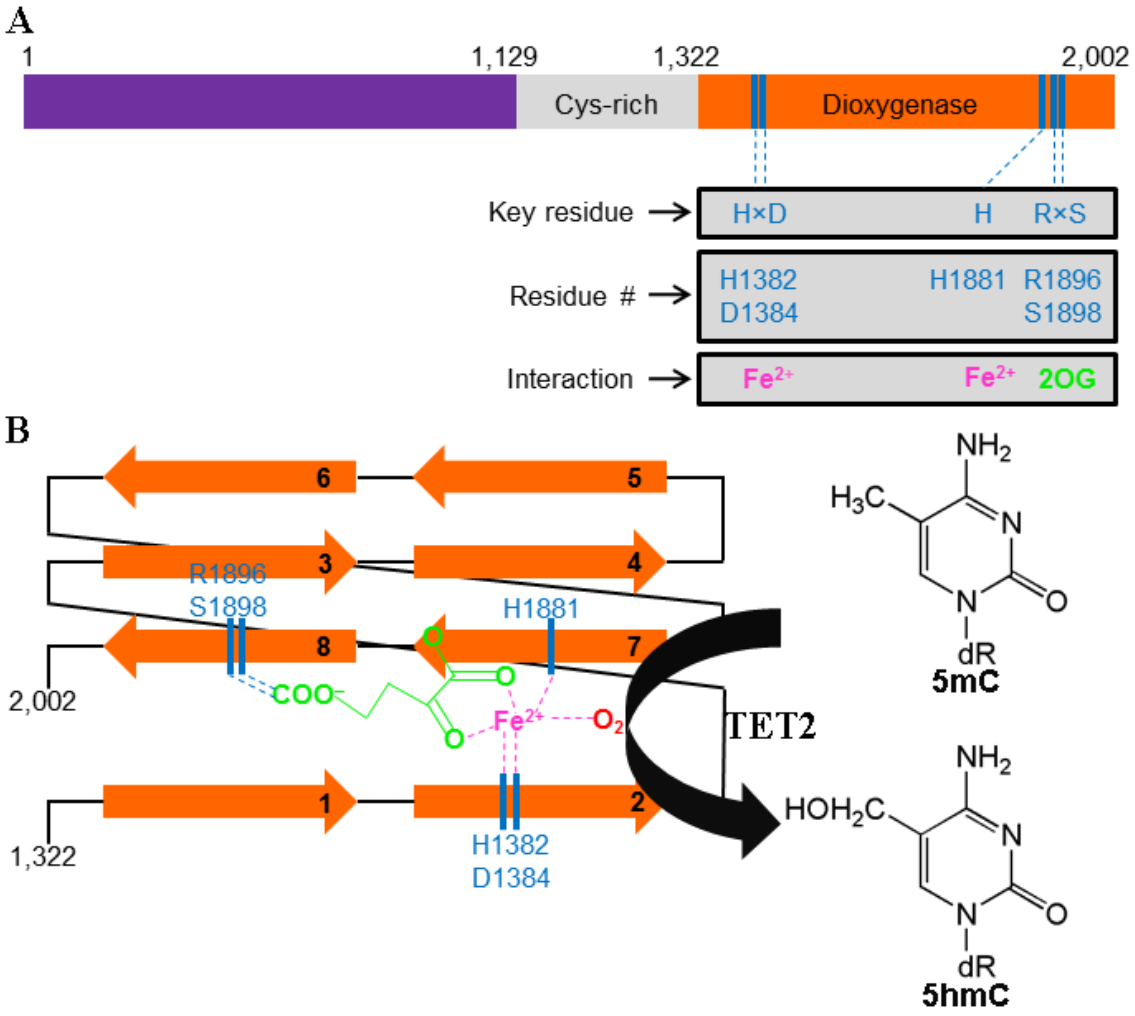

Figure 39: A graphical representation of the full-length TET2 showing the cysteine rich domain and catalytic dioxygenase domain (A). An active site representation of TET2 showing the eight antiparallel β-sheets constituting the Jelly-roll motif (B). The Jelly-

roll motif also represents the bound cosubstrate, 2OG, and cofactors, Fe(II) and O_2, to the active site catalysing the conversion of 5mC into 5hmC.

Structure-function analysis of TET2 mutations in leukemia

The clinically described TET2 mutations include frame-shift, nonsense and missense mutations. Since the dioxygenase domain is present toward the TET2 C-terminus with the critical 2OG binding motif located toward the very end, most frame-shift and nonsense mutations upstream to it will result in an inactive enzyme. In addition to the frame-shift and nonsense mutations, most of the identified TET2 missense mutations are clustered in the dioxygenase domain (Figure **38**). Interestingly, some of the most frequently mutated residues (Asp-1384Val, His-1881Gln/Arg/Ala) and (Arg-1896Met/Ser/Gly, Ser-1898Phe) form the Fe(II) (His-1382×Asp1384…His-1881) and 2OG (Arg-1896×Ser-1898) binding motif in the TET2 active site, respectively. Since it has been shown that inactivation of TET2 alone can cause myeloid malignancies in the mouse model, some of the observed clinical heterogeneity in patients with TET2 mutations could be due to the type of the enzymatic defects.

In the current study, we cloned and expressed a catalytically active hTET2 gene fragment using both baculovirus and bacterial systems. We also developed a HPLC method for evaluating the catalysis of the purified hTET2 protein.

Materials and Methods

Cloning of human TET2

Human cDNA clone for TET2 gene coding for 2420 bp fragment starting at 3590 bp and ending at 6009 bp was used as the template for PCR amplification. Using 5' – TET2-XhoI, AflII, SmaI, SalI: 5' GTCGACACCCGGGACTTAAGCTCGAGATG GGGCATCATCATCATCATCATAAGTGGGTGGTTCGCAGA – 3' as 5' primer and 3' – TET2-KpnI, NotI: 5' – ATGATGGCGGCCGCGGTACCTCATATATATCTGTT GTA – 3' as the 3' primer, 2420 bp hTET2 fragment (fragment A) was PCR amplified. The amplified DNA fragment was gel purified and cloned into pGEM®-T vector (Promega, Madison, WI). Positive clones were verified by sequencing. To include the cysteine rich domain of hTET a 982 bp long fragment (fragment B) was custom synthesized and cloned into pUC57 vector. The 3' end of this fragment B overlapped into the 5' side of the 2420 bp cloned fragment A such that the unique SgrAI site present at 192 bp of fragment A was included for joining the two fragments. Fragment B was joined to fragment A on the 5' side by digesting the two vectors with SacI and SgrAI. The resulting pGEMT clone consisted of the final 3141 bp long hTET2 fragment (fragment C). Generation of this final clone was confirmed by sequencing the clone. Confirmed fragment C was transferred into pGEX-4T1 vector to generate pGEX-4T1-hTET2 bacterial expression construct. Also hTET2 fragment C was transferred into pFASTBAC-1 vector by digesting with SalI and NotI enzymes.

Bacmid generation

Verified hTET2 clones in pFASTBAC-1 vector were transformed into DH10Bac competent cells and platted on selection media containing kanamycin, gentamycin, and tetracycline at 50 µg/ml, 7 µg/ml, and 10 µg/ml respectively. IPTG (0.1M) and X-gal (20 mg/ml) (40 µl each) were spread on the plates prior to spreading the transformation mix for blue white selection. The plates were incubated for 48 hrs at 37°C and white colonies were picked. White colonies obtained after 48 hrs of incubation were re-streaked onto LB-Kanamycin, Gentamycin, Tetracycline plates with IPTG and X-Gal added and incubated for 12-16 hrs at 37°C. Colonies which remained white were selected for growing liquid culture and bacmid was extracted from them. Presence of TET2 fragment in the extracted bacmids was verified by performing PCR analysis using M13 forward and reverse primers to generate a 5414 bp fragment or by using a combination of M13 primers and TET2 specific primers.

Insect Cell Culture

SF9 cells were obtained from Expression Systems (Davis, CA). They were maintained in suspension culture using serum free media (Expression systems, Davis, CA) at 27°C with 130 rpm in a New Brunswick shaker for efficient aeration. Cells were maintained at a density of 1 million cells per ml by diluting the cultures every second day. Cells were allowed to grow to a maximum density of 4-5 million cells per ml.

Virus generation

SF9 cells were platted at a density of 900,000 cells per well in a 6 well plate for transfecting with pFASTBAC-1 vector carrying human TET2 gene fragment. DNA and

celfectine were added into 100µl of transfection media in separate tubes and left at room temperature for 5 mins. DNA:celfectine complex was generated by mixing these two solutions and leaving for 30 mins at room temperature. Final complex was added to the cells and incubated for 4-5 hrs in transfection media. Following this media was changed to complete media and incubated for 3-5 days. Once the size of the cells increased compared to the untransfected cells, virus was harvested by collecting the spent media. Media was spun down to precipitate any debris or cells. The clear supernatant containing the virus was tittered to determine the viral titer in the initial stock (P_0).

Using this P_0 stock secondary infection of cells was performed in suspension culture to amplify the viral titer. For this 30 ml of media was seeded with cells at a density of 1 million cells per ml and allowed to grow over night. Once the cells started to divide 0.5 ml of P_0 was added and the cell count was observed over the next 3-4 days. If the cell count crossed 4 million per ml, then not enough of initial virus stock was added and if the count didn't reach 3-4 million per ml, too much viral stock was added. Based on this the amount of virus to be added could be adjusted to obtain optimal infection of cells for P_1 generation. After 4-5 days of infection, virus is harvested by spinning the culture and collecting the supernatant. Titer of the generated P_1 viral stock was determined.

Protein expression in insect cells

SF9 cells growing in log phase were seeded at a density of 1 million cells per ml in 300 ml of media and allowed to grow overnight at 27°C with agitation. Following this after verifying that the cell numbers increased to 1.5-2 million cells per ml, they

were infected with desired volume of P1 viral stock for obtaining an MOI of 0.3. After infecting the cells, they were cultured for 3-4 days and the cell number and cell size was monitored every day. Cells were harvested once the cell number started to drop and the size increased to ≈ 20 μm due to high degree of infection. Following this, cells were lysed in lysis buffer and processed for western blot analysis.

Protein expression in bacterial system

The bacterial construct coding for hTET2 (pGEX-4T1-hTET2) was transformed into BL21DE3 cells and selected on ampicillin plates. Using selected colonies small-scale protein expression was done in 10 ml culture. Cells were grown to an OD_{600} of 0.8 at 37°C and then maintained at 16°C. Once the temperature came down to 16°C, 0.1 M IPTG was added to induce protein expression. Cells were harvested after 16 hrs of incubation. Following this, cells were lysed in SDS gel loading buffer and loaded onto a SDS-PAGE to check for induction of hTET2 protein. Western blot analysis was also performed to confirm the presence of hTET2 in the induced sample.

Protein purification

Recombinant hTET2 protein was purified from 12 liter of culture. Bacterial cells were pelleted and either stored at –80°C or lysed immediately for protein purification. This step onwards all the steps of protein purification were performed on ice. The cells were resuspended in 50 ml of lysis buffer (20 mM Phosphate buffer, pH 7) and sonicated at an intensity of 5 for 6 mins with 6 pulses every 30 seconds (Sonic Dismembrator 550, Fisher Scientific). The lysate was spun down at 15,000 rpm for 20 min (Beckman J2-HS centrifuge) and the supernatant was collected and filtered through

0.45µ filter. Ion exchange chromatography was employed to purify GST tagged hTET2 protein, as the theoretical pI of the protein is 8.3. CM-Sepharose (Pharmacia now GE Healthcare, Piscataway, New Jersey) was used for the purification. The resin (50 ml) was packed into a XK16 FPLC column (Pharmacia now GE Healthcare, Piscataway, New Jersey) and equilibrated in 10 bed volumes of wash buffer (20 mM Phosphate buffer, pH 7) using an Akta FPLC system (Pharmacia/GE Healthcare). A constant flow rate of 1 ml/min was used for all steps. Clarified cell lysate was loaded onto the column and washed with the wash buffer (~ 10 bed volumes) till the flow through was clear. Elution of the bound protein was carried out using a gradient from the wash buffer to the elution buffer (20 mM Phosphate buffer, 1 M Sodium Chloride, pH 7). 0 to 100% of elution buffer was reached in 5 bed volumes, followed by holding at 100% elution buffer for 4 bed volumes and then dropping down to 0% elution buffer in 3 bed volumes and holding there for another 3 bed volumes. Samples of cell lysate before and after column loading, along with all the elution fractions (10 ml each) were collected and analyzed by SDS-PAGE. 15% glycerol was added to the protein, and aliquotes were stored at –80°C.

HPLC method for Oligonucleotide separation

A liquid chromatography method for separation and quantification of intact oligonucleotide sequences was developed using a Phenomenex Gemini 5µ C18 column. Triethylamine acetate buffer system in combination with acetonitrile was employed for separation. Solvent A was composed of 100 mM triethylamine acetate pH 7.0 with 5% acetonitrile and solvent B was composed of 100 mM triethylamine acetate pH 7.0 with

20% acetonitrile. Column was equilibrated by running 70% of A and 30% of B for 5 mins and then going upto 80% B in the next 45 mins. Over the next 5 mins solvent B concentration was brought down to 50% and then held there for another 10 mins. Detector was set up at 260 nm to monitor oligonucleotides.

Preparation of standard samples for HPLC method validation

All the nucleoside standards (2'-Deoxyadenine monohydrate, Thymidine, 2'-Deoxyguanosine monohydrate, 2'-Deoxycytidine and 5' Hydroxymethyl-2'-deoxycytidine) were purchased from Berry and Associates (Dexter, MI). All nucleosides except 2'-Deoxyguanosine monohydrate were prepared in HPLC grade water. 2'-Deoxyguanosine monohydrate was prepared in acidified water (pH 4.5) and used immediately. Nucleoside standards ranging from 900 μM to 10 mM in concentration were prepared for validating the HPLC method and evaluating the limits of detection and quantification.

HPLC method for analyzing nucleosides

A liquid chromatography method was developed to separate all the individual nucleosides from a mixture. Using a Phenomenex Gemini 5μ C18 column a gradient method was employed to separate the nucleosides using a flow rate of 0.5 ml per minute with solvent A being 10mM ammonium acetate, pH 4.0 and solvent B being 100% acetonitrile with 0.1% acetic acid added. The time profile for the method is as follows: 100% solvent A was run for the first 3 minutes followed by a gradient to reach 5% solvent B in 20 minutes. This was followed by holding 5% solvent B for 3 minutes and then dropping to 0% solvent B (100% solvent A) in the next 2 minutes. The column was

allowed to equilibrate in solvent A for the next 10 minutes. The UV detector was set at 280 nm for the detection.

DNAse I digestion of oligonucleotide

An oligonucleotide of 32 mer was used as the template for doing the digestion with DNAse I. DNAse I works on both single and double stranded DNA to yield 5'-phosphomononucleotides and oligonucleotides. The digestion of the single stranded oligonucleotides was setup using varying concentration of the enzyme ranging from 2 units to 10 units at 37°C for 12 hours. 10 µg of the substrate was used for all the digestions. Following the digestion half of the sample was processed by phenol chloroform and precipitated using isopropanol and the remaining half was used directly for calf intestinal alkaline phosphatase (CIAP) treatment.

Calf intestinal alkaline phosphatase (CIAP) treatment

Conditions for calf intestinal alkaline phosphatase treatment were initially standardized by using commercially available dCTP. For the phosphatase treatment 2-10 units of CIAP was used with 10 µg of dCTP (substrate) for 12 hours. Following this the samples were purified by phenol chloroform extraction, precipitated with isopropanol and finally re-suspended in 10 µl of water. DNAse I digested samples were further processed to remove the phosphate group by treating with CIAP. Crude and phenol chloroform extracted samples were subjected to CIAP treatment for 12 hours and were processed as mentioned earlier.

Mass Spectrometric analysis

Adenosine, Thymidine, Guanosine and Cytidine standards were dissolved in water and infused into the mass spectrometer (MS) in the positive mode as these lacked the phosphate group. To analyze the digested and CIAP treated oligonucleotide samples using either MS or MALDI-TOF we performed HPLC purification. Fractions were collected and the solvent was evaporated using speed vac. Following this samples were re-suspended in nuclease free water and analyzed.

Demethylation reaction

All demethylation reactions were performed in duplicate in 100 µl reaction volume with final concentrations of 500 µM $FeSO_4$, 1 mM 2-oxoglutarate, 2 mM ascorbate, 50 mM HEPES, pH 7.5, and 40 µg of purified enzyme. 2 µg of annealed double stranded oligonucleotide with single methylated CpG island was used as the substrate in the assay. The reactions were carried out at 37 °C for 12 hrs. Following this the reaction mix was processed as mentioned earlier for DNAseI digestion for 12 hrs and CIAP treatment for 12 hrs. The reaction mix was purified and used for HPLC analysis as mentioned earlier.

qPCR analysis

Using RNA extracted from cells exposed to hypoxia in earlier studies as described in materials and methods section of chapter 3, we performed qPCR analysis. Primers used for this study are listed below in Table **7**

Table 7: Sequences of primes used for qPCR analysis of TET1-3 DNA demethylases.

S.No.	Gene - Primer Name	Primer Sequence
1	TET1-F1	TAGCCCAACTCTCTCAGGCT
2	TET1-R1	AGGAGGTACTGACCATTGGC
3	TET1-F2	AGTCCTTAACCTGCAATGGG
4	TET1-R2	GGAGAGTCGCCTGCTAAGAG
5	TET1-F3	TTCCAGTCCAAGGAGAGGTC
6	TET1-R3	GGAACAGGAAGGAAGACAGG
7	TET1-F4	CAAAGTTCATGCAACACGGT
8	TET1-R4	TGACTTTGTGGATGCTTGGT
9	TET2-F1	GTGAGATCACTCACCCATCG
10	TET2-R1	CAGCATCATCAGCATCACAG
11	TET2-F2	AAATGAATCAAGGGCAGTCC
12	TET2-R2	AGAAGTGCACCTGGTGTGAG
13	TET2-F3	TCAACAGCTCTCTTCATGCC
14	TET2-R3	TCCTTGGACACAAGCAGTTC
15	TET2-F4	GGAAGTTTAAGCTGCTTGGG
16	TET2-R4	ATGCATCAGGTGCAAGTTTC
17	TET3-F1	AAGTTTGGGAACAGCACCTC
18	TET3-R1	TCTTGGAACCCAGGACTACC
19	TET3-F2	CATGGTATGAAACCACCCA
20	TET3-R2	ACTCGAGGTAGTCAGGGCA

S.No.	Gene - Primer Name	Primer Sequence
21	TET3-F3	GTGGTGGAGAGCTACTCGGT
22	TET3-R3	ACGCTGTTCATGCTGTAAGG
23	TET3-F4	AAGGCTGAGAACCCACTCAC
24	TET3-R4	CAGGTGTGTCCAGCAGACTC

Results

Cloning of hTET2 and mTET2 fragments

The C-terminal human TET2 fragment was PCR amplified using the MGC clone as the template (Figure **40**). PCR product was cloned into pGEMT cloning vector as described in the materials section. The clone was confirmed by restriction digestion

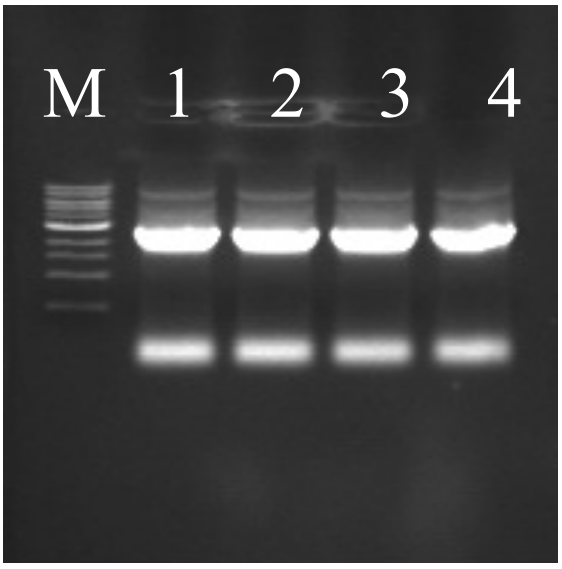

Figure 40: PCR amplification of 2420 bp hTET2 fragment using MGC clone as the template. Lane M – 1Kb ladder and lanes 1-4 PCR product

and positive clones were sent for sequencing (fragment A, Figure 41). Fragment of the hTET2 gene containing the cysteine rich region and overlapping with the 5' side of the fragment A was custom synthesized (fragment B) (Figure 42). Fragment A and fragment B were combined together using SgrAI and SacI restriction sites present in both fragments to generate a 3141 bp fragment C (Figure 42). Obtained clones were double digested using an internal enzyme to release a 2 Kb fragment confirming the

generation of the pGEMT-hTET2 (fragment C) clones (Figure 43). Multiple clones were sent for sequencing for verifying the presence of the entire 3141 bp fragment C. Verified clones were used as the source of the hTET2 fragment for transferring into pFASTBAC1and pGEX-4T1 vectors as described in methods section (Figure 43 and Figure 44).

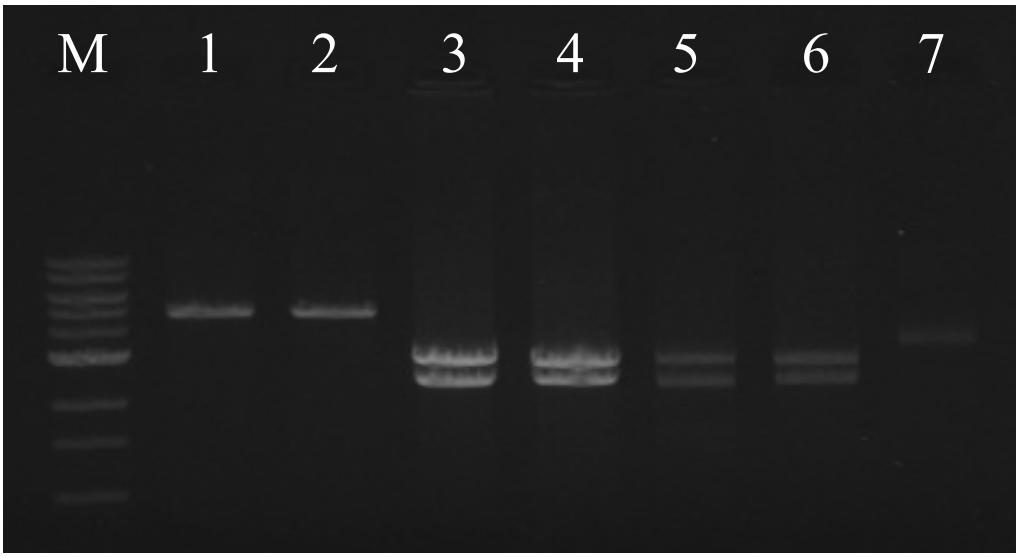

Figure 41: pGEMT-hTET2 double digest for confirming positive clones (Lanes 3-6)

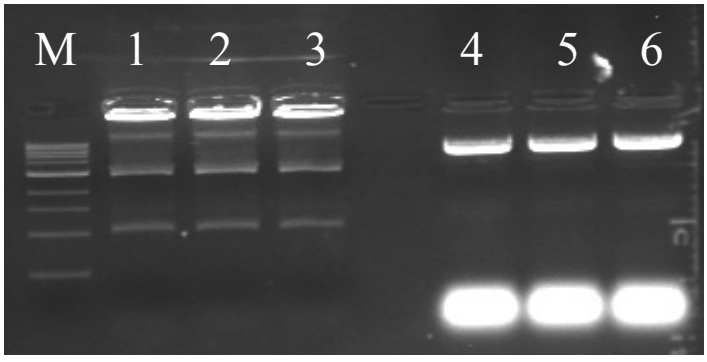

Figure 42: pGEMT-hTET2 (2420 bp) digest for adding synthetic fragment into it. Lane M – 1Kb ladder, lanes 1-3 double digest of pUC57-Synthetic TET2 with SacI and SgrAI and lanes 4-6 double digest of pGEMT-hTET2 (2420bp) with SacI and SgrAI

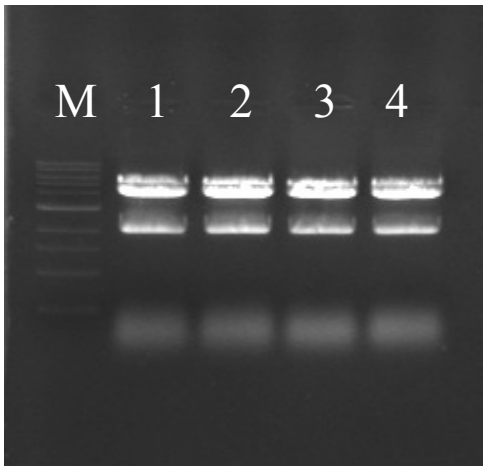

Figure 43: pGEMT-hTET2 (3141 bp) internal digest for confirmation. Lane M – 1Kb ladder

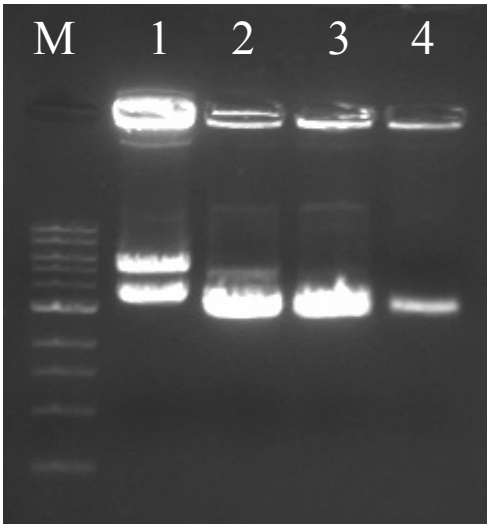

Figure 44: pFASTBAC-1-hTET2 (3141 bp). Lane M – 1Kb ladder and lanes 1-4 pFASTBAC1-hTET2 double digested with SalI and NotI

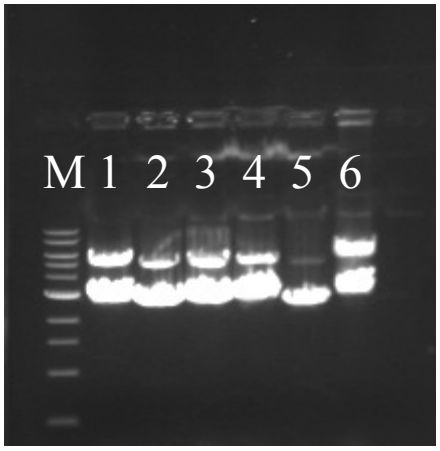

Figure 45: pGEX4T1-hTET2 (3141 bp). Lane M – 1Kb ladder and lanes 1 and 6 double digest

Protein expression in insect cells

Bacmids encoding for hTET2 protein were generated by transforming the pFASTBAC-1 constructs into DH10Bac cells as mentioned earlier. Bacmids extracted from the colonies were screened for the presence of TET2 gene using PCR analysis. Multiple bacmids were positive for the presence of TET2 gene. Two of these bacmids were used for transfecting SF9 cells for virus generation as described in the methods section.

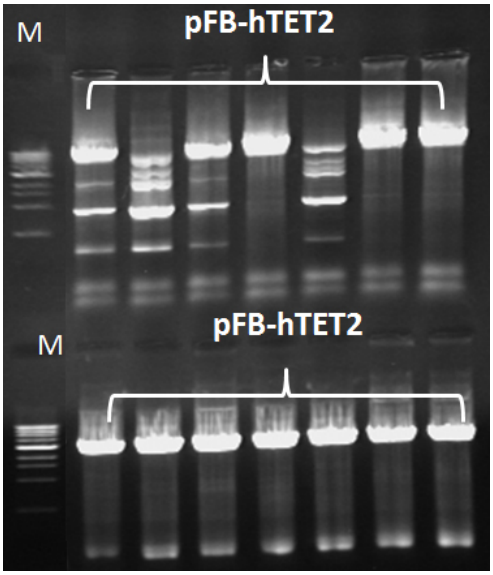

Figure 46: PCR analysis of bacmids extracted from DH10Bac cells transformed with various constructs of TET2. PCR for the top set was done using M13 forward primer and gene specific reverse primer and the expected amplicon size is ≈ 5.5 Kb. PCR for the bottom set was done using gene specific forward and reverse primers and the expected amplicon size is ≈ 3 Kb.

After the transfection the initial viral stock (P0) that was generated had a titer of 3.97 X 10^7 pfu/ml. Using P0 virus more cells were infected at an MOI of 0.1 to generate amplified viral stock (P1). The titer for P1 was found to be 1.23 X 10^9 pfu/ml. Using P1 viral stock, 300 ml of log phase cells were infected and harvested as described earlier for protein expression analysis. Western blot was performed to detect the presence of hTET2 protein in the lysate of the infected SF9 cells (Figure 47).

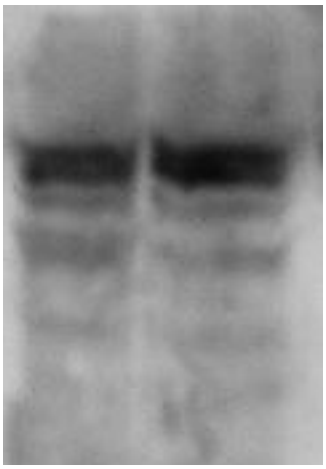

Figure 47: Western blot analysis of cell lysate from SF9 cells infected with TET2 expressing viral particles. Rabbit anti-TET2 polyclonal antibody was used for the detection.

Protein expression and purification of hTET2 using bacterial system

C-terminal fragment of hTET2 coding for cysteine rich domain and the dioxygenase domain cloned into pGEX-4T1 vector was used to express the protein in BL21DE3 cells as mentioned earlier. Small scale expression done in 100 ml culture validated the expression conditions. Western blot analysis showed increased expression

of hTET2 at 16 hrs (Figure 48). Large scale expression of wild type, RM, SF and RMSF mutant proteins was done in 12 liters of culture and the protein was purified (>90% purity) using CM-Sepharose resin. The total size of the GST-tagged hTET2 protein was found to be 145.6 KDa (Figure 49)

.

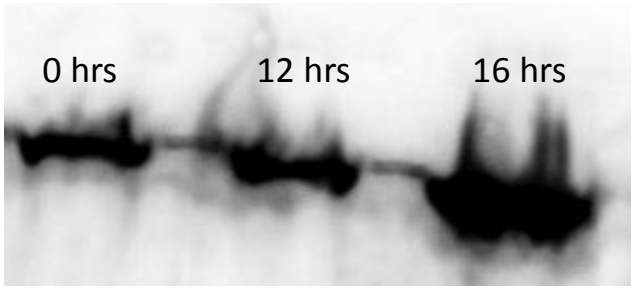

Figure 48: Western blot analysis of cell lysate from BL21DE3-pGEX-4T1-hTET2. Rabbit anti-TET2 polyclonal antibody was used for the detection.

HPLC method for Oligonucleotide separation

To evaluate the enzymatic activity of TET2 protein we wanted to develop a HPLC based analytical method for monitoring the catalysis. We looked at developing an ion-pairing system to effectively separate oligonucleotide substrate and product. For this purpose we utilized TEAA buffer system along with acetonitrile. We were able to separate the complementary forward and reverse strands of a double stranded oligonucleotide (Figure 50). Using this method we were unable to separate the methylated and unmethylated single stranded oligonucleotides. Hence, we had to look at developing an alternative method for evaluating the catalysis by TET2.

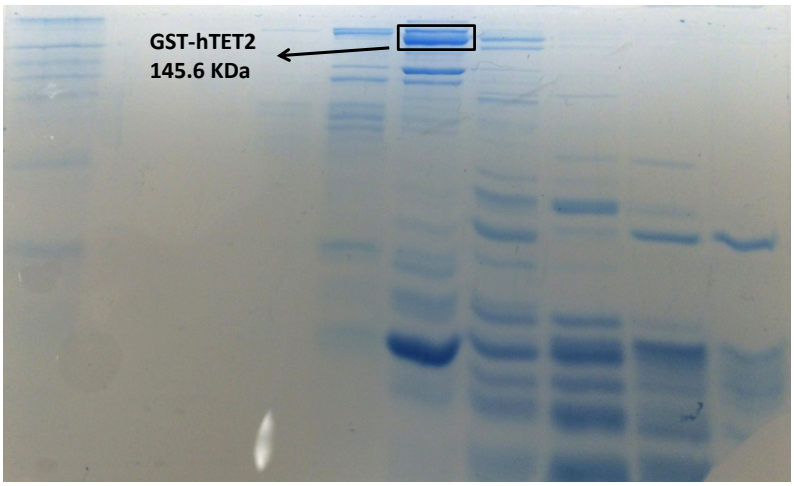

Figure 49: SDS-PAGE analysis of fractions collected during ion exchange purification. Fraction with the desired protein is highlighted in the box.

HPLC method for analyzing nucleosides

As we were not able to separate methylated and unmethylated oligonucleotides using the TEAA buffer system, we looked at developing an HPLC method for evaluating individual nucleosides. An HPLC method was developed using pure nucleosides as starting material for separating and quantitating. Initially we used phosphate buffed as the solvent system and obtained good resolution for the separation. Fractions collected after chromatography with the phosphate buffer system gave poor results in mass spectrometry analysis (data not shown). Hence phosphate buffer was replaced with ammonium acetate, which could be removed by drying the fractions in speed vacuum instrument. Using the conditions mentioned in the methods section we obtained good separation of all the nucleosides.

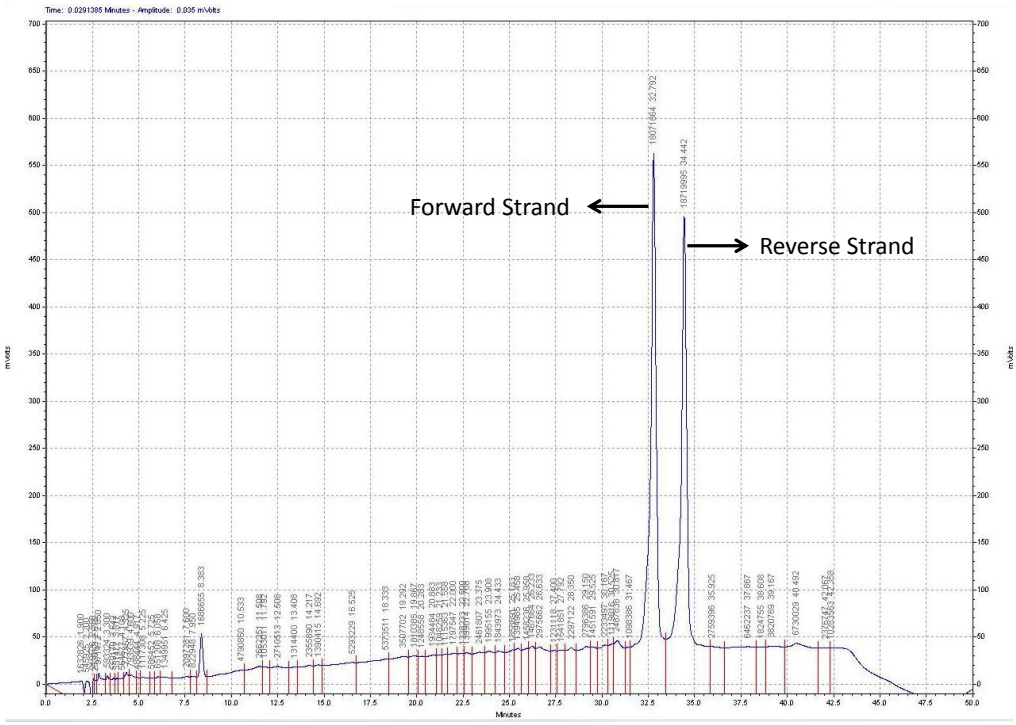

Figure 50: HPLC chromatogram for a mixture of forward and reverse strands separated using TEAA buffer system on a C18 reverse phase column.

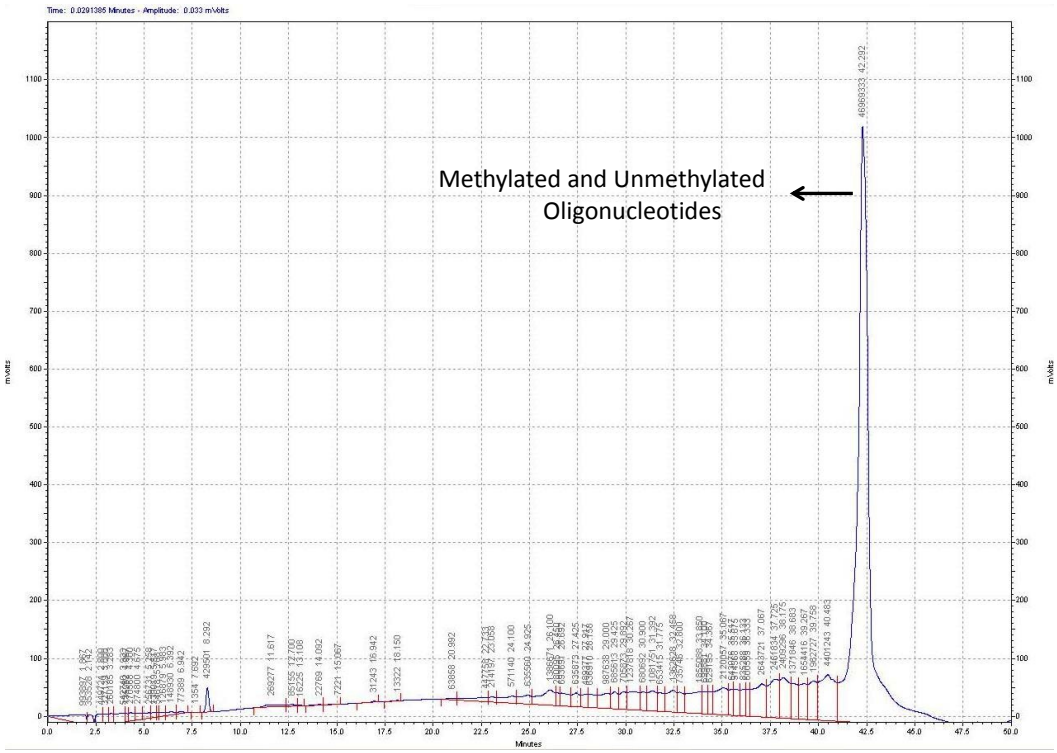

Figure 51: HPLC chromatogram for a mixture of methylated and unmethylated oligonucleotides analyzed using TEAA buffer system on a C18 reverse phase column.

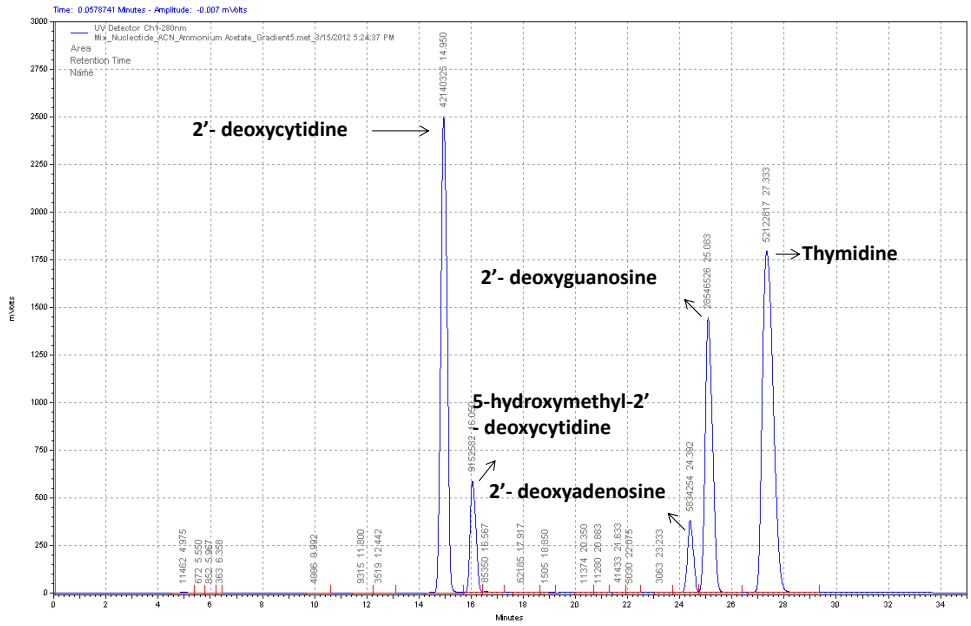

Figure 52: LC profile of a mixure of nucleoside standards resolved using the developed HPLC method.

The limit of detection (LOD) and limit of quantification (LOQ) of these individual nucleosides were determined and listed in Table 8. Multiple concentrations of the individual nucleosides were prepared and each nucleoside at each concentration was run for 5 times to determine LOD and LOQ. The standard plot for these runs is shown in Figure 53.

Table 8: Limit of detection and limit of quantification of nucleosides calculated using the developed HPLC method

Nucleotide	LOD (ng/ml)	LOQ (ng/ml)
Adenosine	30	90
Thymidine	560	1680
Guanosine	50	150
Cytidine	120	360

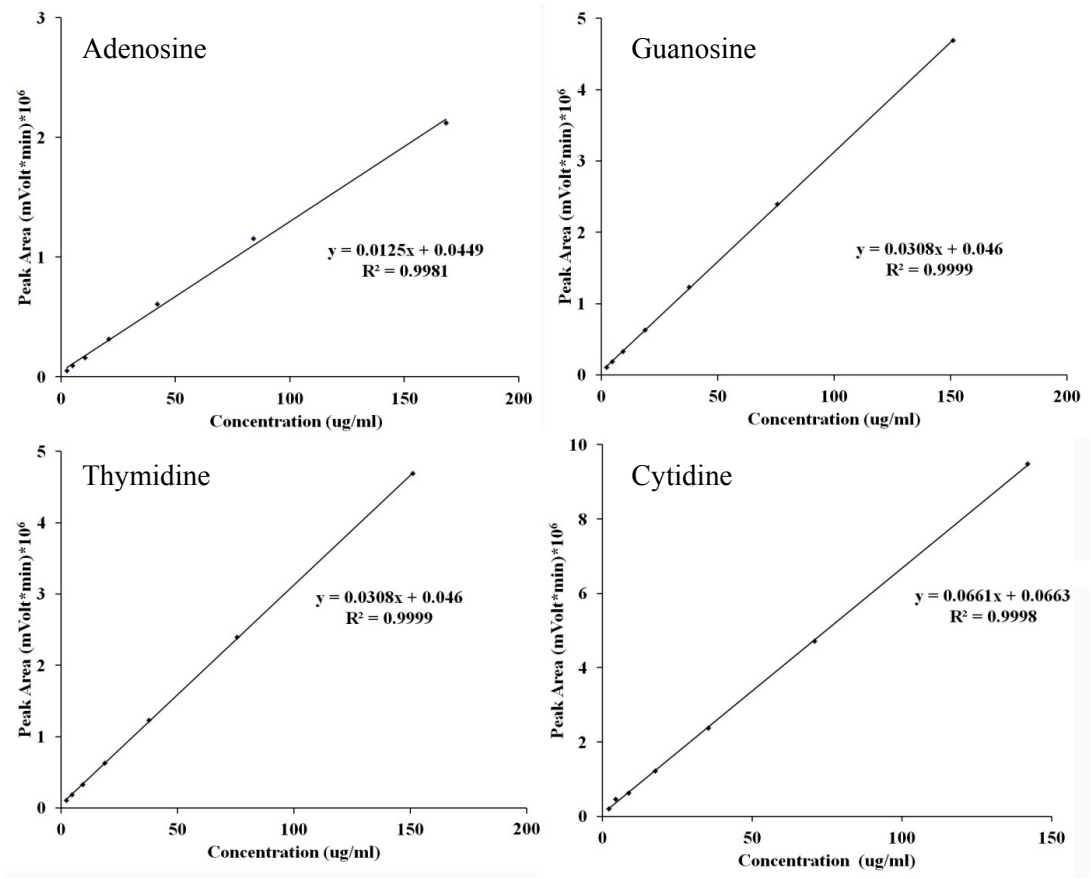

Figure 53: Standard plot for calculating LOD and LOQ of the nucleosides using the developed HPLC method.

Calf intestinal alkaline phosphatase (CIAP) treatment

Commercially available dCTP was run on the HPLC method developed for nucleosides. dCTP eluted at 7.3 minutes as seen in Figure 54. The amount of CIAP needed for compete conversion of 10 μg of dCTP to deoxycytidine was standardized to be 10 units when treated for 12 hrs at 37°C. Following the CIAP treatment the samples were purified as mentioned in the methods section and run on HPLC. More than 90% of dCTP was converted to deoxycytidine and eluted at 14 minutes as seen in Figure 55.

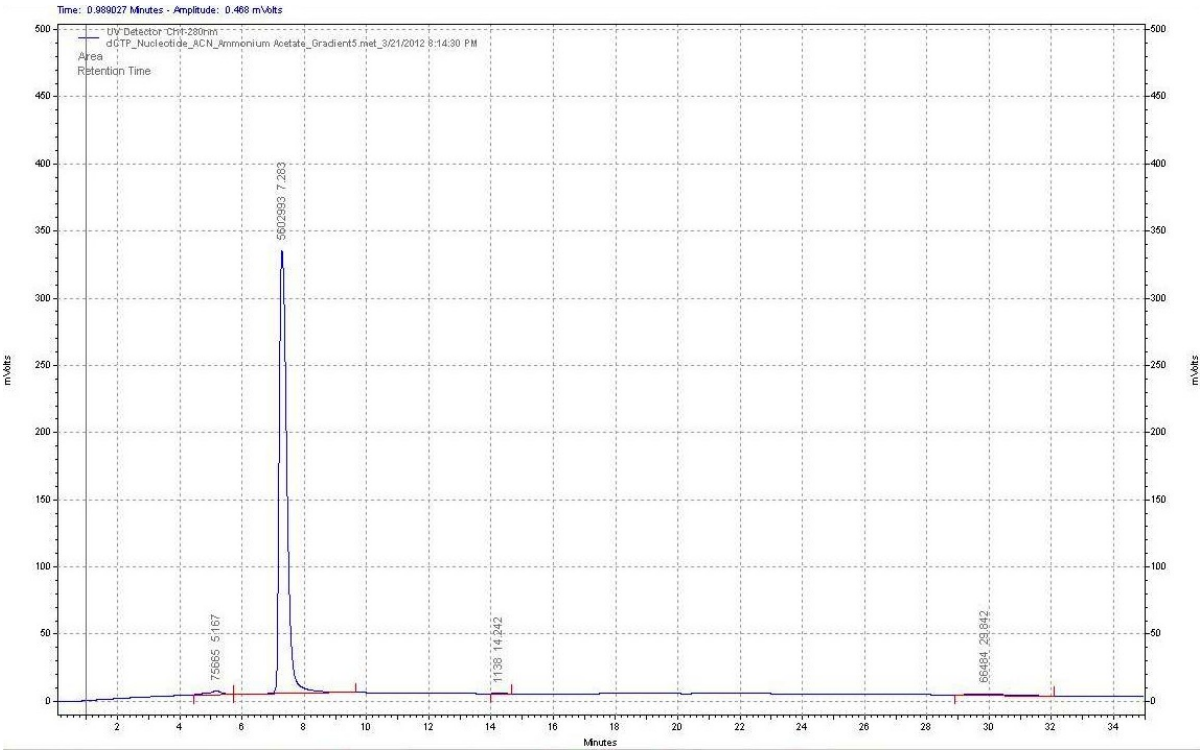

Figure 54: HPLC chromatogram for dCTP

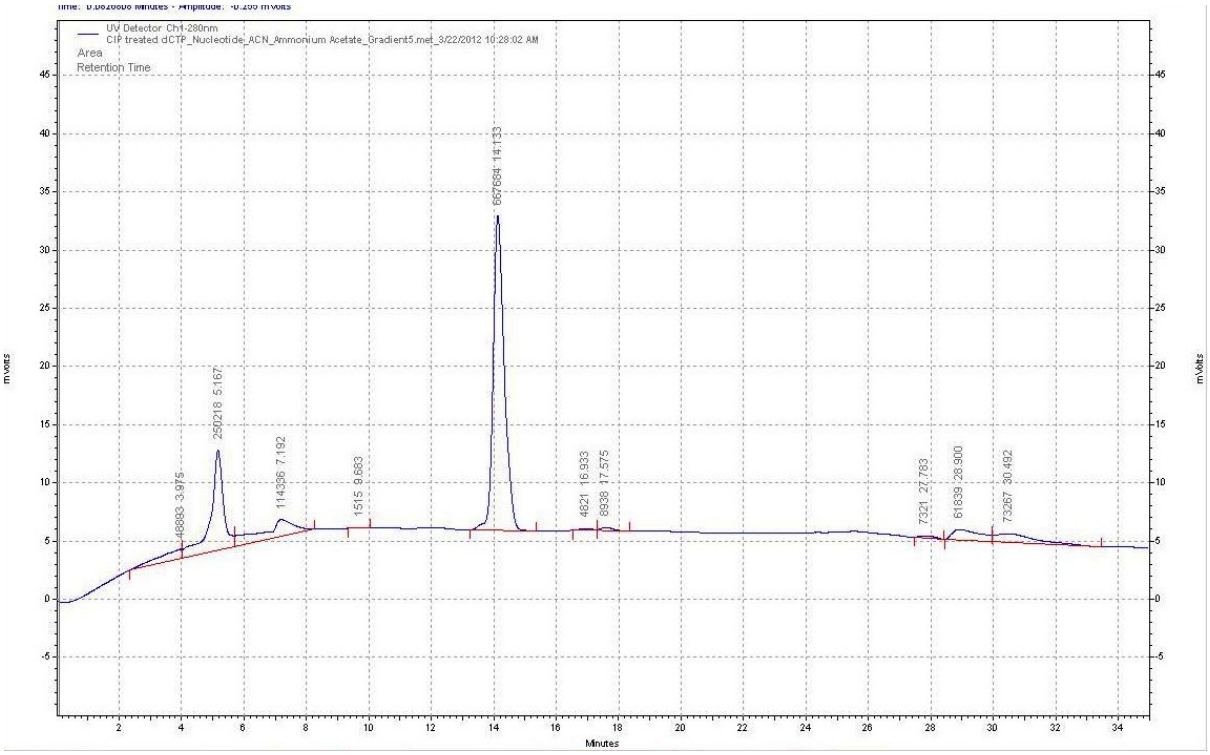

Figure 55: HPLC chromatogram for dCTP treated with 10 units of CIAP.

DNAse I digestion of oligonucleotide

Single stranded oligonucleotide was used as the substrate for the digestion. Using varying concentrations of DNAseI, we standardized the DNAseI concentration needed for efficient digestion of the substrate to be 10 units. The reactions were carried out at 37°C for 12 hrs. Following this samples were subjected to CIAP treatment as described earlier and processed for HPLC analysis. We were able to visualize all four nucleosides clearly resolved on the HPLC profile (Figure 56).

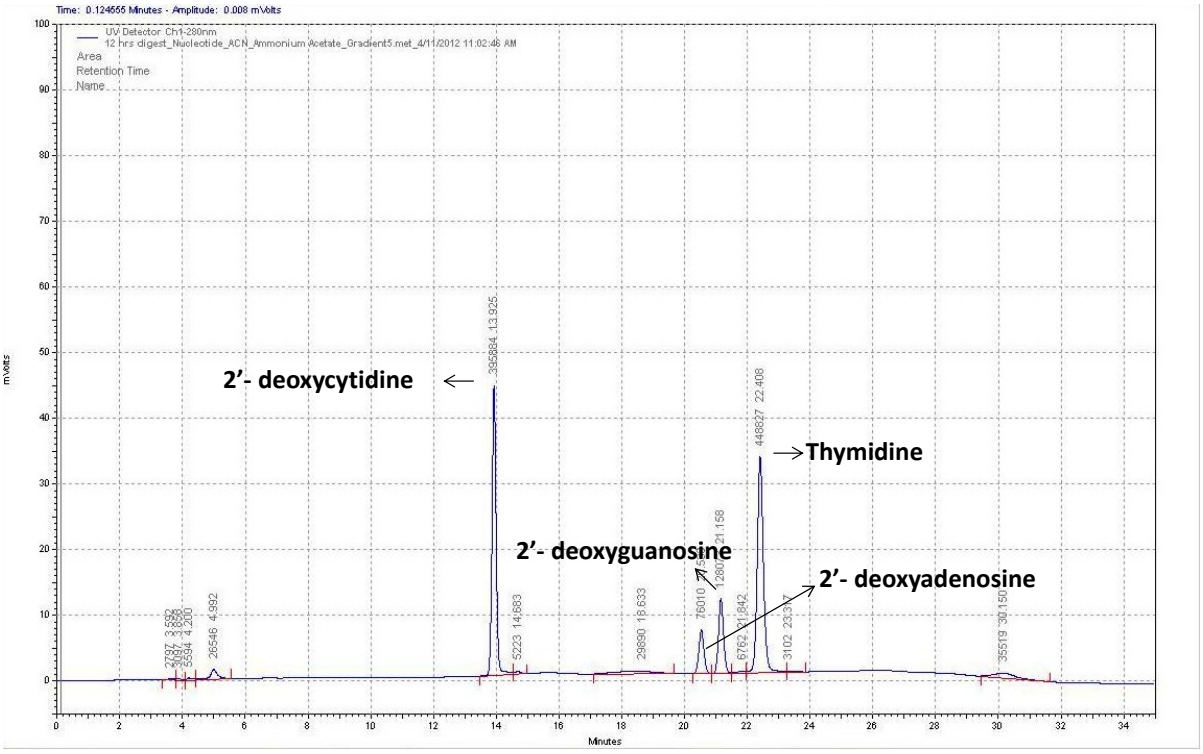

Figure 56: HPLC profile of DNASe I digested and CIAP treated oligonucleotide showing individual nucleosides.

Mass spectrometry analysis

Mass spectrometry and MALDI-TOF analysis was performed to look for the presence of nucleosides in the processed samples. Initially individual nucleoside standards were infused into the mass-spectrometer for determining the MS conditions. HPLC method was modified such that all the nucleosides elute in a short duration facilitating collection of all the nucleosides together as one fraction (Figure 57). Infusion of the processes fraction showed the presence of all four nucleosides (Figure 58). Similar results were obtained when the sample was used for MALDI-TOF analysis (Figure 59).

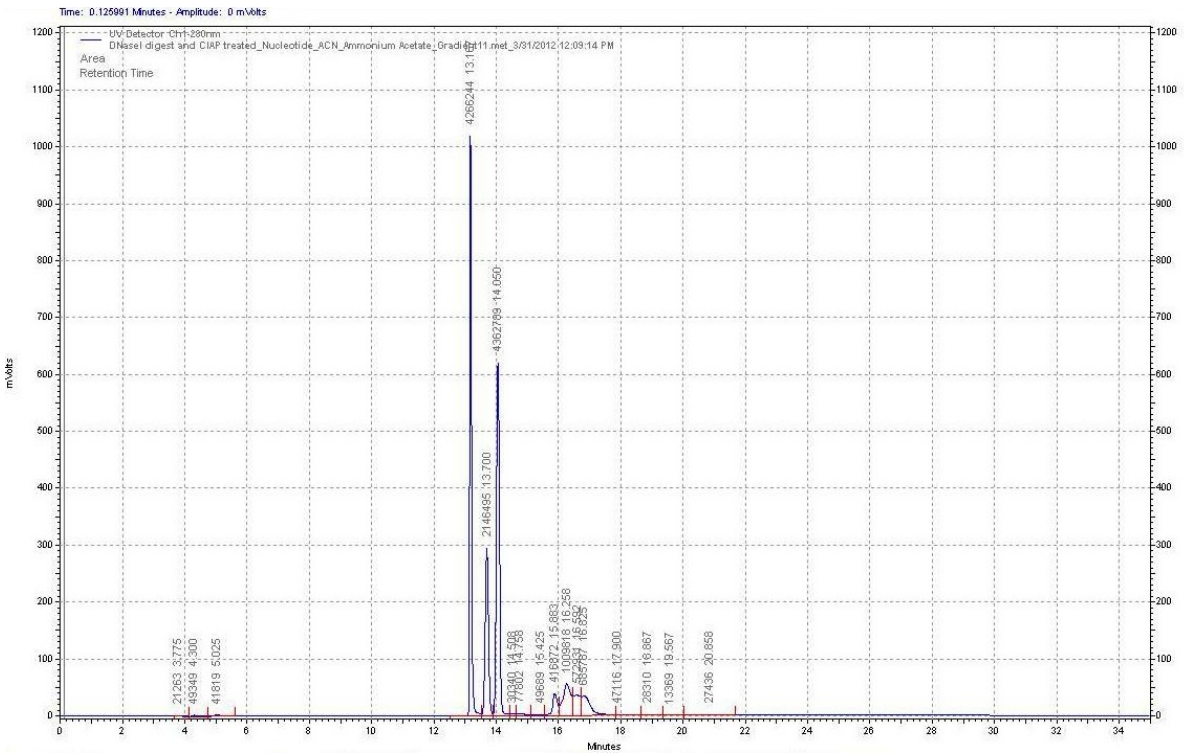

Figure 57: HPLC profile of DNASe I and CIAP treated oligonucleotide using modified method

Demethylation reaction

TET2 DNA demethylases work on double stranded oligonucleotides. Using the assay conditions described earlier we evaluated the catalysis by TET2. Following the incubation with and without the enzyme, oligonucleotide was processed and HPLC analysis was performed. The negative control had the signature profile for all the standard nucleosides (Figure 60). In the chromatogram for the reaction a new peak at 20 min was observed which correlates well with the peak for 5-hydroxymethylcytosine, one of the reaction products (Figure 61). Identity of the new peak was confirmed by performing mass spectrometry analysis of the collected fraction.

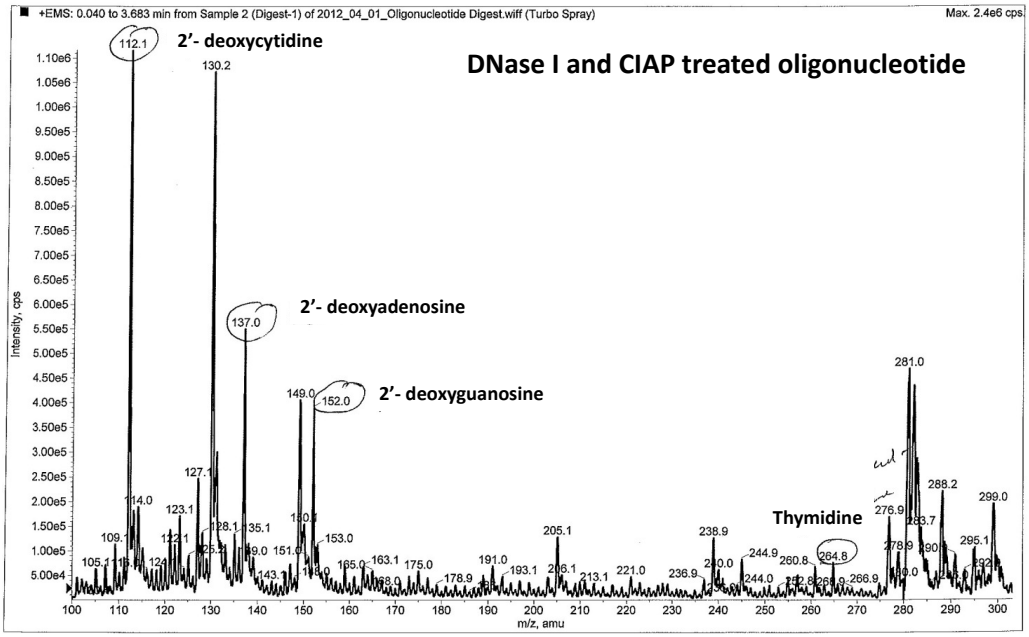

Figure 58: Mass spectrometer infusion of the fraction collected from the modified HPLC method showing all four nucleosides.

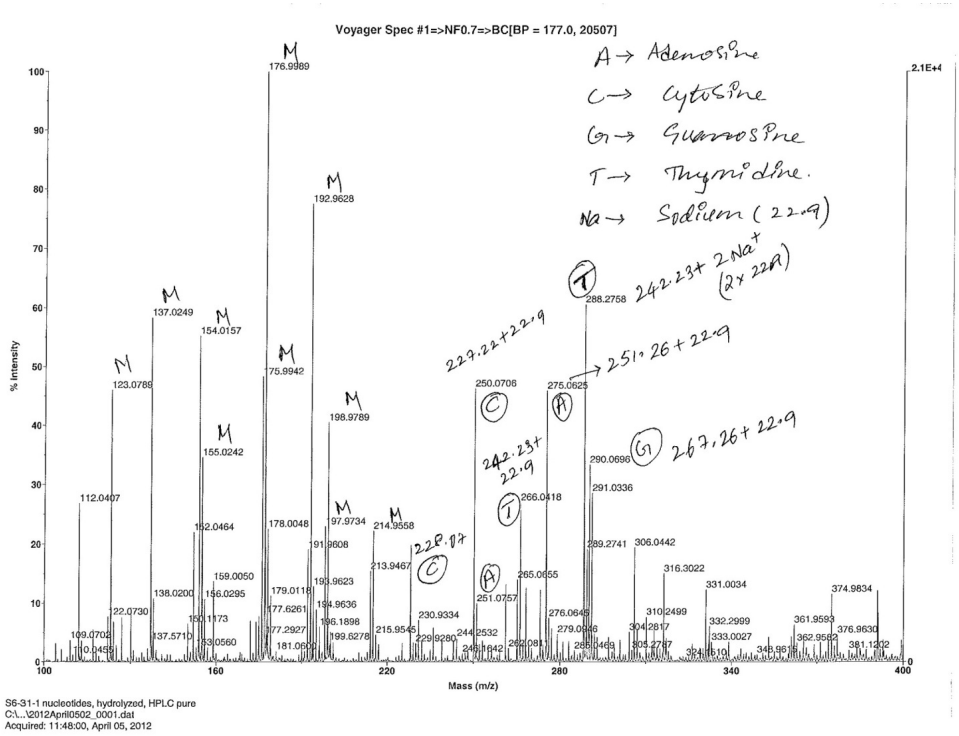

Figure 59: MALDI-TOF analysis of the fraction collected from the modified HPLC method showing all four nucleosides. M represents peaks associated with the matrix, A for adenosine, T for thymidine, G for guanidine, and C for cytidine.

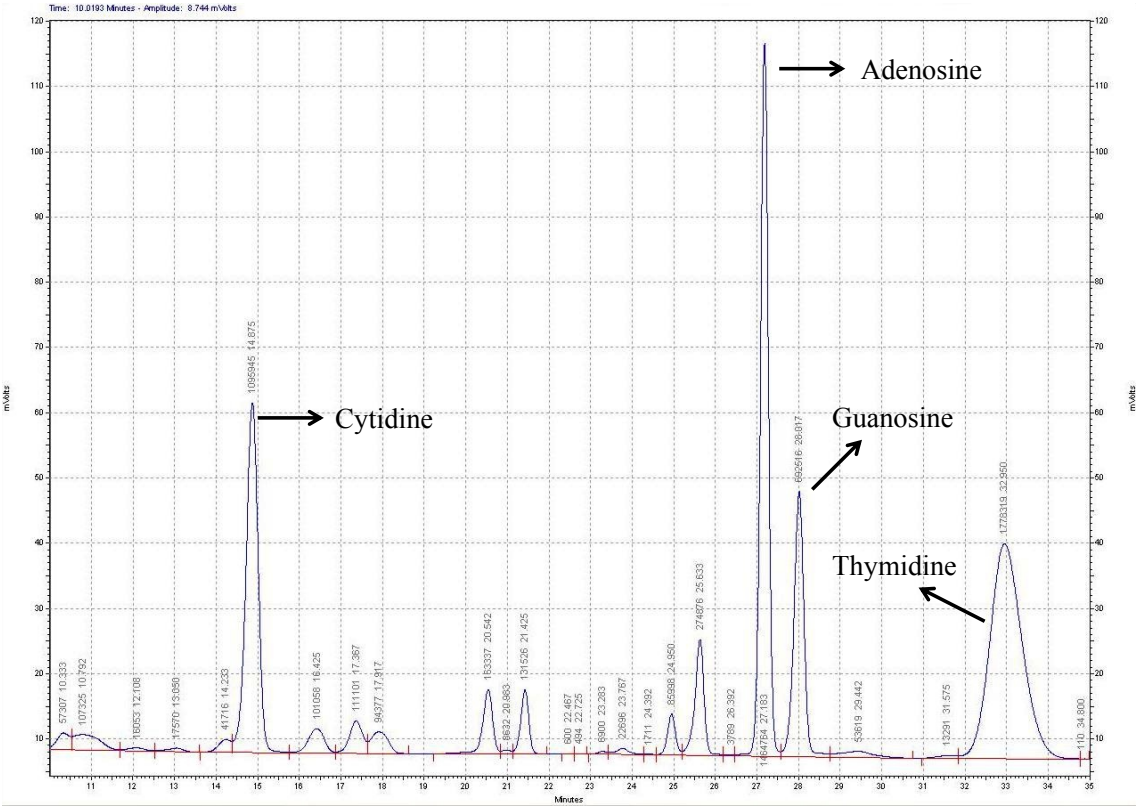

Figure 60: HPLC analysis of demethylation reaction incubated without TET2 (negative control).

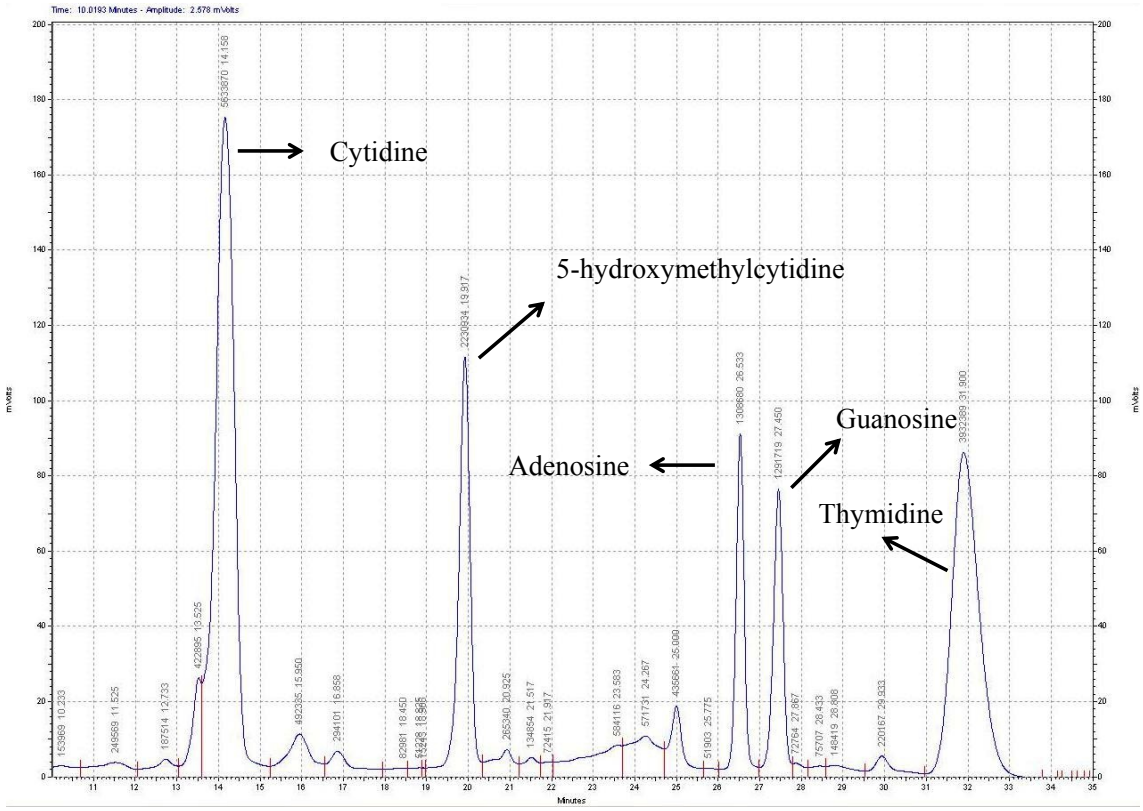

Figure 61: HPLC analysis of demethylation reaction incubated with TET2.

Hypoxia mediated expression of TET family of DNA demethylases

TET family of DNA demethylases belong to Fe(II), 2-OG dependent dioxygenase super family of enzymes. Members of this super family are intimately involved in the regulation and amplification of the HIF pathway. Hence we evaluated the possibility of HIF mediated regulation of TET enzymes in cells originating from different tissues. There was a tissue specific induction of TET enzymes when exposed to 1 % O_2 for 12 hrs suggesting a possibility of HIF mediated regulation (Figure 62).

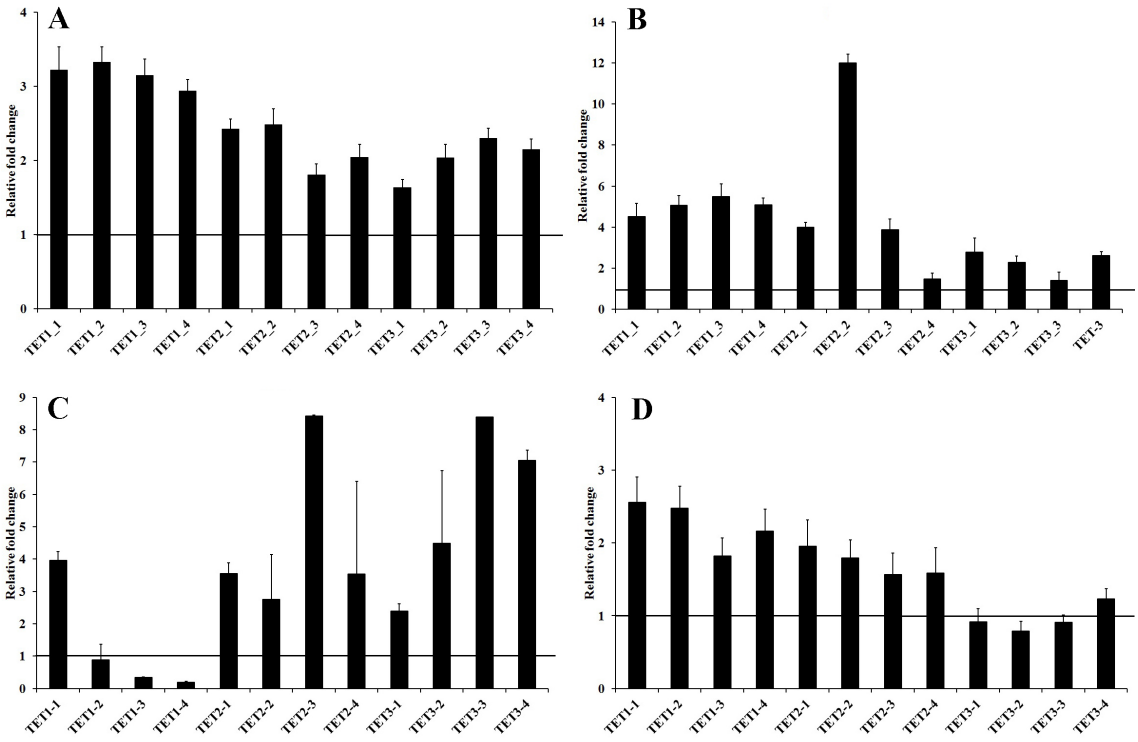

Figure 62: qPCR analysis of expression levels of TET1-3 DNA demethylases mRNA under 1% O_2 in A) 293 cells, B) D407 cells, C) HT29 cells, and D) MCF-7 cells. Horizontal line represents normoxic expression levels of the corresponding mRNA.

Conclusion and future perspectives

5-methylcytosine plays critical role in gene expression and its dynamic regulation by TET dioxygenases have opened a new era in epigenetic regulation of transcription. More interestingly, discovery of TET dioxygenases have helped identify three additional cytosine modifications (5hmC, 5fC, and 5caC), with the possibility of each playing a distinct role in epigenetics. Recent studies have established that HIF pathway plays critical roles in the homeostasis of HSCs, which reside within hypoxic regions of the bone marrow [165]. The HIF pathway itself is regulated by and regulates a number of dioxygenases [112, 166]. For example, isozymes of PHD and factor-inhibiting-HIF (FIH) dioxygenases negatively regulate the HIF pathway in response to increasing oxygen concentration. The apparent K_M values of PHDs and FIH for oxygen are in the range of 65-240 μM depending on the substrate and enzyme used [167-169]. Since the K_M values of PHDs and FIH for oxygen are higher than the observed physiological oxygen concentration of 30-60 μM, these enzymes are the cellular oxygen sensors. Further, we and others have shown that hypoxia-mediated activation of the HIF pathway leading to the induction of iron(II), 2OG-dependent KDMs is a conserved process [122, 166]. Recent studies have shown that the apparent K_M of Jmjd2 family KDMs for oxygen ranges between 50-200 μM, suggesting that KDMs may also function as cellular oxygen sensors [170]. Since dioxygenases, including TETs, have an absolute requirement of oxygen, it will be interesting to see if oxygen availability plays a role in the regulation of TET2 activity during hematopoiesis. Our unpublished data indicates differential expression of TET isoforms under hypoxic conditions in cell

lineages from diverse origin. However, it is not known if TET isoforms are targets of the HIF pathway. Finally, a recent study has shown that in some hypoxic cells 2HG accumulates even in the presence of wild-type IDH1/2 [171]. Although the amount of 2HG in these cells is much lower than that observed in IDH-1/2 mutated AML and glioblastoma patients, whether these levels of 2HG are enough to inhibit TET2 activity, and thereby, keep HSCs undifferentiated under hypoxic conditions remains to be seen.

APPENDIX

ELSEVIER LICENSE
TERMS AND CONDITIONS

Apr 22, 2014

This is a License Agreement between V K Chaithanya Ponnaluri ("You") and Elsevier ("Elsevier") provided by Copyright Clearance Center ("CCC"). The license consists of your order details, the terms and conditions provided by Elsevier, and the payment terms and conditions.

All payments must be made in full to CCC. For payment instructions, please see information listed at the bottom of this form.

Supplier	Elsevier Limited The Boulevard,Langford Lane Kidlington,Oxford,OX5 1GB,UK
Registered Company Number	1982084
Customer name	V K Chaithanya Ponnaluri
Customer address	2464 Charlotte Street Kansas City, MO 64108
License number	3374390124075
License date	Apr 22, 2014
Licensed content publisher	Elsevier
Licensed content publication	Biochemical and Biophysical Research Communications
Licensed content title	Identification of non-histone substrates for JMJD2A–C histone demethylases
Licensed content author	V.K. Chaithanya Ponnaluri,Divya Teja Vavilala,Sandeep Putty,William G. Gutheil,Mridul Mukherji
Licensed content date	11 December 2009
Licensed content volume number	390
Licensed content issue number	2
Number of pages	5
Start Page	280
End Page	284
Type of Use	reuse in a thesis/dissertation
Intended publisher of new work	other
Portion	full article
Format	both print and electronic
Are you the author of this Elsevier article?	Yes
Will you be translating?	No
Title of your thesis/dissertation	Epigenetic regulation of the HIF pathway and novel therapeutic strategies
Expected completion date	May 2014
Estimated size (number of pages)	200
Elsevier VAT number	GB 494 6272 12
Permissions price	0.00 USD
VAT/Local Sales Tax	0.00 USD / 0.00 GBP
Total	0.00 USD

ELSEVIER LICENSE
TERMS AND CONDITIONS

Apr 22, 2014

This is a License Agreement between V K Chaithanya Ponnaluri ("You") and Elsevier ("Elsevier") provided by Copyright Clearance Center ("CCC"). The license consists of your order details, the terms and conditions provided by Elsevier, and the payment terms and conditions.

All payments must be made in full to CCC. For payment instructions, please see information listed at the bottom of this form.

Supplier	Elsevier Limited The Boulevard,Langford Lane Kidlington,Oxford,OX5 1GB,UK
Registered Company Number	1982084
Customer name	V K Chaithanya Ponnaluri
Customer address	2464 Charlotte Street Kansas City, MO 64108
License number	3374390010287
License date	Apr 22, 2014
Licensed content publisher	Elsevier
Licensed content publication	Biochemical and Biophysical Research Communications
Licensed content title	Studies on substrate specificity of Jmjd2a-c histone demethylases
Licensed content author	V.K. Chaithanya Ponnaluri,Divya Teja Vavilala,Mridul Mukherji
Licensed content date	25 February 2011
Licensed content volume number	405
Licensed content issue number	4
Number of pages	5
Start Page	588
End Page	592
Type of Use	reuse in a thesis/dissertation
Intended publisher of new work	other
Portion	full article
Format	both print and electronic
Are you the author of this Elsevier article?	Yes
Will you be translating?	No
Title of your thesis/dissertation	Epigenetic regulation of the HIF pathway and novel therapeutic strategies
Expected completion date	May 2014
Estimated size (number of pages)	200
Elsevier VAT number	GB 494 6272 12
Permissions price	0.00 USD
VAT/Local Sales Tax	0.00 USD / 0.00 GBP
Total	0.00 USD

ELSEVIER LICENSE
TERMS AND CONDITIONS

Apr 22, 2014

This is a License Agreement between V K Chaithanya Ponnaluri ("You") and Elsevier ("Elsevier") provided by Copyright Clearance Center ("CCC"). The license consists of your order details, the terms and conditions provided by Elsevier, and the payment terms and conditions.

All payments must be made in full to CCC. For payment instructions, please see information listed at the bottom of this form.

Supplier	Elsevier Limited The Boulevard,Langford Lane Kidlington,Oxford,OX5 1GB,UK
Registered Company Number	1982084
Customer name	V K Chaithanya Ponnaluri
Customer address	2464 Charlotte Street Kansas City, MO 64108
License number	3374381413174
License date	Apr 22, 2014
Licensed content publisher	Elsevier
Licensed content publication	Biochemical and Biophysical Research Communications
Licensed content title	Hypoxia induced expression of histone lysine demethylases: Implications in oxygen-dependent retinal neovascular diseases
Licensed content author	V.K. Chaithanya Ponnaluri,Ramya Krishna Vadlapatla,Divya Teja Vavilala,Dhananjay Pal,Ashim K. Mitra,Mridul Mukherji
Licensed content date	18 November 2011
Licensed content volume number	415
Licensed content issue number	2
Number of pages	5
Start Page	373
End Page	377
Type of Use	reuse in a thesis/dissertation
Intended publisher of new work	other
Portion	full article
Format	both print and electronic
Are you the author of this Elsevier article?	Yes
Will you be translating?	No
Title of your thesis/dissertation	Epigenetic regulation of the HIF pathway and novel therapeutic strategies
Expected completion date	May 2014
Estimated size (number of pages)	200
Elsevier VAT number	GB 494 6272 12
Permissions price	0.00 USD
VAT/Local Sales Tax	0.00 USD / 0.00 GBP
Total	0.00 USD

ELSEVIER LICENSE
TERMS AND CONDITIONS

Apr 22, 2014

This is a License Agreement between V K Chaithanya Ponnaluri ("You") and Elsevier ("Elsevier") provided by Copyright Clearance Center ("CCC"). The license consists of your order details, the terms and conditions provided by Elsevier, and the payment terms and conditions.

All payments must be made in full to CCC. For payment instructions, please see information listed at the bottom of this form.

Supplier	Elsevier Limited The Boulevard,Langford Lane Kidlington,Oxford,OX5 1GB,UK
Registered Company Number	1982084
Customer name	V K Chaithanya Ponnaluri
Customer address	2464 Charlotte Street Kansas City, MO 64108
License number	3374381294581
License date	Apr 22, 2014
Licensed content publisher	Elsevier
Licensed content publication	Biochemical and Biophysical Research Communications
Licensed content title	A mechanistic overview of TET-mediated 5-methylcytosine oxidation
Licensed content author	V.K. Chaithanya Ponnaluri,Jaroslaw P. Maciejewski,Mridul Mukherji
Licensed content date	28 June 2013
Licensed content volume number	436
Licensed content issue number	2
Number of pages	6
Start Page	115
End Page	120
Type of Use	reuse in a thesis/dissertation
Intended publisher of new work	other
Portion	full article
Format	both print and electronic
Are you the author of this Elsevier article?	No
Will you be translating?	No
Title of your thesis/dissertation	Epigenetic regulation of the HIF pathway and novel therapeutic strategies
Expected completion date	May 2014
Estimated size (number of pages)	200
Elsevier VAT number	GB 494 6272 12
Permissions price	0.00 USD
VAT/Local Sales Tax	0.00 USD / 0.00 GBP
Total	0.00 USD

ELSEVIER LICENSE
TERMS AND CONDITIONS

Apr 22, 2014

This is a License Agreement between V K Chaithanya Ponnaluri ("You") and Elsevier ("Elsevier") provided by Copyright Clearance Center ("CCC"). The license consists of your order details, the terms and conditions provided by Elsevier, and the payment terms and conditions.

All payments must be made in full to CCC. For payment instructions, please see information listed at the bottom of this form.

Supplier	Elsevier Limited The Boulevard,Langford Lane Kidlington,Oxford,OX5 1GB,UK
Registered Company Number	1982084
Customer name	V K Chaithanya Ponnaluri
Customer address	2464 Charlotte Street Kansas City, MO 64108
License number	3374380977435
License date	Apr 22, 2014
Licensed content publisher	Elsevier
Licensed content publication	Biochemical and Biophysical Research Communications
Licensed content title	Hypoxia mediated expression of stem cell markers in VHL-associated hemangioblastomas
Licensed content author	V.K. Chaithanya Ponnaluri,Divya Teja Vavilala,Swami Prakash,Mridul Mukherji
Licensed content date	16 August 2013
Licensed content volume number	438
Licensed content issue number	1
Number of pages	7
Start Page	71
End Page	77
Type of Use	reuse in a thesis/dissertation
Portion	full article
Format	both print and electronic
Are you the author of this Elsevier article?	Yes
Will you be translating?	No
Title of your thesis/dissertation	Epigenetic regulation of the HIF pathway and novel therapeutic strategies
Expected completion date	May 2014
Estimated size (number of pages)	200
Elsevier VAT number	GB 494 6272 12
Permissions price	0.00 USD
VAT/Local Sales Tax	0.00 USD / 0.00 GBP
Total	0.00 USD

REFERENCES

1. Luger, K., *Dynamic nucleosomes.* Chromosome Res, 2006. **14**(1): p. 5-16.
2. Kouzarides, T., *Chromatin modifications and their function.* Cell, 2007. **128**(4): p. 693-705.
3. Klose, R.J. and A.P. Bird, *Genomic DNA methylation: the mark and its mediators.* Trends Biochem Sci, 2006. **31**(2): p. 89-97.
4. Esteller, M., *Aberrant DNA methylation as a cancer-inducing mechanism.* Annu Rev Pharmacol Toxicol, 2005. **45**: p. 629-56.
5. Hanahan, D. and R.A. Weinberg, *The hallmarks of cancer.* Cell, 2000. **100**(1): p. 57-70.
6. Goll, M.G. and T.H. Bestor, *Eukaryotic cytosine methyltransferases.* Annu Rev Biochem, 2005. **74**: p. 481-514.
7. Cheng, X. and R.J. Roberts, *AdoMet-dependent methylation, DNA methyltransferases and base flipping.* Nucleic Acids Res, 2001. **29**(18): p. 3784-95.
8. Klimasauskas, S., et al., *HhaI methyltransferase flips its target base out of the DNA helix.* Cell, 1994. **76**(2): p. 357-69.
9. Sheikhnejad, G., et al., *Mechanism of inhibition of DNA (cytosine C5)-methyltransferases by oligodeoxyribonucleotides containing 5,6-dihydro-5-azacytosine.* J Mol Biol, 1999. **285**(5): p. 2021-34.

10. Wu, J.C. and D.V. Santi, *Kinetic and catalytic mechanism of HhaI methyltransferase.* J Biol Chem, 1987. **262**(10): p. 4778-86.

11. Youngblood, B., et al., *S-adenosyl-L-methionine-dependent methyl transfer: observable precatalytic intermediates during DNA cytosine methylation.* Biochemistry, 2007. **46**(30): p. 8766-75.

12. Zhang, X. and T.C. Bruice, *The mechanism of M.HhaI DNA C5 cytosine methyltransferase enzyme: a quantum mechanics/molecular mechanics approach.* Proc Natl Acad Sci U S A, 2006. **103**(16): p. 6148-53.

13. Turner, B.M., *Defining an epigenetic code.* Nat Cell Biol, 2007. **9**(1): p. 2-6.

14. Yen, Z.C., et al., *A cross-species comparison of X-chromosome inactivation in Eutheria.* Genomics, 2007. **90**(4): p. 453-63.

15. Reik, W., *Stability and flexibility of epigenetic gene regulation in mammalian development.* Nature, 2007. **447**(7143): p. 425-32.

16. Lande-Diner, L., et al., *Role of DNA methylation in stable gene repression.* J Biol Chem, 2007. **282**(16): p. 12194-200.

17. Miranda, T.B. and P.A. Jones, *DNA methylation: the nuts and bolts of repression.* J Cell Physiol, 2007. **213**(2): p. 384-90.

18. Gronbaek, K., C. Hother, and P.A. Jones, *Epigenetic changes in cancer.* APMIS, 2007. **115**(10): p. 1039-59.

19. Wade, P.A., *Methyl CpG-binding proteins and transcriptional repression.* Bioessays, 2001. **23**(12): p. 1131-7.

20. Dobosy, J.R. and E.U. Selker, *Emerging connections between DNA methylation and histone acetylation.* Cell Mol Life Sci, 2001. **58**(5-6): p. 721-7.

21. Wang, Y., et al., *Beyond the double helix: writing and reading the histone code.* Novartis Found Symp, 2004. **259**: p. 3-17; discussion 17-21, 163-9.

22. Wu, S.C. and Y. Zhang, *Active DNA demethylation: many roads lead to Rome.* Nat Rev Mol Cell Biol, 2010. **11**(9): p. 607-20.

23. Zhang, H., et al., *TET1 is a DNA-binding protein that modulates DNA methylation and gene transcription via hydroxylation of 5-methylcytosine.* Cell Res, 2010. **20**(12): p. 1390-3.

24. Tahiliani, M., et al., *Conversion of 5-methylcytosine to 5-hydroxymethylcytosine in mammalian DNA by MLL partner TET1.* Science, 2009. **324**(5929): p. 930-5.

25. Ito, S., et al., *Role of Tet proteins in 5mC to 5hmC conversion, ES-cell self-renewal and inner cell mass specification.* Nature, 2010. **466**(7310): p. 1129-33.

26. Kriaucionis, S. and N. Heintz, *The nuclear DNA base 5-hydroxymethylcytosine is present in Purkinje neurons and the brain.* Science, 2009. **324**(5929): p. 929-30.

27. Cliffe, L.J., et al., *JBP1 and JBP2 are two distinct thymidine hydroxylases involved in J biosynthesis in genomic DNA of African trypanosomes.* Nucleic Acids Res, 2009. **37**(5): p. 1452-62.

28. Iyer, L.M., et al., *Prediction of novel families of enzymes involved in oxidative and other complex modifications of bases in nucleic acids.* Cell Cycle, 2009. **8**(11): p. 1698-710.

29. He, Y.F., et al., *Tet-mediated formation of 5-carboxylcytosine and its excision by TDG in mammalian DNA.* Science, 2011. **333**(6047): p. 1303-7.

30. Mariappa, D., S. Pathak, and D.M. van Aalten, *A sweet TET-a-tete-synergy of TET proteins and O-GlcNAc transferase in transcription.* EMBO J, 2013. **32**(5): p. 612-3.

31. Falnes, P.O., R.F. Johansen, and E. Seeberg, *AlkB-mediated oxidative demethylation reverses DNA damage in Escherichia coli.* Nature, 2002. **419**(6903): p. 178-82.

32. Trewick, S.C., et al., *Oxidative demethylation by Escherichia coli AlkB directly reverts DNA base damage.* Nature, 2002. **419**(6903): p. 174-8.

33. Koivisto, P., et al., *Demethylation of 3-methylthymine in DNA by bacterial and human DNA dioxygenases.* J Biol Chem, 2004. **279**(39): p. 40470-4.

34. Han, Z., et al., *Crystal structure of the FTO protein reveals basis for its substrate specificity.* Nature, 2010. **464**(7292): p. 1205-9.

35. Motorin, Y., F. Lyko, and M. Helm, *5-methylcytosine in RNA: detection, enzymatic formation and biological functions.* Nucleic Acids Res, 2010. **38**(5): p. 1415-30.

36. Kovaleva, E.G. and J.D. Lipscomb, *Versatility of biological non-heme Fe(II) centers in oxygen activation reactions.* Nat Chem Biol, 2008. **4**(3): p. 186-93.

37. Ito, S., et al., *Tet proteins can convert 5-methylcytosine to 5-formylcytosine and 5-carboxylcytosine.* Science, 2011. **333**(6047): p. 1300-3.

38. Murray, K., *The Occurrence of Epsilon-N-Methyl Lysine in Histones.* Biochemistry, 1964. **3**: p. 10-5.

39. DeLange, R.J., et al., *Calf and pea histone IV. II. The complete amino acid sequence of calf thymus histone IV; presence of epsilon-N-acetyllysine.* J Biol Chem, 1969. **244**(2): p. 319-34.

40. Patterson, B.D. and D.D. Davies, *Specificity of the enzymatic methylation of pea histone.* Biochem Biophys Res Commun, 1969. **34**(6): p. 791-4.

41. Gershey, E.L., et al., *Chemical studies of histone methylation. Evidence for the occurrence of 3-methylhistidine in avian erythrocyte histone fractions.* J Biol Chem, 1969. **244**(18): p. 4871-7.

42. Allis, C.D., et al., *New nomenclature for chromatin-modifying enzymes.* Cell, 2007. **131**(4): p. 633-6.

43. Shi, Y., et al., *Histone demethylation mediated by the nuclear amine oxidase homolog LSD1.* Cell, 2004. **119**(7): p. 941-53.

44. Cloos, P.A., et al., *The putative oncogene GASC1 demethylates tri- and dimethylated lysine 9 on histone H3.* Nature, 2006. **442**(7100): p. 307-11.

45. Tsukada, Y., et al., *Histone demethylation by a family of JmjC domain-containing proteins.* Nature, 2006. **439**(7078): p. 811-6.

46. Klose, R.J., E.M. Kallin, and Y. Zhang, *JmjC-domain-containing proteins and histone demethylation.* Nat Rev Genet, 2006. **7**(9): p. 715-27.

47. Shilatifard, A., *Chromatin modifications by methylation and ubiquitination: implications in the regulation of gene expression.* Annu Rev Biochem, 2006. **75**: p. 243-69.

48. Schubert, H.L., R.M. Blumenthal, and X. Cheng, *Many paths to methyltransfer: a chronicle of convergence.* Trends Biochem Sci, 2003. **28**(6): p. 329-35.

49. Zhang, X. and T.C. Bruice, *Enzymatic mechanism and product specificity of SET-domain protein lysine methyltransferases.* Proc Natl Acad Sci U S A, 2008. **105**(15): p. 5728-32.

50. Ng, S.S., et al., *Crystal structures of histone demethylase JMJD2A reveal basis for substrate specificity.* Nature, 2007. **448**(7149): p. 87-91.

51. Couture, J.F., et al., *Specificity and mechanism of JMJD2A, a trimethyllysine-specific histone demethylase.* Nat Struct Mol Biol, 2007. **14**(8): p. 689-95.

52. Hegg, E.L. and L. Que, *The 2-His-1-carboxylate facial triad. An emerging motif in mononuclear non-heme iron(II) enzymes.* Eur. J. Biochem., 1997. **250**: p. 625-629.

53. Mukherji, M., et al., *Structure-function analysis of phytanoyl-CoA 2-hydroxylase mutations causing Refsum's disease.* Hum Mol Genet, 2001. **10**(18): p. 1971-82.

54. Lopez-Barneo, J., R. Pardal, and P. Ortega-Saenz, *Cellular mechanism of oxygen sensing.* Annu Rev Physiol, 2001. **63**: p. 259-87.

55. Hardie, D.G., *Minireview: the AMP-activated protein kinase cascade: the key sensor of cellular energy status.* Endocrinology, 2003. **144**(12): p. 5179-83.

56. Brahimi-Horn, M.C. and J. Pouyssegur, *Oxygen, a source of life and stress.* FEBS Lett, 2007. **581**(19): p. 3582-91.

57. Li, J., et al., *Altered metabolic responses to intermittent hypoxia in mice with partial deficiency of hypoxia-inducible factor-1alpha.* Physiol Genomics, 2006. **25**(3): p. 450-7.

58. Sharp, F.R., et al., *Hypoxic preconditioning protects against ischemic brain injury.* NeuroRx, 2004. **1**(1): p. 26-35.

59. Biagas, K., *Hypoxic-ischemic brain injury: advancements in the understanding of mechanisms and potential avenues for therapy.* Curr Opin Pediatr, 1999. **11**(3): p. 223-8.

60. Lee, K.A., R.A. Roth, and J.J. LaPres, *Hypoxia, drug therapy and toxicity.* Pharmacol Ther, 2007. **113**(2): p. 229-46.

61. Semenza, G.L. and G.L. Wang, *A nuclear factor induced by hypoxia via de novo protein synthesis binds to the human erythropoietin gene enhancer at a site required for transcriptional activation.* Mol Cell Biol, 1992. **12**(12): p. 5447-54.

62. Wang, G.L. and G.L. Semenza, *Purification and characterization of hypoxia-inducible factor 1.* J Biol Chem, 1995. **270**(3): p. 1230-7.

63. Wang, G.L., et al., *Hypoxia-inducible factor 1 is a basic-helix-loop-helix-PAS heterodimer regulated by cellular O2 tension.* Proc Natl Acad Sci U S A, 1995. **92**(12): p. 5510-4.

64. Jiang, B.H., et al., *Hypoxia-inducible factor 1 levels vary exponentially over a physiologically relevant range of O2 tension.* Am J Physiol, 1996. **271**(4 Pt 1): p. C1172-80.

65. Ema, M., et al., *A novel bHLH-PAS factor with close sequence similarity to hypoxia-inducible factor 1alpha regulates the VEGF expression and is potentially involved in lung and vascular development.* Proc Natl Acad Sci U S A, 1997. **94**(9): p. 4273-8.

66. Mahon, P.C., K. Hirota, and G.L. Semenza, *FIH-1: a novel protein that interacts with HIF-1alpha and VHL to mediate repression of HIF-1 transcriptional activity.* Genes Dev, 2001. **15**(20): p. 2675-86.

67. Lando, D., et al., *FIH-1 is an asparaginyl hydroxylase enzyme that regulates the transcriptional activity of hypoxia-inducible factor.* Genes Dev, 2002. **16**(12): p. 1466-71.

68. Lando, D., et al., *Asparagine hydroxylation of the HIF transactivation domain a hypoxic switch.* Science, 2002. **295**(5556): p. 858-61.

69. Krieg, A.J., et al., *Regulation of the histone demethylase JMJD1A by hypoxia-inducible factor 1 alpha enhances hypoxic gene expression and tumor growth.* Mol Cell Biol, 2010. **30**(1): p. 344-53.

70. Sar, A., et al., *Identification and characterization of demethylase JMJD1A as a gene upregulated in the human cellular response to hypoxia.* Cell Tissue Res, 2009. **337**(2): p. 223-34.

71. Beyer, S., et al., *The histone demethylases JMJD1A and JMJD2B are transcriptional targets of hypoxia-inducible factor HIF.* J Biol Chem, 2008. **283**(52): p. 36542-52.

72. Uemura, M., et al., *Jumonji domain containing 1A is a novel prognostic marker for colorectal cancer: in vivo identification from hypoxic tumor cells.* Clin Cancer Res, 2010. **16**(18): p. 4636-46.

73. Zhang, Y. and D. Reinberg, *Transcription regulation by histone methylation: interplay between different covalent modifications of the core histone tails.* Genes Dev, 2001. **15**(18): p. 2343-60.

74. Klose, R.J., et al., *The transcriptional repressor JHDM3A demethylates trimethyl histone H3 lysine 9 and lysine 36.* Nature, 2006. **442**(7100): p. 312-6.

75. Klose, R.J. and Y. Zhang, *Regulation of histone methylation by demethylimination and demethylation.* Nat Rev Mol Cell Biol, 2007. **8**(4): p. 307-18.

76. Pavel, E.G., et al., *Circular dichroism and magnetic circular dichroism spectroscopic studies of the non-heme ferrous active site in clavaminate synthase and its interaction with a-ketoglutarate cosubstrate.* J. Am. Chem. Soc., 1998. **120**: p. 743-753.

77. Zhou, J., et al., *Substrate binding to the a-ketoglutarate-dependent non-haem iron enzyme clavaminate synthase 2: Coupling mechanism of oxidative decarboxylation and hydroxylation.* J. Am. Chem. Soc., 1998. **120**: p. 13539-13540.

78. Chen, Z., et al., *Structural insights into histone demethylation by JMJD2 family members.* Cell, 2006. **125**(4): p. 691-702.

79. Elkins, J.M., et al., *Structure of factor-inhibiting hypoxia-inducible factor (HIF) reveals mechanism of oxidative modification of HIF-1 alpha.* J Biol Chem, 2003. **278**(3): p. 1802-6.

80. McDonough, M.A., et al., *Structure of human phytanoyl-CoA 2-hydroxylase identifies molecular mechanisms of Refsum disease.* J Biol Chem, 2005. **280**(49): p. 41101-10.

81. McDonough, M.A., et al., *Cellular oxygen sensing: Crystal structure of hypoxia-inducible factor prolyl hydroxylase (PHD2).* Proc Natl Acad Sci U S A, 2006. **103**(26): p. 9814-9.

82. Valegård, K., et al., *Structure of a cephalosporin synthase.* Nature, 1998. **394**: p. 805-809.

83. Wilmouth, R.C., et al., *Structure and mechanism of anthocyanidin synthase from Arabidopsis thaliana.* Structure, 2002. **10**(1): p. 93-103.

84. Zhang, Z.-H., et al., *Structural origins of the selectivity of the trifunctional oxygenase clavaminic acid synthase.* Nat. Struct. Biol., 2000. **7**: p. 127-133.

85. Clifton, I.J., et al., *Structure of proline 3-hydroxylase. Evolution of the family of 2-oxoglutarate dependent oxygenases.* Eur J Biochem, 2001. **268**(24): p. 6625-36.

86. Baldwin, J.B., et al., *Incorporation of ^{18}O-labelled water into oxygenated products produced by the enzyme deacetoxy/deactycephalosporin C synthase.* Tetrahedron, 1993. **49**: p. 7499-7518.

87. Whetstine, J.R., et al., *Reversal of histone lysine trimethylation by the JMJD2 family of histone demethylases.* Cell, 2006. **125**(3): p. 467-81.

88. Mukherji, M., et al., *Utilization of sterol carrier protein-2 by phytanoyl-CoA 2-hydroxylase in the peroxisomal alpha oxidation of phytanic acid.* Chem Biol, 2002. **9**(5): p. 597-605.

89. Cockman, M.E., et al., *Posttranslational hydroxylation of ankyrin repeats in IkappaB proteins by the hypoxia-inducible factor (HIF) asparaginyl hydroxylase, factor inhibiting HIF (FIH).* Proc Natl Acad Sci U S A, 2006. **103**(40): p. 14767-72.

90. Coleman, M.L., et al., *Asparaginyl hydroxylation of the Notch ankyrin repeat domain by factor inhibiting hypoxia-inducible factor.* J Biol Chem, 2007. **282**(33): p. 24027-38.

91. Rathert, P., et al., *Protein lysine methyltransferase G9a acts on non-histone targets.* Nat Chem Biol, 2008. **4**(6): p. 344-6.

92. Ponnaluri, V.K., et al., *Identification of non-histone substrates for JMJD2A-C histone demethylases.* Biochem Biophys Res Commun, 2009. **390**(2): p. 280-4.

93. Wissmann, M., et al., *Cooperative demethylation by JMJD2C and LSD1 promotes androgen receptor-dependent gene expression.* Nat Cell Biol, 2007. **9**(3): p. 347-53.

94. Shin, S. and R. Janknecht, *Activation of androgen receptor by histone demethylases JMJD2A and JMJD2D.* Biochem Biophys Res Commun, 2007. **359**(3): p. 742-6.

95. Tachibana, M., et al., *Set domain-containing protein, G9a, is a novel lysine-preferring mammalian histone methyltransferase with hyperactivity and specific selectivity to lysines 9 and 27 of histone H3.* J Biol Chem, 2001. **276**(27): p. 25309-17.

96. Wu, H., et al., *Structural biology of human H3K9 methyltransferases.* PLoS One, 2010. **5**(1): p. e8570.

97. Xiao, B., et al., *Specificity and mechanism of the histone methyltransferase Pr-Set7.* Genes Dev, 2005. **19**(12): p. 1444-54.

98. Southall, S.M., et al., *Structural basis for the requirement of additional factors for MLL1 SET domain activity and recognition of epigenetic marks.* Mol Cell, 2009. **33**(2): p. 181-91.

99. Couture, J.F., et al., *Structural and functional analysis of SET8, a histone H4 Lys-20 methyltransferase.* Genes Dev, 2005. **19**(12): p. 1455-65.

100. Xiao, B., et al., *Structure and catalytic mechanism of the human histone methyltransferase SET7/9.* Nature, 2003. **421**(6923): p. 652-6.

101. Zhang, X., et al., *Structure of the Neurospora SET domain protein DIM-5, a histone H3 lysine methyltransferase.* Cell, 2002. **111**(1): p. 117-27.

102. Qian, C., et al., *Structural insights of the specificity and catalysis of a viral histone H3 lysine 27 methyltransferase.* J Mol Biol, 2006. **359**(1): p. 86-96.

103. Choudhary, C., et al., *Lysine acetylation targets protein complexes and co-regulates major cellular functions.* Science, 2009. **325**(5942): p. 834-40.

104. Olsen, J.V., et al., *Global, in vivo, and site-specific phosphorylation dynamics in signaling networks.* Cell, 2006. **127**(3): p. 635-48.

105. Tedford, N.C., F.M. White, and J.A. Radding, *Illuminating signaling network functional biology through quantitative phosphoproteomic mass spectrometry.* Brief Funct Genomic Proteomic, 2008. **7**(5): p. 383-94.

106. Ueda, J., et al., *Zinc finger protein Wiz links G9a/GLP histone methyltransferases to the co-repressor molecule CtBP.* J Biol Chem, 2006. **281**(29): p. 20120-8.

107. Shi, Y., et al., *Coordinated histone modifications mediated by a CtBP co-repressor complex.* Nature, 2003. **422**(6933): p. 735-8.

108. Carmeliet, P., et al., *Role of HIF-1alpha in hypoxia-mediated apoptosis, cell proliferation and tumour angiogenesis.* Nature, 1998. **394**(6692): p. 485-90.

109. Gibson, J.S., A.R. Cossins, and J.C. Ellory, *Oxygen-sensitive membrane transporters in vertebrate red cells.* J Exp Biol, 2000. **203**(Pt 9): p. 1395-407.

110. Brown, J.M., *Exploiting the hypoxic cancer cell: mechanisms and therapeutic strategies.* Mol Med Today, 2000. **6**(4): p. 157-62.

111. Jaakkola, P., et al., *Targeting of HIF-alpha to the von Hippel-Lindau ubiquitylation complex by O2-regulated prolyl hydroxylation.* Science, 2001. **292**(5516): p. 468-72.

112. Epstein, A.C., et al., *C. elegans EGL-9 and mammalian homologs define a family of dioxygenases that regulate HIF by prolyl hydroxylation.* Cell, 2001. **107**(1): p. 43-54.

113. Arjamaa, O. and M. Nikinmaa, *Oxygen-dependent diseases in the retina: role of hypoxia-inducible factors.* Exp Eye Res, 2006. **83**(3): p. 473-83.

114. Yang, J., et al., *Role of hypoxia-inducible factors in epigenetic regulation via histone demethylases.* Ann N Y Acad Sci, 2009. **1177**: p. 185-97.

115. Kim, W.Y. and W.G. Kaelin, *Role of VHL gene mutation in human cancer.* J Clin Oncol, 2004. **22**(24): p. 4991-5004.

116. Chan, C.C., et al., *Expression of stem cells markers in ocular hemangioblastoma associated with von Hippel-Lindau (VHL) disease.* Mol Vis, 2005. **11**: p. 697-704.

117. Park, D.M., et al., *von Hippel-Lindau disease-associated hemangioblastomas are derived from embryologic multipotent cells.* PLoS Med, 2007. **4**(2): p. e60.

118. Ma, D., et al., *Hemangioblastomas might derive from neoplastic transformation of neural stem cells/progenitors in the specific niche.* Carcinogenesis, 2011. **32**(1): p. 102-9.

119. Glasker, S., et al., *Hemangioblastomas share protein expression with embryonal hemangioblast progenitor cell.* Cancer Res, 2006. **66**(8): p. 4167-72.

120. Wong, W.T., et al., *Intravitreal ranibizumab therapy for retinal capillary hemangioblastoma related to von Hippel-Lindau disease.* Ophthalmology, 2008. **115**(11): p. 1957-64.

121. Wong, W.T. and E.Y. Chew, *Ocular von Hippel-Lindau disease: clinical update and emerging treatments.* Curr Opin Ophthalmol, 2008. **19**(3): p. 213-7.

122. Vavilala, D.T., et al., *Honokiol inhibits HIF pathway and hypoxia-induced expression of histone lysine demethylases.* Biochem Biophys Res Commun, 2012.

123. Hu, C.J., et al., *Differential roles of hypoxia-inducible factor 1alpha (HIF-1alpha) and HIF-2alpha in hypoxic gene regulation.* Mol Cell Biol, 2003. **23**(24): p. 9361-74.

124. Slomiany, M.G. and S.A. Rosenzweig, *IGF-1-induced VEGF and IGFBP-3 secretion correlates with increased HIF-1 alpha expression and activity in retinal pigment epithelial cell line D407.* Invest Ophthalmol Vis Sci, 2004. **45**(8): p. 2838-47.

125. Geisen, P., et al., *Characterization of barrier properties and inducible VEGF expression of several types of retinal pigment epithelium in medium-term culture.* Curr Eye Res, 2006. **31**(9): p. 739-48.

126. Forooghian, F., R. Razavi, and L. Timms, *Hypoxia-inducible factor expression in human RPE cells.* Br J Ophthalmol, 2007. **91**(10): p. 1406-10.

127. Xia, X., et al., *Integrative analysis of HIF binding and transactivation reveals its role in maintaining histone methylation homeostasis.* Proc Natl Acad Sci U S A, 2009. **106**(11): p. 4260-5.

128. Yamane, K., et al., *JHDM2A, a JmjC-containing H3K9 demethylase, facilitates transcription activation by androgen receptor.* Cell, 2006. **125**(3): p. 483-95.

129. Kitamura, K., et al., *Adrenomedullin: a novel hypotensive peptide isolated from human pheochromocytoma.* Biochem Biophys Res Commun, 1993. **192**(2): p. 553-60.

130. Le, Q.T., N.C. Denko, and A.J. Giaccia, *Hypoxic gene expression and metastasis.* Cancer Metastasis Rev, 2004. **23**(3-4): p. 293-310.

131. Thalhammer, A., et al., *Human AlkB homologue 5 is a nuclear 2-oxoglutarate dependent oxygenase and a direct target of hypoxia-inducible factor 1alpha (HIF-1alpha).* PLoS One, 2011. **6**(1): p. e16210.

132. Iliopoulos, O., et al., *Tumour suppression by the human von Hippel-Lindau gene product.* Nat Med, 1995. **1**(8): p. 822-6.

133. Maxwell, P.H., et al., *The tumour suppressor protein VHL targets hypoxia-inducible factors for oxygen-dependent proteolysis.* Nature, 1999. **399**(6733): p. 271-5.

134. Kondo, K., et al., *Inhibition of HIF2alpha is sufficient to suppress pVHL-defective tumor growth.* PLoS Biol, 2003. **1**(3): p. E83.

135. Iliopoulos, O., et al., *Negative regulation of hypoxia-inducible genes by the von Hippel-Lindau protein.* Proc Natl Acad Sci U S A, 1996. **93**(20): p. 10595-9.

136. Kondo, K., et al., *Inhibition of HIF is necessary for tumor suppression by the von Hippel-Lindau protein.* Cancer Cell, 2002. **1**(3): p. 237-46.

137. Zimmer, M., et al., *Inhibition of hypoxia-inducible factor is sufficient for growth suppression of VHL-/- tumors.* Mol Cancer Res, 2004. **2**(2): p. 89-95.

138. Guo, X., et al., *The expression of histone demethylase JMJD1A in renal cell carcinoma.* Neoplasma, 2011. **58**(2): p. 153-7.

139. Song, H., D. Yin, and Z. Liu, *GDF-15 promotes angiogenesis through modulating p53/HIF-1alpha signaling pathway in hypoxic human umbilical vein endothelial cells.* Mol Biol Rep, 2012. **39**(4): p. 4017-22.

140. Rudnicki, M., et al., *Hypoxia inducible factor-dependent regulation of angiogenesis by nitro-fatty acids.* Arterioscler Thromb Vasc Biol, 2011. **31**(6): p. 1360-7.

141. Mathieu, J., et al., *HIF induces human embryonic stem cell markers in cancer cells.* Cancer Res, 2011. **71**(13): p. 4640-52.

142. Mazumdar, J., et al., *O2 regulates stem cells through Wnt/beta-catenin signalling.* Nat Cell Biol, 2010. **12**(10): p. 1007-13.

143. Mazumdar, J., V. Dondeti, and M.C. Simon, *Hypoxia-inducible factors in stem cells and cancer.* J Cell Mol Med, 2009. **13**(11-12): p. 4319-28.

144. Bestor, T.H., *The DNA methyltransferases of mammals.* Hum Mol Genet, 2000. **9**(16): p. 2395-402.

145. Williams, K., et al., *TET1 and hydroxymethylcytosine in transcription and DNA methylation fidelity.* Nature, 2011. **473**(7347): p. 343-8.

146. Wu, H., et al., *Dual functions of Tet1 in transcriptional regulation in mouse embryonic stem cells.* Nature, 2011. **473**(7347): p. 389-93.

147. Pastor, W.A., et al., *Genome-wide mapping of 5-hydroxymethylcytosine in embryonic stem cells.* Nature, 2011. **473**(7347): p. 394-7.

148. Ficz, G., et al., *Dynamic regulation of 5-hydroxymethylcytosine in mouse ES cells and during differentiation.* Nature, 2011. **473**(7347): p. 398-402.

149. Lorsbach, R.B., et al., *TET1, a member of a novel protein family, is fused to MLL in acute myeloid leukemia containing the t(10;11)(q22;q23).* Leukemia, 2003. **17**(3): p. 637-41.

150. Ko, M., et al., *Impaired hydroxylation of 5-methylcytosine in myeloid cancers with mutant TET2.* Nature, 2010. **468**(7325): p. 839-43.

151. Langemeijer, S.M., et al., *Acquired mutations in TET2 are common in myelodysplastic syndromes.* Nat Genet, 2009. **41**(7): p. 838-42.

152. Smith, A.E., et al., *Next-generation sequencing of the TET2 gene in 355 MDS and CMML patients reveals low-abundance mutant clones with early origins, but indicates no definite prognostic value.* Blood, 2010. **116**(19): p. 3923-32.

153. Moran-Crusio, K., et al., *Tet2 loss leads to increased hematopoietic stem cell self-renewal and myeloid transformation.* Cancer Cell, 2011. **20**(1): p. 11-24.

154. Li, Z., et al., *Deletion of Tet2 in mice leads to dysregulated hematopoietic stem cells and subsequent development of myeloid malignancies.* Blood, 2011. **118**(17): p. 4509-18.

155. Ko, M., et al., *Ten-Eleven-Translocation 2 (TET2) negatively regulates homeostasis and differentiation of hematopoietic stem cells in mice.* Proc Natl Acad Sci U S A, 2011. **108**(35): p. 14566-71.

156. Quivoron, C., et al., *TET2 inactivation results in pleiotropic hematopoietic abnormalities in mouse and is a recurrent event during human lymphomagenesis.* Cancer Cell, 2011. **20**(1): p. 25-38.

157. Dawlaty, M.M., et al., *Tet1 is dispensable for maintaining pluripotency and its loss is compatible with embryonic and postnatal development.* Cell Stem Cell, 2011. **9**(2): p. 166-75.

158. Dang, L., et al., *Cancer-associated IDH1 mutations produce 2-hydroxyglutarate.* Nature, 2009. **462**(7274): p. 739-44.

159. Figueroa, M.E., et al., *Leukemic IDH1 and IDH2 mutations result in a hypermethylation phenotype, disrupt TET2 function, and impair hematopoietic differentiation.* Cancer Cell, 2010. **18**(6): p. 553-67.

160. Chowdhury, R., et al., *The oncometabolite 2-hydroxyglutarate inhibits histone lysine demethylases.* EMBO Rep, 2011. **12**(5): p. 463-9.

161. Pasini, B., et al., *Clinical and molecular genetics of patients with the Carney-Stratakis syndrome and germline mutations of the genes coding for the succinate dehydrogenase subunits SDHB, SDHC, and SDHD.* Eur J Hum Genet, 2008. **16**(1): p. 79-88.

162. Lehtonen, H.J., et al., *Increased risk of cancer in patients with fumarate hydratase germline mutation.* J Med Genet, 2006. **43**(6): p. 523-6.

163. Hewitson, K.S., et al., *Structural and mechanistic studies on the inhibition of the hypoxia-inducible transcription factor hydroxylases by tricarboxylic acid cycle intermediates.* J Biol Chem, 2007. **282**(5): p. 3293-301.

164. Clifton, I.J., et al., *Structural studies on 2-oxoglutarate oxygenases and related double-stranded beta-helix fold proteins.* J Inorg Biochem, 2006. **100**(4): p. 644-69.

165. Takubo, K., et al., *Regulation of the HIF-1alpha level is essential for hematopoietic stem cells.* Cell Stem Cell, 2010. **7**(3): p. 391-402.

166. Ponnaluri, V.K., et al., *Hypoxia induced expression of histone lysine demethylases: implications in oxygen-dependent retinal neovascular diseases.* Biochem Biophys Res Commun, 2011. **415**(2): p. 373-7.

167. Ehrismann, D., et al., *Studies on the activity of the hypoxia-inducible-factor hydroxylases using an oxygen consumption assay.* Biochem J, 2007. **401**(1): p. 227-34.

168. Hirsila, M., et al., *Characterization of the human prolyl 4-hydroxylases that modify the hypoxia-inducible factor.* J Biol Chem, 2003. **278**(33): p. 30772-80.

169. Koivunen, P., et al., *Catalytic properties of the asparaginyl hydroxylase (FIH) in the oxygen sensing pathway are distinct from those of its prolyl 4-hydroxylases.* J Biol Chem, 2004. **279**(11): p. 9899-904.

170. Cascella, B. and L.M. Mirica, *Kinetic analysis of iron-dependent histone demethylases: alpha-ketoglutarate substrate inhibition and potential relevance to the regulation of histone demethylation in cancer cells.* Biochemistry, 2012. **51**(44): p. 8699-701.

171. Wise, D.R., et al., *Hypoxia promotes isocitrate dehydrogenase-dependent carboxylation of alpha-ketoglutarate to citrate to support cell growth and viability*. Proc Natl Acad Sci U S A, 2011. **108**(49): p. 19611-6.

VITA

Venkata Krishna Chaithanya Ponnaluri was born on December 3rd, 1983, in Hyderabad, Andhra Pradesh, India. He completed his high school from Kakatiya Vidya Niketan High School, Hyderabad, India. He obtained his Master of Science. (Hons.) in Biological Sciences from Birla Institute of Technology and Science, Pilani, Rajasthan, India in May 2005. He later obtained his Master of Engineering in Biotechnology from Birla Institute of Technology and Science, Pilani, India in December 2007.

Venkata Krishna Chaithanya Ponnaluri joined University of Missouri-Kansas City in Spring-2008 in pursuit of an interdisciplinary doctorate degree in Pharmaceutical Sciences and Molecular Biology and Biochemistry. He completed his doctoral studies in May 2014 under the guidance of Dr. Mridul Mukherji.

He was awarded the National Merit Award by Human Resource Department, Government of India for ranking 24th in the State of Andhra Pradesh, India in Intermediate Public Examinations. He was also awarded the best trainee award at NIH for BIO-TRACK 15 – Yeast Two Hybrid system 2010 and best speaker award in UMKC Pharmaceutical Sciences Spring seminar series 2011.

He did a summer internship at Stowers Institute for Medical Research, Kansas City in Dr. Sue Jasperson lab. He has authored/co-authored 12 peer reviewed research/review articles in reputed international journals.